SOUND GENERATION BY A CENTRIFUGAL VOLUTE PUMP AT BLADE PASS FREQUENCY

BY

MICHAEL MORGENROTH, DIPL. ING.

A Thesis
Submitted to the School of Graduate Studies
in Partial Fulfilment of the Requirements
for the Degree

Doctor of Philosophy
(Mechanical Engineering)

McMaster University

PUMP ACOUSTICS AT BLADE PASS FREQUENCY

DOCTOR OF PHILOSOPHY (1995) (Mechanical Engineering)	MCMASTER UNIVERSITY HAMILTON, ONTARIO, CANADA
TITLE:	Sound Generation by a Centrifugal Volute Pump at Blade Pass Frequency
AUTHOR:	Michael Morgenroth, Dipl. Ing. (Stuttgart, Germany)
SUPERVISOR:	Professor D.S. Weaver
NUMBER OF PAGES:	xv, 214

ABSTRACT

The behaviour of a centrifugal volute pump as a source of pressure pulsations as well as the role that the pump-pipeline interaction plays in the amplification of these pressure pulsations were experimentally investigated.

A test apparatus was designed and built which features acoustic tuning by pump shaft speed control, dynamic pressure measurements at different locations of the system and qualitative flow visualization capabilities.

A semi-empirical model based on a combination of a Green's function solution for the one-dimensional acoustic boundary value problem and a decay function, corresponding to the break down of large vortex structures in the cascade of turbulence, was developed to separate pressure pulsations of acoustic and hydraulic nature.

Flow visualization in the acoustic near field around the pump's cut-water region was correlated with the acoustic pressure pulsations. A study, parametric in Helmholtz number, relative pump flow rate and cut-water tip radius, was conducted.

Results pertain to the acoustic behaviour of a pump in a piping system:

The pump acts primarily as a pressure source that may be acoustically reflective or transparent depending on the prevailing flow conditions. The near field shows pulsing flow separation which occurs on either side of the cut-water depending on relative flow rate. For cut-water geometries with a clear separation point (sharp tip), a strong sound generation dependence on the relative flow is displayed. A well defined point of flow separation at the cut-water tip leads to the largest separation region and also the largest acoustic pressure pulsations. Rounding the cut-water has the effect to permit motion of the stagnation point, thereby reducing the size of the separation region as well as the acoustic pressure pulsations. Clearly, the geometrical details of the cut-water region play a significant role for sound generation without obvious changes in hydraulic performance.

To

my mother, Ilka,

who gave me the freedom,

my sister, Sylvia,

who let me be responsible,

my wife, Ula,

who anchors my world,

and my children, Josephine and Sebastian,

who share their learning and growing with me.

ACKNOWLEDGEMENT

The persistent and intelligent critique and the academic and financial support provided by my supervisor has greatly contributed to this work and is gratefully acknowledged. - Thank You Dr. Weaver.

My supervisory committee Professors Round, Wood and Hartlen have helped this research through their open ears and minds.

For linking this research to the industry I thank Drs. Hartlen and Rzentkowski, whose technical expertise and great availability were invaluable.

The financial support of Ontario Hydro Technologies, the CANDU Owners Group, Atomic Energy of Canada Limited and the province of Ontario was also appreciated.

Thanks go to the staff of the mechanical engineering department for their tireless attempt to make things work.

For grammatically correcting the manuscript I am obliged to Anthony Black.

Finally, the students of the Flow Induced Vibration research group and of the department deserve recognition for creating a friendly, productive atmosphere of scholarship and academic aspiration.

TABLE OF CONTENTS

LIST OF FIGURES AND TABLES

NOMENCLATURE

Symbols

A	cross sectional area	$[m^2]$
b	impeller width	[m, mm]
B	stagnation enthalpy	$[m^2/s^2]$
c	speed of sound	[m/s]
c^*	speed of sound in infinite space	[m/s]
D	diameter	[m, mm]
D_2	impeller tip diameter	[m, mm]
e	pipe wall thickness	[m, mm]
	Euler number, 2.71	
E	elastic bulk modulus	[Pa]
	Young's modulus of elasticity	[Pa]
f	frequency	$[s^{-1}$, Hz]
$f_{ac,n}$	acoustic natural frequency	$[s^{-1}$, Hz]
f_{BP}	blade passing frequency	$[s^{-1}$, Hz]
f_r	frequency ratio	$[f_r = f/f_n]$
F	force	[N]
	dipole strength	$[m^4/s]$
g	solution function	
g_v	vortex growth rate	[m/s]
G	Green's function	
H	admittance	
He	Helmholtz number	$[He = L/\lambda]$
I	sound intensity	$[W/m^2]$
k	decay rate	
Ma	Mach number	$[Ma = v/c]$
Ma_v	vortex Mach number	$[Ma_v = g_v/c]$
n	shaft speed	[rpm]
	integer number	
n_B	number of impeller blades	
n_c	number of cycles	
n_s	specific speed	$[n_s = \omega Q^{1/2} / (g H)^{3/4}]$
p	pressure	[Pa, mbar]
P	power	[W, kW]
q	flow vector: q_1, q_2	$[m^3/s]$
Q	flow rate	$[m^3/s$, l/s]
	monopole strength	$[m^4/s]$
r	radius	[m, mm]
R	residual	
	crosscorrelation	
R_T	cut-water tip radius	[m, mm]
Re	Reynolds number	$[Re = u\ D/\nu]$
S	specific entropy	[kJ/(kg K)]

St	Strouhal number	[St = f D/u]
t	time	[s]
T	temperature	[K,°C]
	period	[s, ms]
T_R	reflection time	[s, ms]
$T_{11}..T_{22}$	elements of transfer matrix	
T_{ij}	Lighthill stress tensor	[N/m²]
u	(tangential) velocity	[m/s]
u_T	tangential impeller tip speed	[m/s]
v	velocity	[m/s]
V	volume	[m³]
x	coordinate	[m]
	observation	
y	spatial location	[m]
Z_0	charcteristic impedance	[kg/(m⁴ s)]
$\Box$	wave operator	
α	proportional to	
α_v	tongue angle of casing	
γ	volumetric gas portion	
δ	Dirac delta	
δ_{ij}	Kronecker delta	
Δ	difference	
λ	wave length	[m]
Γ	circulation	[m²/s]
ν	kinematic viscosity	[m²/s]
∇	Nabla operator	
π	circle constant	
ϕ	perimetral volute angle	[rad]
	flow potential function	
Φ	flow coefficient	[$\Phi = Q / (\omega D_2^2 b)$]
Ψ	head coefficient	[$\Psi = \Delta p / (1/2\ \rho\ u_T^2)$]
ρ	fluid density	[kg/m³]
θ	angle	
ω	vorticity	[1/s]
	shaft speed	[rad/s]

Subscripts and Superscripts

0	steady state
1	impeller inlet
2	impeller exit
3	casing
ac	acoustic
BEP	best efficiency point
Fl	fluid
gas	gas
hyd	hydraulic
i	at location i
	coordinate i
ij	from point i to point j
M	model
	mixture

n	natural
p	pump
'	fluctuating
^	peak

Abbreviations

AECL	Atomic Energy of Canada Limited
ALT	Anechoic Liquid Termination
b.c.	boundary condition
BEP	Best Efficiency Point
BPF	Blade Passing Frequency
CANDU	CANadian Deuterium Uranium reactor
CJC	Cold Junction Compensation
COG	CANDU Owners Group
FFT	Fast Fourier Transformation
FIV	Flow Induced Vibration
LDV	Laser Doppler Velocimetry
NPSH	Net Positive Suction Head
OHT	Ontario Hydro Technologies
PC	Personal Computer
PHT	Primary Heat Transport
PIV	Particle Image Velocimetry
TTL	Transistor Transistor Logic

CHAPTER 1: INTRODUCTION

"Do you really believe that the sciences
would ever have originated and grown
if the way had not been prepared
by magicians, alchemists, astrologers and witches
whose promises and pretentions first
had to create a thirst, a hunger, a taste
for hidden and forbidden powers?"
Friedrich Wilhelm Nietzsche, 1887

Turbo pumps are generally employed to convert the mechanical energy of a rotating shaft into potential energy of a fluid. In other words, pumps move the fluid against friction or a gravity potential. In all centrifugal pumps the process of adding potential energy to the fluid - the desirable aspect of the energy conversion - is accompanied by an introduction of pressure pulsations into this same fluid. These pulsations are mostly undesirable and are the object of the present investigation, an investigation centring on fluid borne as opposed to air borne noise, however important the latter may be under the noise pollution aspect.

The typical pressure frequency spectrum of a centrifugal pump is dominated by peaks at the Blade Pass Frequency (BPF), the harmonics of which stand out against a turbulent background noise that only rises to significant values at frequencies typically below the shaft speed. Figure

1.1 depicts such a typical spectrum where the abscissa shows a frequency normalized by the pump speed and the ordinate represents the pressure pulsations normalized by the stagnation pressure at the pump impeller's tip.

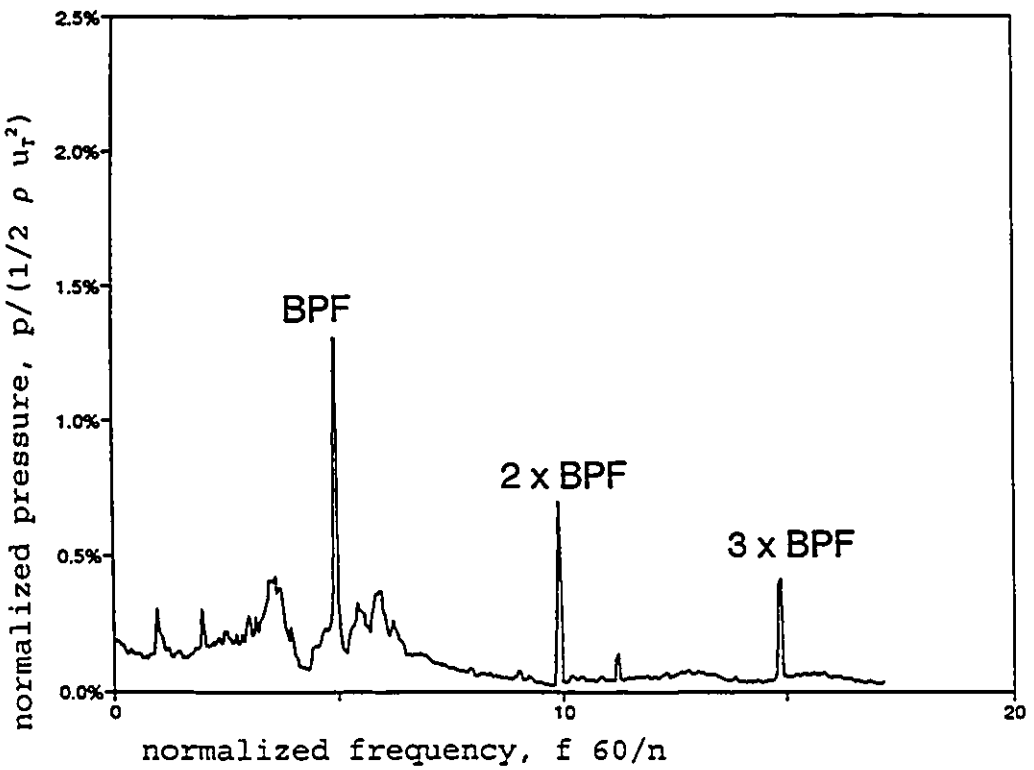

Figure 1.1: Pressure Spectrum of a 5 Vaned Volute Pump

The peaks in this spectrum occur mainly at integer multiples of five, of the BPF (which is the shaft speed times the number of impeller vanes for a volute pump, times the number of diffuser vanes in the case of a diffuser pump). This frequency represents the impeller's jet/wake flow interacting with the stationary cut-water of the pump volute. A minor peak exists due to impeller asymmetry at 1, the shaft speed itself.

From the point of view of structural discrete frequency

excitation in the connected circuit, which can sometimes cause dangerous vibration or costly component failure, the fundamental BPF and higher harmonics are of special interest. Therefore, this research focuses on the pressure pulsations at BPF only.

1.1 Motivation for Research

The need for understanding and possibly reducing pressure pulsations that originate from centrifugal pumps is a generic problem and deserves serious attention. However, to demonstrate that the conducted research is not only of academic interest, but also constitutes a contribution to technology, the example of the nuclear power generation station in Darlington, Ontario, Canada, a station of the CANadian Deuterium Uranium (CANDU) type, will be briefly summarized.

A generating unit at Darlington of the type shown in figure 1.2 is rated at 880 MW power output at the steam turbine. The primary tube side of the tube-and-shell steam generator is operated with radioactive heavy water (deuterium) at elevated system temperatures and pressures, clearly a hostile environment that does not allow easy access or tolerate easily intricate maintenance operations.

The Primary Heat Transport (PHT) pump requires about

a...calandria
b...pressure tubes
c...fuel
m...PHT pump
A...moderator
(deuterium)
B...helium
C...primary coolant
(deuterium)
D...secondary coolant
(water)

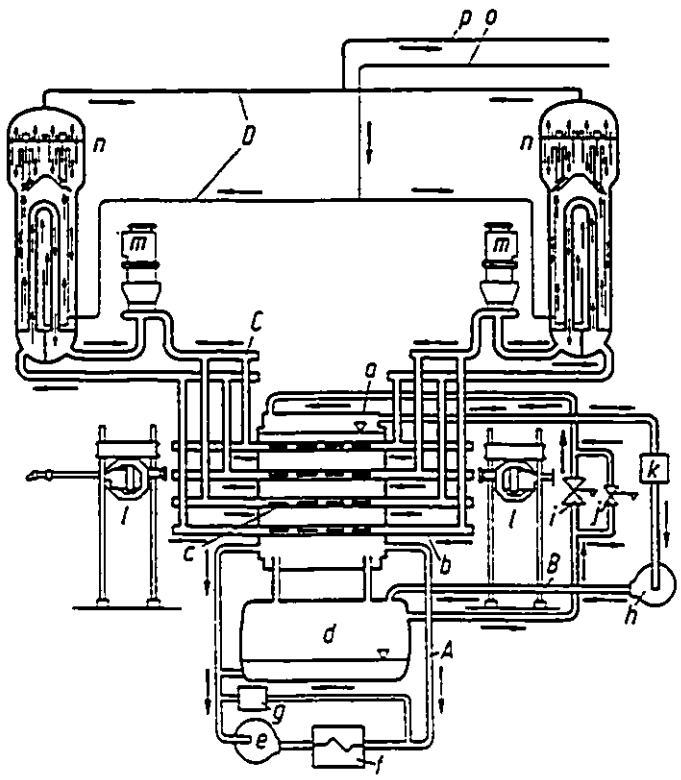

Figure 1.2: Schematic of a CANDU Nuclear Power Generation Station

10MW shaft power for constant speed operation. At these power levels it can be expected that even small fractions of the power are capable of harming or damaging structural components in the circuit by forced vibration or under resonance conditions.

Table 1.1 shows the case history of one of the Darlington units. The breakage of the fuel end-plates was attributed to acoustic excitation by the PHT pump which resulted in fatigue cracks that led to a failure to refuel the pressure tubes of the calandria and ultimately of a shut down of the unit for nearly one year.

Table 1.1: Case History Darlington CANDU Reactor, Unit 2

July to November 1990:
Operation at 100% Power Level
November 1990:
Refuelling of Channel N12 Fails
December 1990:
Unit Shutdown
January 1991:
Brief Restart, than Again Shut Down
Video Inspection of Pressure Tubes Shows Fuel End Plate Cracking and Fretting Wear on Tubes and Pressure Pads due to
► **Acoustic Excitation** by PHT Pump ◄
Remedied by Impeller Change from 5 to 7 Vanes
September 1991:
Start at 30% Power Level
Since November 1991:
Operation at 100% Power Level

The urgency for a fix can easily be seen by the large monetary loss suffered in not selling the expected electricity of approximately Can$ 2 M. per day. A fix was obtained through mismatching the pump BPF by changing the number of impeller blades from five to seven. This fix probably worked due to the absence of a natural acoustic frequency with a low enough acoustic damping-equivalent in the close neighbourhood of the new BPF. However, this success should not lead us to the false conclusion that the problem has been solved in a fundamental sense or would be accessible to a priori assessment of expected pressure levels. Some tube fretting still occurs and is the object of ongoing investigation.

1.2 Outline of Research Work

As a consequence of the previous section the objectives of this research are to investigate for a centrifugal pump:

- Mechanisms of Sound Generation
- Pump-Pipeline Acoustic Interaction
- Cut-Water Geometry Dependence of Sound Levels

in order to develop better understanding of the phenomena and devise possible design recommendations to reduce pressure fluctuations at BPF.

In order to follow the specific steps and methodology of this research it is imperative to understand the following concepts.

First, a clear understanding of the phenomena of noise and "pseudo-noise" is necessary to separate the two because, while a superposition of both types of pressure pulsations is measured close to the sound source, only the real acoustic noise is of practical importance in the far field away from the source.

The key in making such a distinction lies in the spatial distribution of pressure pulsations measured at different locations in a given domain. The acoustic excitation renders a spatial distribution governed by the wave equation and the corresponding boundary conditions resulting in the possibility of a Green's function description. The hydraulic part typically decays exponentially due to the breakdown of

Table 1.2: Acoustic vs. Hydraulic Pressure Pulsation

Acoustic	**Hydraulic**
Noise	Pseudo Noise
<u>Fluid Mechanics of Generation</u>	
Compressible	Incompressible
<u>Propagation</u>	
Speed of Sound	Mean Flow Velocity
<u>Attenuation</u>	
Long Sustaining	Fast Decaying
<u>Spatial Distribution</u>	
Wave Pattern	Decay Function

larger eddy structures into smaller ones and ultimately into broad band turbulence.

Hydraulic pressure fluctuations are seen as momentum (discrete eddies) but also produce sound. Altering the far field acoustic fluctuations can be accomplished by modifying the near field fluid mechanics, i.e. the interaction of the discrete eddies with the flow, which generates the sound.

The pump and piping system is characterized by its acoustic natural frequencies and the corresponding spatially dependent admittance function. Therefore, depending on the frequency ratio between BPF and acoustic natural frequency of the system, the acoustic damping, and the location of measurement the measured spectrum (figure 1.3), can look very different in spite of measurement at identical pump shaft speeds and flow rates.

Consequently, a careful recording not only of pump

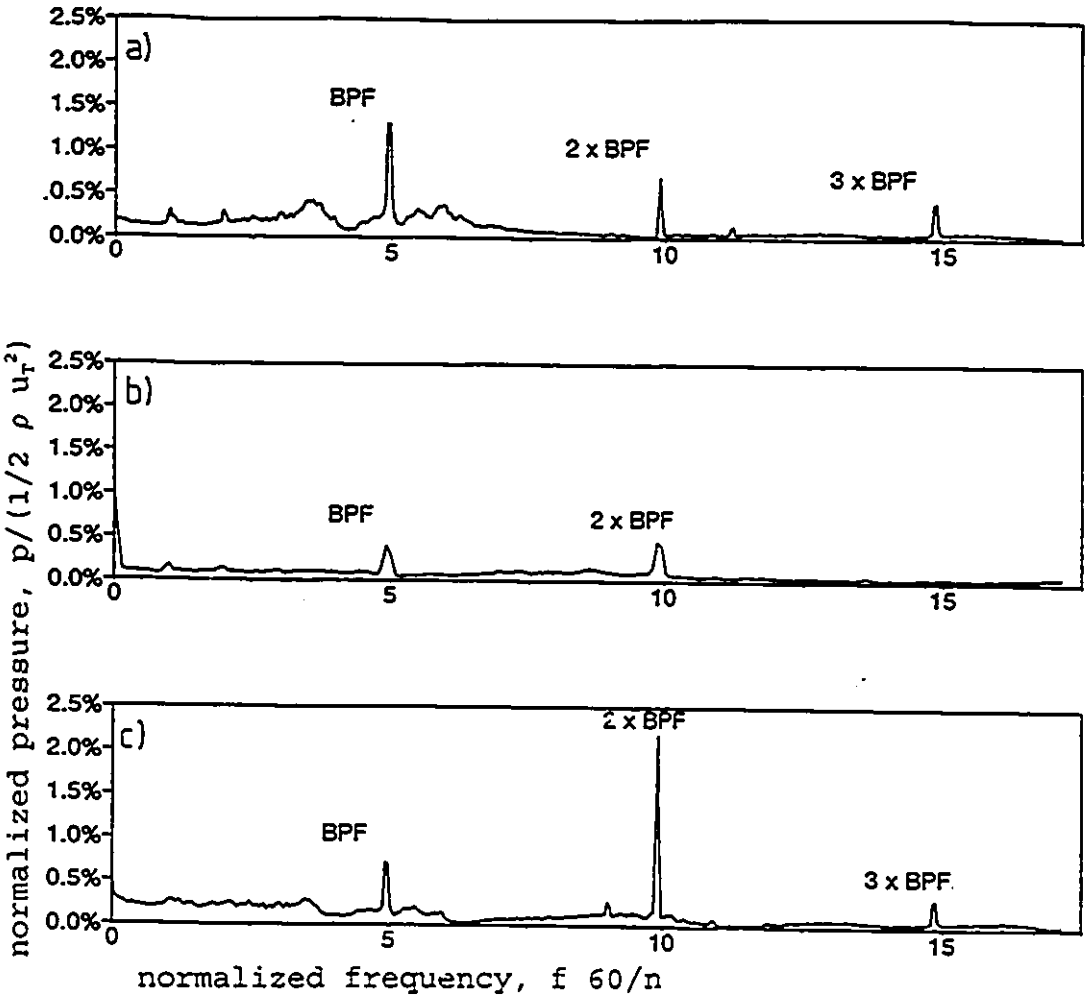

Figure 1.3: Pressure Spectra of Pump: a) Reference Spectrum, b) System with 1.6 Times Acoustic Natural Frequency, c) Measurement Location Changed

operating parameters, but also of the system characteristics is necessary to make measurements comparable.

Though all of the foregoing finds explanation in close analogy to the concepts of forced mechanical vibration, the present research investigates the distinct possibility for a self-excited phenomenon as suggested by Hartlen [123].

The free shear layer that separates at a clear point of

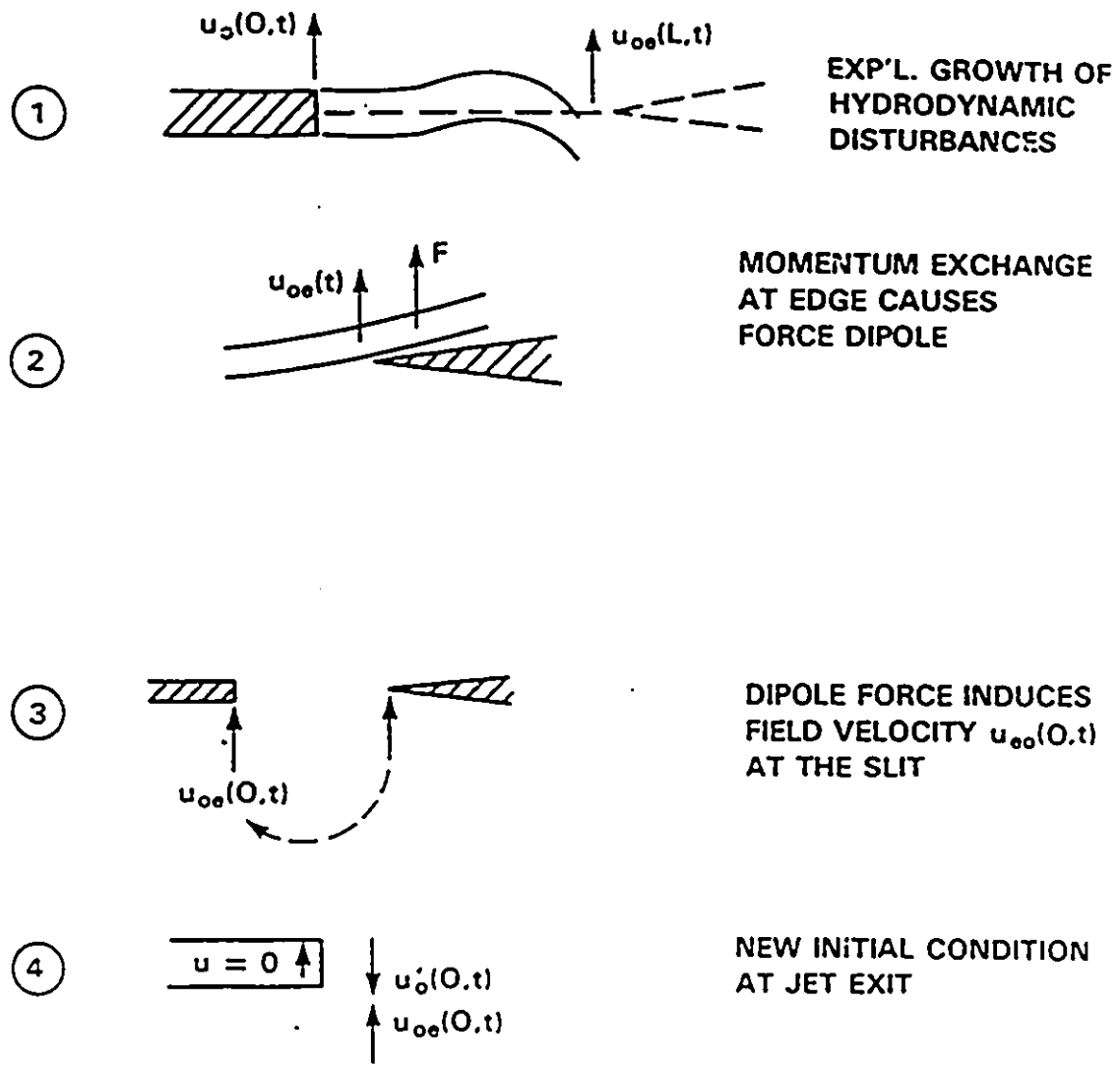

Figure 1.4: Mechanism of Self-Excitation, from Blake and Powell [64]

separation from the solid boundary extracts energy from the mean flow as it grows exponentially (1). The impingement on the downstream wedge (2) creates an acoustic signal that propagates back (3) to the separation point. This signal provides a new initial condition for the shear flow (4) at the separation point that is enhancing for the correct phase.

We know that the cut-water tip in the pump flow provides a point of separation. Further, we can speculate that a flow field exists where vorticity travels transversely to mean stream lines which produces an acoustic signal. Now, the further assertion that an acoustic feedback from the piping system would modify the acoustic near field around the cut-water appears possible.

Identification of this mechanism can, therefore, be twofold: First, a resonant amplitude of acoustic pressure fluctuations beyond the level expected from acoustic damping, and second, a modification of local fluid mechanics in the sound generating region around the cut-water of the pump would be evidence that self-excitation is a significant phenomenon in the acoustic excitation by a pump.

After this brief introduction to the important concepts an outline of the work presented is as follows: Chapter 2 summarizes the literature relevant for this research while chapter 3 portrays the experimental apparatus used. The methodology of separating acoustic from hydraulic pressure pulsations is described in chapter 4. The acoustic properties of the system as well as parametric trends of the acoustic component of pressure pulsation for hydraulic operating point and geometry are identified in chapter 5. Chapter 6 deals with the matter of self-excitation and the flow field inside the pump. Finally, chapter 7 concludes the work and gives recommendations for future research.

CHAPTER 2: LITERATURE REVIEW

"Ignorance is ignorance, no right to believe that anything can be derived from it."
Sigmund Freud, 1917

At the outset of this research, the literature on pump acoustics and, in particular, on sound generation and interaction of the sound source-piping system was rather scarce. The few last years have seen a substantial increase in the published literature on the sound generation by centrifugal pumps, but the subject of the interaction between local fluid mechanics in the pump and acoustic feedback has remained untouched. Some confusion of hydraulic pressure pulsations with acoustic pressure pulsations seems to remain and no attempt to carefully distinguish between the two has been reported.

However scarce the literature dealing specifically with the problem tackled in the present research may be, there exists a rich basis of related publications. This chapter will start with the field of classical acoustics in its application to pipeline acoustics, followed by a summary of sound generation models. The literature on pump flow fields will then be summarized. Finally, a section on the state of knowledge on the acoustics of centrifugal pumps, including

some attempts at theoretical formulations, experimental findings and design measures, will be presented.

2.1 Pipeline Acoustics

The field of classical acoustics is an old and rather well understood field of scholarship. This chapter is devoted to providing the basic acoustic equations derived from fluid mechanics with a view to explaining the acoustics of ducts and pipelines. The summarized knowledge can typically be found in texts such as [2, 4, 24, 53 or 117].

To derive the acoustic wave equation from general fluid mechanics, the underlying assumptions need to be understood. The governing equations are, in the most general case, the compressible form of the Navier-Stokes equations and the continuity equation.

The first important simplification which results from observation of sound propagation is that viscous losses are of negligible influence. The characteristic Reynolds number of sound propagation is formed with the speed of sound (in water about 1450 m/s) as a typical velocity and the wave length (at BPF of about 100 Hz) as a typical length scale:

$$Re = \frac{uD}{\nu} = \frac{c\lambda}{\nu} = \frac{c^2}{BPF\nu} \approx 2\times10^{10} \tag{2.1}$$

The symbol c stands for the speed of sound, f for the frequency of the sound wave and ν for the kinematic viscosity of the fluid.

The enormous magnitude of the Reynolds number encourages the assumption that viscous action is negligible compared to inertial. Because both viscous and compressible terms in the Navier-Stokes equation are multiplied by the now vanishing viscosity this equation reduces to the Euler equation (without body forces):

$$\rho\left(\frac{\partial\bar{v}}{\partial t}+(\bar{v}\nabla)\,\bar{v}\right)=\nabla p \qquad (2.2)$$

Here ρ denotes the fluid density, $\bar{v}$ the velocity vector (u,v,w), t the time, ∇ the Nabla operator ($\partial/\partial x$, $\partial/\partial y$, $\partial/\partial z$) and p the pressure.

A second important assumption is that the order of acoustic pressure fluctuations is small enough to allow for linearization of the governing equations. This ensures that sound fields can be superimposed without being distorted which again agrees well with observation. Because of linearity in the governing equation the physical quantities are related linearly as well. This is of particular importance for the relation between acoustic pressure p′ and density fluctuation

$$p'=c^2\rho' \qquad (2.3)$$

Here the ′ stands for the fluctuating, acoustic component of a quantity.

The linearized Euler equation with neglected second order terms is:

$$\rho_0 \frac{\partial \vec{v}}{\partial t} + \nabla p' = 0 \tag{2.4}$$

Here the subscript ρ_0 means the steady state part of the density

By linearization, the compressible continuity equation becomes:

$$\frac{\partial \rho'}{\partial t} + \rho_0 \nabla \vec{v} = 0 \tag{2.5}$$

Finally the wave equation is obtained if the partial time derivative of the continuity equation is subtracted from the Euler equation on which the Nabla operator was applied and the relation between pressure and density fluctuation is inserted:

$$\frac{\partial^2 p'}{\partial t^2} - c^2 \nabla^2 p' = \Box p' = 0 \tag{2.6}$$

The square $\Box$ denotes the wave operator $\partial^2/\partial t^2 - c^2 \nabla^2$.

The solution to the one-dimensional linear wave equation, where the wave operator assumes the form $\partial^2/\partial t^2 - c^2 \partial^2/\partial x^2$, has the general form:

$$p(x,t) = f_1(x-ct) + f_2(x+ct) \tag{2.7}$$

This solution contains only functions of the argument x - ct (x + ct) which represent a wave of the form f_1 (f_2) travelling

with unchanged shape in positive (negative) x-direction.

The field of duct or pipeline acoustics is concerned with sound propagation, transmission and reflection in piping systems where the sound field is mainly one-dimensional. This is the case for sound of wave lengths large compared to the pipe diameter. For the present research this can certainly be ensured by a wave length (about 14.5 m) to pipe diameter (0.075 m) ratio of 200. Therefore, two- and three-dimensional acoustic modes are virtually non-existent in the piping system.

In determining the pattern of an acoustic standing wave in a pipe loop, the influential parameters are length and acoustic boundary conditions (b.c.) of the pipe. The idea of b.c.'s can better be captured by the notion of a spatial change of characteristic impedance Z_0 along the line.

$$Z_0 = \frac{\rho c}{A} \tag{2.8}$$

Any change of cross-sectional area A, wave speed c (most likely by change of pipe material and/or wall thickness) or density of the fluid ρ will change the impedance Z_0 and induce a part of the wave into being reflected and a part into being transmitted. The superposition of all travelling waves constitutes the acoustic standing wave pattern.

In a three-dimensional domain, with a known sound source located in a compact region where the wave equation is

non-homogeneous, the sound source reduces. If it assumes the form of a point monopole source of source strength Q with the mathematical description

$$q(\vec{x},t)=Q(t)\,\delta(\vec{x}) \tag{2.9}$$

the solution in the region where the wave equation is homogeneous, or the sound field, is

$$p'(\vec{x},t)=\frac{Q(t-|\vec{x}|/c)}{4\pi|\vec{x}|} \tag{2.10}$$

Opposed to that, a point dipole source of the form:

$$q(\vec{x},t)=-\nabla\vec{f}(\vec{x},t) \tag{2.11}$$

has the sound field

$$p'(\vec{x},t)=-\frac{\partial}{\partial x_i}\left[\frac{F_i(t-r/c)}{4\pi r}\right] \tag{2.12}$$

In the more revealing cylindrical form it is

$$p'(r,\theta,t)=\frac{\cos\theta}{4\pi}\left[\frac{1}{cr}\frac{\partial F}{\partial t}+\frac{F}{r^2}\right] \tag{2.13}$$

Physical representation of a monopole can be thought to be a pulsing sphere and a dipole to be a body oscillating along a linear degree of freedom..

Two aspects of the dipole field as opposed to the monopole field should be pointed out. First, the directivity of the dipole field is contained in the cosine term and results in a maximum sound pressure in the direction of the dipole axis and complete cancellation at 90° to it. And

second, a distinction of a near field (F/r^2) and a far field is present. The near field takes account of the lower effectiveness of two monopoles approaching each other (the dipole) because of local cancellation of sound radiation. It contains pressure pulsations that will not propagate outside of the compact region but are only locally important or of a rather hydraulic nature.

In the one-dimensional framework the monopole type of source will produce pressures up and downstream of the source that are in phase. For the case of a dipole source these pressure pulsations are out of phase. The monopole or pressure source will hence produce a pressure antinode at the source location while a pressure node will coincide with a dipole source.

2.2 Sound Generation

This section on sound generation is subdivided into a brief review of the field of aeroacoustics and a very selective section on self-excitation of flow tones.

2.2.1 Theories of Sound Generation

Aeroacoustics is the science investigating sound production by flows, a discipline that was historically first concerned with air-borne noise from jet engines. Meanwhile the term "hydroacoustics", sound in water, is used similarly for sound produced by water flows.

Aeroacoustics is a relatively new science. Lighthill [3,5] developed an approach of acoustic analogy to describe the aerodynamic sound generation in the early 1950's with the main purpose of predicting the noise from aircraft jet engines. Since then many researchers have built upon his theory. This chapter will extract the significant features of Lighthill's theory in the context of our research, as well as subsequent additions by other researchers.

Lighthill's acoustic analogy is based on a comparison of the earlier derived acoustic wave equation with the complete flow field. A description of the flow field in Einstein summation convention is given by the continuity equation:

$$\frac{\partial \rho}{\partial t} + \frac{\partial (\rho v_i)}{\partial x_i} = 0 \tag{2.14}$$

and the momentum equation:

$$\frac{\partial (\rho v_i)}{\partial t} + \frac{\partial}{\partial x_j}(p_{ij} + \rho v_i v_j) = 0 \tag{2.15}$$

The stress tensor p_{ij} consists of the pressure (normal stresses) on the main diagonal and the shear stresses τ_{ij} of compressible flow:

$$p_{ij}=p^{*}\delta_{ij}-\tau_{ij} \tag{2.16}$$

Here δ_{ij} denotes the Kronecker Delta operator.

A similar mathematical transformation as used above in the case of the wave equation leads to the equation:

$$\frac{\partial^2\rho}{\partial t^2}=\frac{\partial^2}{\partial x_i\partial x_j}(p_{ij}+\rho v_i v_j) \tag{2.17}$$

Subtracting from both sides the term:

$$c^2\nabla^2\rho=c^2\frac{\partial^2}{\partial x_i\partial x_j}\rho\delta_{ij} \tag{2.18}$$

leads to the equation:

$$\frac{\partial^2\rho}{\partial t^2}-c^2\nabla^2\rho=\frac{\partial^2}{\partial x_i\partial x_j}T_{ij} \tag{2.19}$$

where the Lighthill stress tensor T_{ij} is defined as:

$$T_{ij}=p_{ij}+\rho v_i v_j-c^2\rho\delta_{ij} \tag{2.20}$$

The Lighthill stress tensor contains the Reynolds stresses that quantifies the turbulent shear stresses.

The equivalent source term is of quadrupole type with a flow field ρ:

$$\rho=\frac{\partial}{\partial x_i\partial x_j}\int_V\frac{T_{ij}(\bar{y},t-t/c)}{4\pi c^2 r}d^3\bar{y} \tag{2.21}$$

It should be noted that Lighthill's equation was derived without any simplifications to the governing equations but only by equivalent transformations. This stands opposed to the derivation of the wave equation where major assumptions were introduced. For this reason Lighthill's theory is called an analogy. The resulting equation has the appearance of a wave equation with a quadrupole source term on the right hand side. The denomination of the right hand side as a source term includes the requirement that it is non-zero in a compact source region and zero in the sound field where sound is merely propagated.

As a matter of fact the Lighthill equation is a rearranged form of the Navier-Stokes and continuity equations. This means that in order to predict the sound field the complete non-linear equation needs to be solved inside the source region. Even approximately, this task can only be accomplished for flow fields of a particularly simple nature.

Curle [6] extended Lighthill's theory to incorporate the influence of solid boundaries. An interesting finding is that besides reflecting and diffracting sound waves the solid walls change the source term from the quadrupole to the more efficient dipole type.

While Curle provided a solution in terms of an order of magnitude analysis, Doak [9] gives a solution in terms of

Green's functions for the sound field of turbulent flow containing arbitrary shaped foreign bodies submersed in it. Doak extends Curle's work in providing a proof of the assumption that all dipole radiation comes from a surface distribution of dipoles on the submersed bodies.

The theory for boundary layer noise is further developed by Ffowcs-Williams [14], Meecham [15] and Ffwocs-Williams and Hawkins [26]. The latter contribution included moving surfaces as sound sources.

Summarizing the work up to mid the 1960's, the prediction methodology was particularly successful for turbulent noise levels in sound fields produced by flows that display a clearly distinguishable compact source region.

A major step in relating a given flow field to its sound radiation was achieved by Powell [16]. The statement that "vorticity induces the whole flow field, of which the acoustic field is an integral part" means that the sound field produced by slightly compressible flow can be determined from the vortex motion of the corresponding incompressible one. This is a slightly different approach than Lighthill's but yields consistent results for model cases treated by either theory.

Flow sound is calculated by comparing the

incompressible velocity field of a closed vortex loop with that due to a uniform dipole distribution. The result is that those fields are identical where the constant circulation of the vortex is identical to the strength of an equivalent point dipole:

$$Q=\Gamma\int_A d^2\bar{y} \tag{2.22}$$

The hydrodynamic near field of a slightly compressible flow will be almost identical to that of the corresponding incompressible flow. The far field or sound radiation which essentially relies on compressible effects will be determined by changes in the vortex strength either by area or circulation changes:

$$p'\propto\frac{d^2(\Gamma A)}{dt^2} \tag{2.23}$$

Lighthill's theory undergoes a useful reformulation by Howe [33] in terms of the stagnation enthalpy. He considers this physical quantity to be the natural one for the formulation of the acoustic analogy. It is defined as an extension of the Bernoulli integral:

$$B=\int\frac{1}{\rho}dp+\int TdS+\frac{1}{2}u^2 \tag{2.24}$$

with T being the temperature and S the entropy.

Howe overcomes difficulties that existed in the

presence of extensive non-acoustic, non-uniform mean flow at low Mach number. He also provides analytical tools in the form of free space Green's functions for solving his convected wave equation.

Howe further develops Powell's vortex sound theory by applying it to the sound field of a turbulent discrete vortex which leads to an equation of the form:

$$\frac{\partial^2 \rho}{\partial t^2} - c^2 \nabla^2 \rho = \rho_0 \nabla (\vec{\omega} \times \vec{v}) \tag{2.25}$$

In this equation the source term on the right hand side is determined, as Powell suggested, by the incompressible flow independent of the (weak) compressibility of the fluid. The vector product will exist for motion of the vortex that is not parallel to the mean flow velocity. The acoustic source strength is proportional to the rate at which the vorticity cuts across the flow field.

An elucidating physical interpretation of the equation can be given for a vortex travelling around the edge of a rigid semi-infinite plate. In that case the instantaneous sound pressure level is "proportional to the rate at which the vortex cuts across the hypothetical field of [...] streamlines which describes irrotational flow [...around this flat plate.]"

Texts on this subject matter were published by

Goldstein [37] in 1976 and Comte-Bellot and Ffowcs-Williams [65] in 1986 and a useful paper review was published by Mueller [41] in 1979.

2.2.2 Flow Tones and Self-Excitation

The important topic of free shear layer mechanics will be covered here to illustrate the relation between impinging shear layers and the resulting acoustics. These kinds of flow phenomena can be encountered in the flow field around the cut water of a centrifugal pump in a more complex form but with common features preserved.

Rockwell and Naudascher [42] explain very clearly the phenomena involved in self-sustained oscillations of impinging shear layers in their review paper. The phenomena involved are common to all self-excited flow tones: An unstable free shear layer is produced. Unstable implies that an amplification of the shed vorticity fluctuation takes place as it is convected downstream. The vortex impinges on a downstream surface where an acoustic disturbance is generated. The disturbance propagates upstream to the sensitive region of flow separation where it organizes the process of vorticity generation into discrete vortices.

From the description of the mechanism it is obvious

that there are limits to the distance between the region of separation or vorticity generation and the impingement zone or acoustic source region. The lower limit is imposed by the time the disturbance needs to travel upstream, the wave speed of the medium. The associated time must produce exactly the right phase relation to enhance the shedding of vortices at the separation point. The upper limit is imposed by the requirement that coherent vortices need to arrive at the impingement surface in order to produce a discrete frequency disturbance. This is, of course, no longer the case if the initially discrete vortex experiences a breakdown in the turbulence cascade, and hence, constitutes a random signal as it arrives. So only for well matched fluid properties and geometry can a flow oscillation sustain itself. Various models for predicting such oscillations are discussed.

Two companion publications by Nelson, Halliwell and Doak [50,54] constitute an excellent investigation of two-dimensional flow in the mouth of a Helmholtz resonator excited by grazing flow. An experimental and analytical treatment of the flow-acoustic interaction for a flow excited resonance is presented. A theory is developed that divides the flow field into a reciprocating acoustic potential part which is superimposed to the vortically induced flow of the shear layer across the resonator neck. It is shown that the only term that can account for the feeding of energy from the mean flow field

into the acoustic far field is a coriolis term of the form:

$$2\overline{\omega}\times\nabla\phi' \tag{2.26}$$

This vector product involves the mean vorticity of the vortical flow and the fluctuating velocity of the potential flow.

Assuming the Kutta condition at the upstream edge to be fulfilled, the theory shows the convection speed of a discrete vortex, shed at the upstream edge, to accelerate towards the downstream impingement edge. Flow visualization and laser velocimetry confirm this acceleration of the vortex convection. Interpretation of that observation in the context of Powell's vortex sound and Howe's theory is consistent with Rockwell and Naudascher's explanation that the downstream region plays the most important role in terms of sound generation.

A comprehensive review of self-excitation and flow tones is given by Blake and Powell [64] in 1986.

2.3 Flow Field in Centrifugal Pumps

Investigations of the flow field inside centrifugal turbomachinery has a long history. However, only in recent years with the advent of modern experimental techniques, in particular Particle Image Velocimetry (PIV) and Laser-Doppler Velocimetry (LDV), has reliable quantitative information been found in the literature.

Texts covering the basics of the subject are published by Lazarkiewicz and Troskolanski [18], Stepanoff [23], Karassik [69] and Lein [71] and the list is certainly not exhaustive.

Generally, the flow inside the impeller receives more attention because it is considered more important for the pump efficiency than the volute flow. For design purposes the assumption about the volute flow is one of steady state. Only the Best Efficiency operation Point (BEP) is taken into account for the design. However, it is acknowledged qualitatively that the flow actually is unsteady, especially at off-design operation. The contribution to the flow rate is assumed to come in equal parts from flow around the perimeter

$$Q_\phi = \frac{\phi}{360^\circ} Q \tag{2.27}$$

where ϕ is the angle around the volute measured from the cut-

water. This assumption results in the spiral casing design. For the radial velocity distribution two schools of thought exist. The one considers the circumferential velocity v_c and the other the angular momentum or v_c/r to be constant.

The angle of the volute tongue is designed according to the Euler velocity triangles of the impeller transformed into a stationary reference frame. The efficiency is reported not to depend to any significant extent on the tongue angle. This sums up the state of the art as reported in pump text books.

Dean and Senoo [10] provide, using hot wire measurements on an air compressor with vaneless diffusor, the experimental proof of the unsteadiness of the flow field inside the casing. Additionally, they establish the jet/wake phenomenon of the impeller outlet velocity. The term "jet" describes the increased radial velocity near the pressure side and the term "wake" describes a decreased velocity near the suction of the impeller blade in a reference frame rotating with the impeller. This is an observation of the circulation flow around the blade that produces the lift or the momentum on the impeller and more complex secondary impeller flows.

With radial thrust on the impeller in mind, Iversen, et al. [11] measure the static pressure in a water operated volute pump. Their success in relating casing wall pressures to fluid loading on the impeller - and taken one step further,

shaft vibrations - triggered a long line of investigations (Acosta, Arndt, Brennen, etc. [87,91,93,102,107]). These will not be described in more detail here because the principal thrust of this work is pump vibration.

Krain [49] reported experimental work with laser velocimeters applied to impeller-, vaned and vaneless diffuser-flows of centrifugal air compressors. The laser velocimetry permits investigation of the detailed velocity field non-intrusively.

Yuasa and Hinata [45] compared potential flow calculations with experimental data of a volute pump to predict the internal flow of the pump as well as the air-borne noise. Numerical predictions failed for fluctuating flow quantities while they were able to approximate averaged pressures along the casing wall quite well. This indicates that viscous effects play an important role in the development of the unsteady flow field.

Brownell, et al. [60] mark an important contribution to the understanding of the flow field around the cut-water. Their results were obtained by an experimental investigation of an industrial pump with characteristics and dimensions comparable to the pump of the present study. Findings include a relatively low sensitivity of the hydraulics to varying

shaft speed. However, significant differences in streakline patterns are found for a variation of flow rate and instantaneous impeller blade position. While operating at the design flow rate the stagnation point is located at the tip of the cut-water. The stagnation point moves to the discharge side for low flow rates and into the recirculation channel for high flow rates featuring a flow separation on the discharge side. Stagnation point variation is found to be particularly large for low flow rates but is not quantified.

Lorett and Gopalakrishnan [75] performed a numerical research on the two-dimensional interaction of impeller and casing flow. An important result of this work is to invalidate the classic assumption about the steadiness of the internal impeller flow. Their argument that this flow cannot be steady given that the impeller rotates in a non-axissymmetric casing is numerically confirmed. From their numerical model, it can be seen that only for operation at BEP does the flow receive contributions from along the perimeter evenly. Flow rates below BEP result in a smaller, flow rates above BEP in a larger flow contribution from the region around the cut-water.

Thomas, et al. [79] reported laser velocimetry experiments with a 32 forward facing blade impeller that ought to simulate the "mean" flow field of a moving impeller. By getting rid of the fluctuating velocity components, a steady

state reference data base is produced that serves as a benchmark for computational simulation. For the present purpose, the results do not provide any useful information because the sound generation is attributed exactly to those suppressed fluctuating components.

Hamkins and Flack [82] investigated, using the same test apparatus as Thomas, et al. [79], the influence of shrouds on the impeller flow. They experimented with shrouded and unshrouded impellers and mapped velocity at different flow rates and blade positions. Secondary flows in the unshrouded impellers are more differently developed than in a totally enclosed impeller vane passage.

Miner, et al. [99] reported results from experiments on a centrifugal volute pump, again mainly to determine the impeller flow. Findings on the flow regime around the volute tongue confirmed Brownell, et al.'s work [60] by showing an averaged stagnation point at flows below BEP on the discharge side of the tongue, moving with increasing flow rate to the tip at BEP and further to the recirculation side at flow beyond BEP. A dependence of the stagnation point on blade position at constant flow was generally given as +/- 6° angle.

Paone, et. al [100] introduce the powerful technique of Particle Image Velocimetry (PIV) to measurements of the flow

field in a centrifugal pump, this paper being mainly a publication on the methodology. Limitations were stated mainly to be in the computational power required. The technique basically allows for quantitative information about a two-dimensional slice (newer techniques even obtain three-dimensional information by using different coloured light sheets simultaneously) instantaneously through a whole flow field. The details of illumination, tracer particles, recording and postprocessing vary according to application and complete systems are nowadays available commercially.

Very detailed experimental results from quantitative flow visualization of the volute flow of a vaneless diffuser pump are found in a series of publications from Dong, Chu and Katz [114,115,118,119].

Some of the more important results are that the jet/wake phenomenon is confined to a region within 1.4 times the tip radius of the impeller blade. When an impeller blade lines up with the volute tongue the mean circumferential flow increases throughout the volute. The design assumption of constant v_c/r holds true within 5 - 10 %. The flow contribution around the impeller perimeter is not equal and the uneven distribution depends on the operating condition. And finally, the recirculating leakage at the tongue is recognized to strongly fluctuate with blade position and depend, as well, on operating condition. Personal

correspondence with the authors revealed that the motivation for their research is similar to ours. For this reason it can be expected that more interesting publications are yet to come.

A numerical parametric study was carried out by the author of this work [124] investigating the influence of different design parameters such as impeller speed, radius, vane length and width. Due to software and hardware limitations the study used a simplified impeller geometry with parallel vanes. It did not incorporate any turbulence model and secondary flows could not be represented. Given theses limitations, this control volume model showed that the single most important parameter for the asymmetry of the outlet profile is the width of the vane passage. This suggests a strong significance of the number of vanes for an otherwise unchanged impeller design. Besides lowering the BPF a lower number of vanes has the effect of creating a wider vane passage wit a more asymmetric velocity profile across the impeller outlet, the so called jet/wake phenomenon.

Croba, et al. [134] report close agreement of numerical results obtained by a finite volume computation with multi-domain overlapping grids with LDV measurements on a physical model everywhere except in the relevant cut-water region.

2.4 Pump Acoustics

2.4.1 Theories of Sound Generation in Pumps

The most prominent and often quoted publication on prediction of sound generated in a centrifugal pump is by Simpson, et al. [22]. A theory and its experimental confirmation for sound generated in a two-dimensional centrifugal volute or diffuser type pump is provided. The theory is based on a hydrodynamic rather than an acoustical approach. It considers a fluctuating blade circulation based on potential flow theory superimposed by the viscous flow of the impeller blade wake interacting with a simplified volute geometry. Experimental results for the blade frequency noise are reported to be conservatively over predicted by about 20dB (factor of 10 between pressure amplitudes). However, trends for parametric variation in flow rate (minimum noise level at about 120 % of best efficiency flow), impeller tip to cut-water clearance (minimum at 1.0") and pump shaft speed (noise level proportional to shaft speed squared) agree well between theory and experiment. Finally, an empirical correlation between the pump's specific speed its power level and the overall noise level at BEP was presented. Clearly, the work does not address the geometry of the cut-water which the author of this work recognized as a major factor in sound generation. The amplification in the acoustic system which

determines the experimental measurements used to compare results in Simpson, et al. [22] is also not reported. Therefore, while detecting useful trends, the theory is not considered advanced enough to allow for accurate predictions.

Blake [64] acknowledges the complicated interaction of rotor and casing in fan noise. Internal acoustics of fans are treated, particularly, for large machines. In comparison to water pumps an importance of internal acoustics is more common in fans because of the shorter wave lengths in air than in water. Blake states the basic proportionality between sound pressure and rotor tip speed squared. Further, a linearized model contains two unspecified functions. One of the functions is dependent on the blade harmonic number (frequency f over BPF), the Reynolds number and the flow rate of the fan. The other aeroacoustic coupling function is dependent on a tip speed determined Mach number, Reynolds number and flow rate. He references to noise control of fans [13,39,51] as dealt with in section 2.4.3 of this thesis.

Afonin and Novozhilov [126] propose a prediction method based on empirical factors, shaft speed, pump head and flow rate at BEP and a single length scale representing the size of the machine. Detailed sound generating mechanisms are not accounted for and thus need to be incorporated in the adjustable factors. It is not clear how this approach is

timely or stands even a chance of being successful for either the wide array of geometries in use or for the off-design operation.

Until the present time the theory put forward in Simpson, et al. [22] finds application. Jaremczak and Caignaert [139] transform geometry and hydraulic characteristic data into a two-dimensional domain to use the theory provided by [22]. The assumed transformation allows to reduce the initially large discrepancies with experimental data of up to 20 dB to more moderate levels of as little as 3dB. Obviously, in the design stage new geometries can not be assessed to this degree of accuracy because adjusting the transformation is then not possible.

Lee and Im [158] use the sound pressure predictions from [22] in an analytical model to formulate an acoustical pressure source (monopole) boundary condition of a model incorporating a Green's function solution for pressure distribution in a pressurized water reactor. Although claiming "good agreement", ratios between measured and predicted data range from 212 % to 32 %, i.e. predictions are neither reliable nor conservative.

The attempt until most recent times to continue using the theory of Simpson, et al. [22] after almost 30 years of proven deficiencies as a basis to predict sound pressure

levels of radial pumps provides a strong indicator of how complicated the actual subject is and how far away from an accurate prediction in the design stage we still are.

2.4.2 Experimental Findings on Pump-Pipeline Acoustics

While research on noise pollution by pumps appears rather common place, research specific to pump-pipe line acoustics is extremely sparse.

Chen [12] investigated fluid loading on impeller blades in a centrifugal diffuser pump. A theory was developed to minimize the negative interaction effects between impeller blades and guide vanes that take the pump internal wave patterns into account. This theory relies on the negligibility of higher order modes inside the casing and results in a recommendation for the number of impeller and diffuser blades.

Neise [34] laid the ground work for non-dimensional representation of experimental fan noise data. The formulation for the rms pressure in the duct depends on four scaling parameters:

the Mach number

$$Ma = u_T / c \tag{2.28}$$

with u_T being the tangential impeller tip speed and c the speed of sound propagation,

the Reynolds number

$$Re=\frac{u_T D_2}{\nu} \tag{2.29}$$

with D_2 being the outer impeller diameter and ν the fluid kinematic viscosity,

a form of Strouhal number

$$St=\frac{fD_2 \pi}{u_T n_B} (=f/f_{BP}) \tag{2.30}$$

with f being the frequency, n_B the number of blades and f_{BP} the BPF,

and the Helmholtz number

$$He=D_2 /\lambda \tag{2.31}$$

with λ being the wavelength.

In the application to fan noise the length scale for the Helmholtz number is chosen appropriately to be the fan diameter D_2. This is useful because compared to water pumps the wavelengths are about a factor 3 smaller due to the slower sound speed. Therefore, fan internal acoustics are important. In the present work the piping length L is thought to be a much more significant length scale to capture acoustic interaction.

Tourret et al. [61,62] reported work on pipe acoustics related to the pump as a source. The tested pump is of single stage type and corresponds to the French standard NFE 44 111. An Anechoic Liquid Termination (ALT, French patent number 8304560) in the suction and pressure pipe of the test apparatus is featured to eliminate standing wave patterns and allow only for waves travelling away from the pump. This removes the importance of transducer location and provides a frozen acoustic pressure signal travelling along the pipe, i.e. a direct (not amplified) measurement of the acoustic source term. Dynamic pressure measurements were taken in the normal and parallel directions along the volute and it was found that the level of pressure pulsation decreases with distance from the volute tongue where the pressure is a mixture of acoustic and hydrodynamic components. The energy of the measured frequency spectrum is concentrated below 1000 Hz, mainly at the BPF. Another interesting result is that while the time dependency of the pressure fluctuation is regularly harmonic at high flow rates it is quite irregular at low flow rates. This is explained by the influence of recirculation but could as well be attributed to local back flow in the impeller.

Saxena et. al. [78] investigated air-borne noise from a single-stage volute pump. The experimental parameters were operating condition, number of impeller blades, pump speed,

foundation of pump and the presence or absence of cavitation. Among their results is that at flow rates Q below BEP (Q = 50 % Q_{BEP}), the noise measurements peak and, at BEP, a minimum occurs.

Tourret and Bernard [80] expanded the concept of air-borne noise as representative for the acoustic power emitted by taking an overall acoustic energy balance of a hydraulic pump. By considering the sound emitted out of a control surface around the sound generating pump fluid-borne and structure-borne acoustic energy entered the picture.

Stirnemann et al. [84] analyzed pumping systems with respect to dynamic stability. A transfer matrix model for the passage of waves through the pump in a system was proposed:

$$[p_i, q_i] = \begin{bmatrix} T_{11} & T_{12} \\ T_{21} & T_{22} \end{bmatrix} \begin{bmatrix} p_{i-1} \\ q_{i-1} \end{bmatrix} \tag{3.1}$$

A major underlying assumption is that the transfer matrix can uniquely, independent of resonance condition of the system, describe a given pump. This is an assumption which the present research has to question since it would negate the presence of a modifying influence from the system. Further, the theory presented is only designed to model the pump as a passive component of the system, through which a wave is travelling, not as a source of such a wave. Even with these

limitations understood, the paper reports an error of up to 100 %, i.e. a difference between matrix components of one pump, but different pump location, at certain frequencies.

Further studies on the transfer matrix approach are given in the bibliography [103,111,128,129,137,142].

Zogg et al. [86] reported an investigation on air-borne noise of a range of single stage radial impeller pumps (two double volute and two single volute models). Measurements were taken at BEP. The smaller pumps and all pumps in a frequency range below 500 Hz were acoustically best represented as an acoustic dipole source as determined from far field measurement in the sound field. The largest pump, for frequencies higher than 500 Hz, is better represented as an acoustic monopole. This is only natural because with increasing frequencies the wavelengths decrease. Hence, the fixed location of the sound measurement the distance normalized by the wavelength increases, i.e. the location of measurement moves more into the far field of the source.

Bolleter [88] mainly investigated the optimization of diffuser to impeller blade number ratios in centrifugal diffuser pumps. The main source of pressure pulsations is identified to be the impeller wake interacting with the stationary diffuser blades. An increase in the gap between impeller tip and diffuser blades is reported to decrease the

pressure pulsations at BPF but is limited for hydraulic reasons to about 4 % for diffuser pumps and 6 to 13 % for volute pumps. Stronger occurrence of the higher harmonics of the BPF in the pressure spectra is also noted to be possible.

Gühlich and Bolleter [122] published a review of physical mechanisms causing pressure pulsations in centrifugal pumps and the design parameters influencing these pulsations. The mechanisms are classified into impeller wake phenomena and turbulence. They point out that what is a wake, a minimum of the velocity, in the rotating reference frame becomes a velocity peak by the transformation into the stationary frame, i.e. the vectorial addition of the impeller tip speed. The associated stagnation pressure is equal to $0.75\ \rho\ u_T^2$, where u_T is the impeller tip speed. Resulting from the impeller tongue (or diffuser) interaction, the pressure spectra show peaks at the blade passing frequency and its harmonics and, due to rotational non-symmetry, peaks occur at the rotational frequency and its harmonics. Of greater importance to the amplitudes than just the shed eddies themselves is their impingement on solid boundaries. These secondary sources introduced into the primary hydrodynamic near field act as stronger sources then the original primary sources. The turbulence provides a white noise background that is weak at BEP but increases at off-design conditions because of recirculation effects. Design parameters governing the pump

behaviour are the geometry of the impeller, especially the blade tips, and the volute. For the volute the most important aspect is the tongue shape. As the single most influential design parameter, the gap between volute tongue and impeller tip is recognized. This gap has, of course, a strong influence on the hydraulic performance of the pump, as well. Additionally, the system parameters influence the pressure pulsations measured. The system parameters discussed are the standing wave pattern in the pipe, the location of pressure measurement and the type of instrumentation used, the gas content of the fluid and the intake swirl of pump and cavitation conditions. Finally, the scaling of pressure fluctuations is discussed. In the near field, the Bernoulli equation provides a valid energy balance and therefore a velocity squared scaling can be expected. However, the air-borne sound radiation from experiments shows rather a 2.5 power relation. This is explained by the different Mach number dependence for different acoustic sources like monopoles, dipoles and quadrupoles in terms of their far field solution. The Reynolds number dependence for sound radiation is considered to be negligible.

Based on full scale testing of a PHT pump, Hartlen [123] suggested that not only the piping magnifies acoustic excitation from the pump but that some kind of a interaction of the acoustic source and the feedback from the pump takes

place. From the experiments, it is apparent that a resonant hydraulic circuit magnifies the pressure pulsations beyond the level that could be expected by a mere resonance phenomenon. Experimental data taken with pump impellers of different diameter and taper indicate an increase in pressure pulsations with increasing gap. This is opposed to normal expectations since increasing the gap is commonly used to reduce pump vibration. Unfortunately a systematic change of design parameters was not investigated in this work.

From pressure measurements on the impeller, in the volute and connected pipe Barrand, et al. [127] gained insight into pump internal acoustics. Interestingly, pressure fluctuations on the impeller reached amplitudes of up to 14 % of the pump static head, much higher than fluctuations typical in the piping. Therefore, hydraulic near field pulsations must play a major role in that region. Another interesting detail is that while generally the BPF is dominant at one of the measured shaft speeds (944 rpm) the second harmonic dominates the spectrum. Vaguely this is attributed to acoustic resonance of the piping but no further details are reported.

Bolleter [128,129] and Zogg and Bolleter [154], besides repeating earlier findings, reinforces the importance of the connected system. They find it experimentally difficult to measure the pulsations of pressure in pumps properly because

of the interference of the acoustic system properties.

For practical reasons, a lumped parameter model is preferred over the transfer matrix model for the dynamic behaviour of the pump as a component in a circuit. In an AC circuit analogy they proposed options to incorporate source terms into the model that behave like a monopole or a dipole. Neither of the suggested models is able to simulate the self-excited component suggested by Hartlen [123] due to enhancement of the source mechanism by acoustic feedback from the circuit. A need for further research on dynamic pump models which include the source mechanism is recognized. In a private communication, Bolleter admits that work on self-excitation in pumps has so far not been attempted and would be particularly interesting.

Chatel, et al. [1..] related the dipole nature of a centrifugal pump as a sound source to the blade-turbulence interaction and the monopole characteristic to the fluctuating outflow from the impeller channels. Attempts to model experimental results failed by up to 40 dB.

Chu, et al. [132] used velocity field data from PIV measurements to compute the pressure field in a volute pump. Modification of the cut-water tip clearance from 7 to 11 % revealed a reduction in the rms pressure level measured 1 m into the downstream pipe by a factor of about 2.8. Further

increase up to 23 % clearance only yielded marginal reduction in pressure pulsations. Given the hydraulic efficiency penalty paid for the increase in clearance, it is surprising that no attempt for optimization in the region yielding high return (below 7 % clearance) was attempted. Further, since the reported geometry significantly changes at the same time tip radii, it is not clear which effect (clearance or radius) is really affecting the sound generation more effectively.

De Jong, et al. [135] mainly conducted their experimental investigation on a centrifugal pump to improve the transfer matrix approach to acoustic pump modelling. At BPF and harmonics they find a pressure source (dipole) model for the pump satisfactory.

Hartlen, et al. [138] reported from a large scale test with several impeller variations a relation between the "hook" in the hydraulic head-flow rate characteristic and the maximum pressure pulsations. Also, a hope is expressed for a standardized test and modelling methodology to validate comparison between data of different origin, a task which is currently impeded by the fact that decomposition into source strength and loop amplification is often impossible.

Akin and Rockwell [155,156] reported PIV results for a radial pump. A significant finding is the importance of

instantaneous versus ensemble averaged vorticity contours in accurately determining the resulting sound levels. Further, the pump inlet conditions are reported to bear a significant influence on the internal flow structures to an extent where they can be used for sound generation control. In particular, pulsing the inflow at 2/3 of the BPF with optimized phase and amplitude can achieve reattachment of otherwise separated flow regions and therefore reduce sound generation at the BPF. However, this is accomplished at the expense of sound generated at the excitation and related frequencies.

Chu, et al. [161,162] extended the previously reported experimental results on the internal flow field of a volute pump by measurements of local pressure time histories in the cut-water region. These measurements were correlations with pipe pressure pulsations. Noise maxima were believed to be generated by tongue oscillations due to local pressure differences. This sounds rather like a peculiarity of their model than a generic cause for sound generation in pumps. Industrial pump volutes typically are of a rigid and conservative cast design making vibrations less likely than in a plexiglas laboratory design.

Finally, Cooper [133] and Verhoeven [148] gave recent examples of pump-pipeline acoustically caused problems arising from outside the nuclear industry.

Basically, two approaches to solve the problem of sound generation in pumps exist up to the most recent publications: First, modelling the pump as a system element represented by a transfer matrix or lumped parameter approach and second, visualization and measurement of local flow fields in correlation with pressure measurements locally or in connected piping. However, none of the publications addresses the investigation of a possible interaction between the sound generating mechanism and a feed back from the acoustic wave pattern in the connected piping.

2.4.3 Design Measures to Reduce Sound Generation in Centrifugal Fans and Pumps

Many of the reported design improvements to minimize sound generation in centrifugal machinery result from investigations on air blowers. However, fundamental ideas can be transferred to water pumps although the density and sound speed differences need to be kept in mind since they result in significantly different space requirements for some of the measures.

Neise [39] reviewed the literature on noise reduction in centrifugal fans. Some of the more interesting reported design measures are summarized:

Inclining the impeller outlet edge of the blades with respect to the shaft axis or similarly skewing the cut-off edge is clearly aimed at generating a longer, less instantaneous interaction between impeller outflow and cut-off. Sound reductions at BPF of 10 to 12 dB were stated.

Enclosing the impeller outlet surface in wire mesh increases the turbulence level. In combination with tripping wires in the casing that facilitate transition to turbulent boundary layers this not only reduces noise at BPF, but also turbulent noise by up to 15 dB.

Slots in the impeller blades to allow for flow of fluid from the pressure side to the suction side of the blade can avoid boundary layer separation on the blade surface but has only small noise effects of 1 to 2 dB.

Florjancic, et al. [48] investigated the primary noise reduction in a volute pump. The broad band turbulent air-borne noise reduces proportionally as the efficiency increases. A detailed study of the influence of the local design of impeller tip and volute tongue on casing vibration, efficiency of the pump, pump head and sound pressure level in the surrounding of the pump was conducted. Design variations, that were investigated, include for the impeller blade-tip tapers, holes or slots to decrease the pressure difference between the pressure and suction sides of the blade exit. The cut-water was altered by a tapered tongue or a pattern of holes

connecting discharge and recirculation side. Ambient sound reductions at BPF up to 6 dB were achieved. Generally, most of the proposed measures to improve sound generation had to be paid for by an efficiency penalty of up to 3 percentage points.

Neise's review [51] adds to his earlier work [39] the following further noise reduction methods for sound at BPF:

Spacing impeller blades irregularly reduces the peak pressure fluctuations around BPF effectively but does not help to reduce the overall sound level.

Sound pressure levels are lowered at BPF up to 5 dB by fabricating the volute from perforated sheet metal and placing it in a fabric and rock wool lined enclosure. Overall sound pressure levels are reduced by about the same amount.

By connecting a tuneable quarter-wavelength resonator to the cut-water the BPF noise could be reduced by 29 dB while not affecting the aerodynamic performance noticeably. In water flows such a resonator could assume lengths of several meters but nevertheless the idea sounds attractive.

In summary, the know-how existing in the field of silencing centrifugal fans can provide useful ideas of how to optimize centrifugal pumps with respect to their acoustic performance. More information is available on fan acoustics because the topic seems to have come up in this context at

least a decade earlier.

2.5 Summary of Literature Survey

The level of understanding on the acoustics of piping systems is very well established and accessible to analytical treatment (except the reliable prediction of acoustic damping).

The theories of sound generation are only sufficiently advanced for simple geometries and compact source regions and self-excited flow tones lack models for complicated geometries and unsteady approaching flows.

Flow fields in centrifugal pumps have experienced considerable attention. A major feature of the impeller flow is the jet/wake phenomenon that results in an interaction with the stationary cut-water at a stagnation point whose mean location moves with increasing flow rate from the discharge to the recirculation side of the tongue and oscillates with blade position.

The only serious theory for sound generation in pumps needs many simplifying assumptions and does not appear capable of predicting noise levels within 20 dB.

Reported experiments of pump-pipeline acoustics mostly do not allow for a clear separation of source term and pipeline admittance and are therefore difficult to compare.

The pump as a sound source is assumed to be of the pressure type.

Design measures to silence pumps must primarily be transferred from blower investigations. The ideas appear to have potential, but for the most part have not yet been tried on pumps.

Neither a self-excited source pipeline interaction for a centrifugal pump nor a separation of hydraulic from acoustic pressure pulsations have so far been reported in the open literature.

CHAPTER 3: EXPERIMENTAL APPARATUS

"Physics is experience, arranged in economical order"
Ernst Mach, 1882

The present research on the sound generation by a centrifugal pump at BPF and its interaction with pipeline acoustics is of an experimental nature.

The experimental apparatus is designed to obtain quantitative data on pressure fluctuations in the flow loop and to do qualitative flow visualisation in the pump cut-water region. The pricipal parameters that were experimentally varied are the acoustic excitation frequency via pump shaft speed, acoustic natural frequency of the loop, pump operating point by in-line flow rate regulation and incorporation of different pump geometries.

Design criteria are classified into hydraulic and acoustic which will be treated in the first two sections. The particular features of the laboratory pump will be described in 3.3 and the instrumentation in 3.4. The hardware implementation for visualisation of the flow field at the pump cut-water is reported in chapter 6 together with flow visualization results.

3.1 Hydraulic Design of Apparatus

Figure 3.1: Photograph of Pump Noise Flow Loop

The test loop is of a closed type pumping from and back

into an overhead tank, i.e a purely frictional system. Figure 3.1 provides a photograph of the loop and figure 3.2 a schematic depiction of the laboratory set-up.

Upstream of the pump the pipe diameter is 4" and the downstream pipe diameter is 3" matching the suction and discharge dimensions of the pump. All pipe [h] (letters in square brackets refer to the list in appendix A) is stainless steel and the pump is an all bronze construction to avoid corrosion in the loop.

The pipe support structures are welded from 2" x 2" square tubing. These, as well as the pump frame, are mounted on neoprene pads [ah] for vibration isolation and bolted to the concrete floor with steel anchors.

The tank contains about 7 m^3 of drinking quality water at ambient temperature. The loop can be isolated from the large volume of water in the tank by means of a ball valve [a] upstream of the pump and a globe valve [c] that acts also as flow control valve in the downstream part of the loop.

The water surface in the tank is located about 1.75 m above the pump [b] suction flange providing the necessary Net Positive Suction Head (NPSH) to prevent pump cavitation at all operating conditions.

Being a purely frictional system the hydraulic energy introduced by the pump must be dissipated by friction losses in the loop. The most significant pressure drop is concentrated in the control valve which makes this valve prone

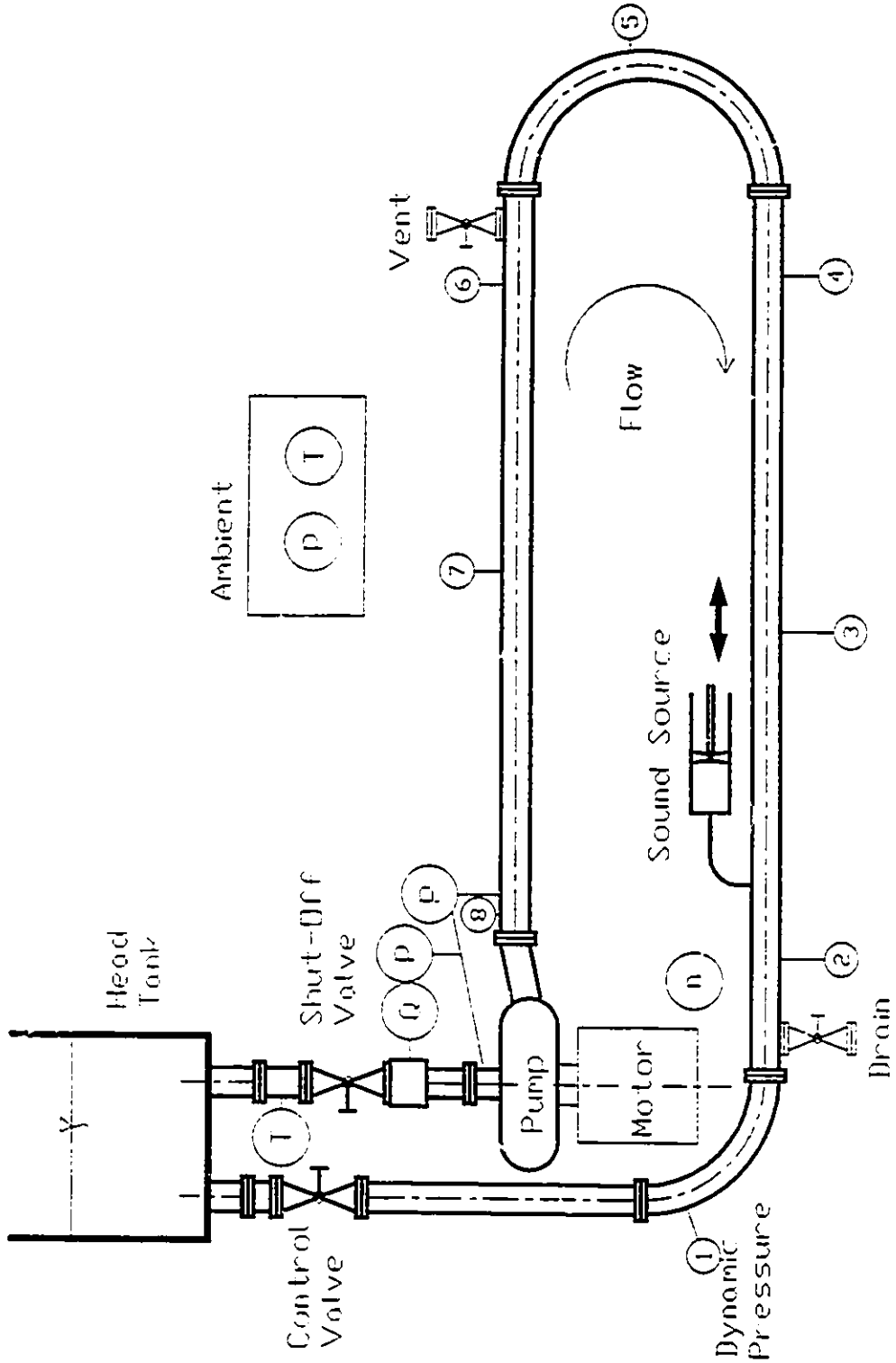

Figure 3.2: Schematic of Pump Noise Flow Loop

to cavitation at higher flow rates.

The major hydraulic design criterion is to allow the widest possible flow rate range for the pump. Figure 3.3 shows the match of hydraulic characteristic for pump and system. Static measurements of volumetric flow rate and pump head represent the pump characteristic. The system characteristic is the parabola described by the friction factor equivalent to the overall system's friction losses for the control valve in a completely open position. This yields a flow of about 125 % of the nominal flow.

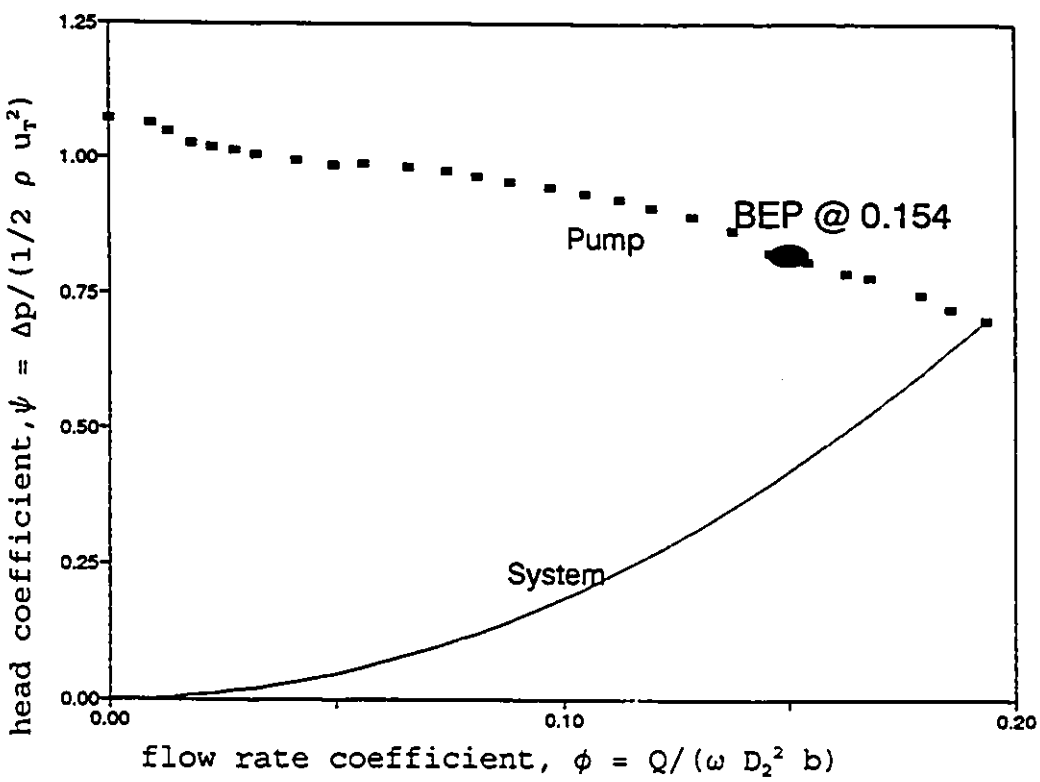

Figure 3.3: Hydraulic Characteristic of Pump and System

The non-dimensionalization in this diagram is done by

the use of flow rate coefficient

$$\Phi = \frac{Q}{\omega D_2^2 \, b} \tag{3.1}$$

and head coefficient

$$\Psi = \frac{\Delta p}{1/2 \; \rho u_T^2} \tag{3.2}$$

where Q is the flow rate, ω the shaft speed, D_2 the impeller exit diameter, b the impeller passage width at exit, Δp the pump head corrected for pressure tap elevation and difference between flow speed in suction and discharge pipe, ρ the fluid density and u_T the circumferential speed of the impeller tip.

The flow rate coefficient for the BEP is 0.154. For the lack of instrumentation for shaft torque, this value is based on an extrapolation of manufacturer's data and measurements of the electrical power supplied to the motor driving the pump. Efficiency is calculated by comparing electrical input power to hydraulic power delivered to the fluid with the underlying (certainly quite inaccurate) assumption of constant motor efficiency. On this basis the flow rate in the loop can be adjusted within the limits of 0 to 125 % of nominal best efficiency flow Q_{BEP}.

3.2 Acoustic Design of Apparatus

In the context of acoustic design the central notion is that the loop can be treated as a one-dimensional continuous system due to the large ratio between wave length and transverse pipe dimension. This large ratio results in the three-dimensional modes being too far removed from one-dimensional modes in the frequency domain to cause any confusion. Figure 3.4 shows the acoustically equivalent system.

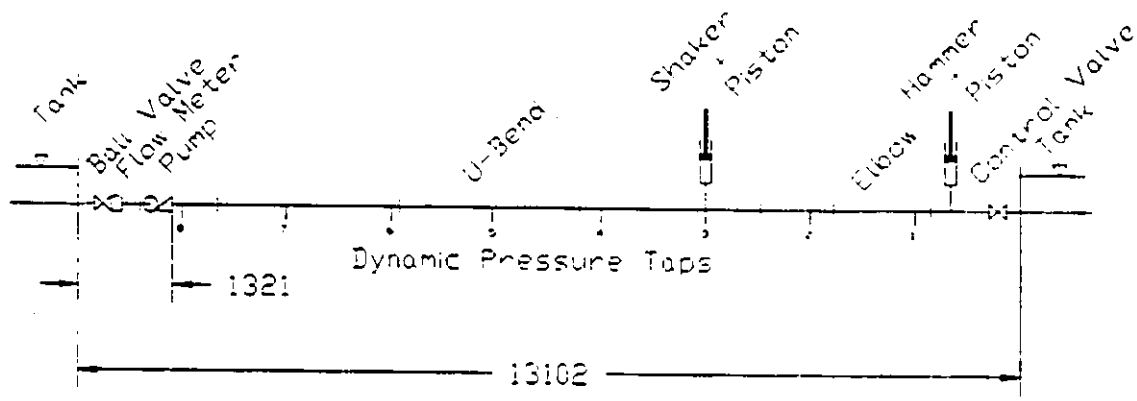

Figure 3.4: One-Dimensional Acoustically Equivalent Pump Noise Flow Loop

Therefore, the acoustically relevant parameter to describe the system becomes the acoustic natural frequency, $f_{ac,n}$, which obviously depends on the speed of sound c and the acoustically relevant length L. The condition for the acoustic natural frequency $f_{ac,n}$ is for open-open boundary conditions such that the wavelength be an integer multiple of twice the length L between open boundaries:

$$f_{ac,n} = n\frac{c}{2L} \tag{3.3}$$

The speed of sound in free undisturbed pure water c^* is approximately 1450 m/s. This can be computed from the ratio of the elastic bulk modulus and the density of the liquid:

$$c^* = \sqrt{\frac{E}{\rho_0}} \tag{3.4}$$

This value is only modestly modified by pressure and temperature given the pressure and temperature (2.5 bar, 20°C) encountered in this work. Further, the large fluid volume in the overhead tank prevents any major temperature changes of the fluid during test runs. (The calculated temperature increase over a two hour continuous working period is only about 0.7 K. Actual operating time during all experiments reported was only about 2 minutes.) The potentially largest effect, however, results from the degree of aeration of the fluid. A volumetric portion $\gamma = V_{Gas}/V$ of gas in the fluid affects the elastic property of the mixture according to:

$$E_M = \frac{E_{Fl}}{1+\gamma\left(\frac{E_{Fl}}{E_G}-1\right)} \tag{3.5}$$

and the density of the mixture:

$$\rho_M = \rho_{Fl}\left[1-\gamma\left(1-\frac{\rho_G}{\rho_{Fl}}\right)\right] \tag{3.6}$$

Here the indices Fl mean fluid, G gas and M mixture.

Because of the dominance of the decrease in elasticity over the decrease of density of the mixture it is observed that with increasing gas content, γ, the wave speed in the mixture decreases. Unfortunately, our only means of controlling the aeration was to follow a rigid procedure for collecting data. However, the sound speed was monitored for all experiments.

Additionally, inside a fluid conveying pipe the elasticity and stress condition (structural boundary condition of piping) bear an influence on wave speed. For an elastic pipe without axial stress induced by structurally clamped boundary conditions a modification of the free sound speed c^*, to that actually present in the pipe, c, is given by Lein [72]:

$$c=\frac{c^*}{\sqrt{1+\frac{E_{Fl}\,D}{E_{Pipe}\,e}}} \tag{3.7}$$

with e being the wall thickness and D the mean diameter of a thin walled pipe.

The calculated wave speed in the discharge pipe (1339 m/s) compares very well to the measured value, 1368 m/s.

The acuostically relevant pipe length is determined by points of (partial) reflections in the pipe like orifices,

expansion chambers, and open or closed end conditions. Open end conditions experience end corrections which, however, only amount to fractions of the pipe diameter and are not very important. In this test rig configuration potential reflection points are the pump, valves, elbows and bends for the loop. Partial reflections could only be measured for the pump. Of course, a change of acoustic boundary condition from open to closed occurred for the control valve completely closed.

The acoustic natural frequency is examined more closely in section 5.1. The equipment utilized for some of the experimental determination of the acoustic natural frequency consists of a side branch piston source driven by an electromagnetic shaker [p]. The signals for this shaker are generated by the function generator [r], the sine random generator [t] or the dynamic analyzer [z] and amplified by the power amplifier [s].

As a design concept, the acoustical tuning was achieved by a change in the pipe lengths and regulation of the pump speed with an AC variable frequency drive [u]. The available parameters allow, while maintaining reasonable pump shaft speeds from a hydraulic point of view, a range for the Helmholtz number L/λ from 0.2 to 1, i.e from a ratio of BPF to first acoustic natural frequency of 0.4 to 2.

3.3 Pump Design

The pump [b] is a single discharge centrifugal volute pump of end suction type with five vane impeller. The best efficiency is from the manufacturer's data greater than 70% at 1150 rpm, a head of 63 ft and 275 gpm flow. The specific speed in its non-dimensional form is

$$n_s = \frac{\omega\sqrt{Q}}{(g\,H)^{3/4}} = 0.312 \tag{3.8}$$

With the engineering definitions common in North America and Europe the values are 853 rpm $gpm^{1/2}$ $ft^{-3/4}$ and 16.5rpm $m^{3/4}.\,s^{-1/2}$ respectively.

Figure 3.5 shows a photograph of the pump motor assembly before any modifications for flow visualization were applied.

As the specific speed suggests, the pump is very radial which was selected for the relatively large area available for flow visualization and the more two-dimensional flow regime in the cut-water area.

3.3.1 Pump Impeller

The detailed geometry of the pump impeller was obtained in three different ways: First, an agreement was reached with

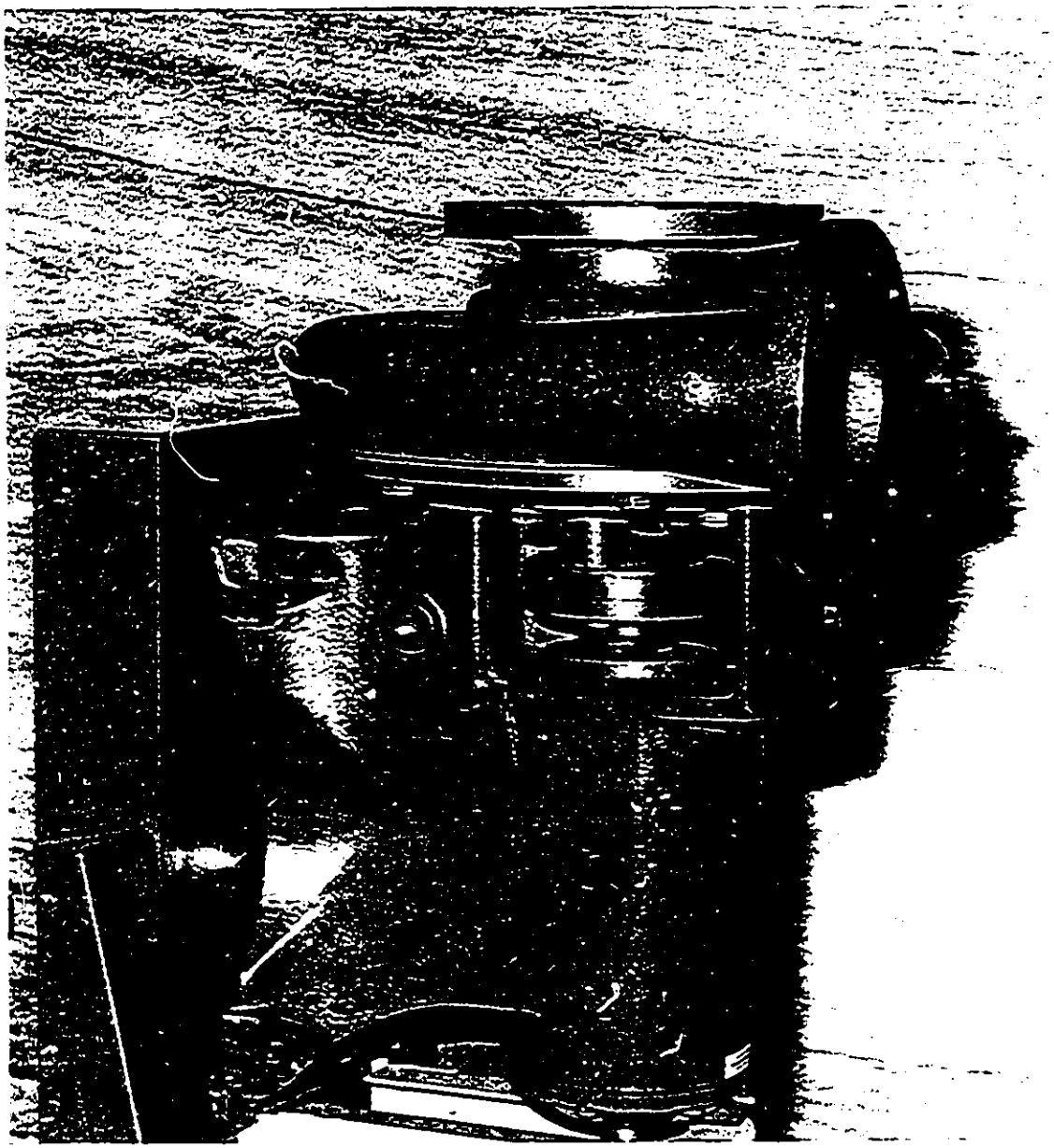

Figure 3.5: Photograph of Pump Motor Assembly before Modification

the pump manufacturer to release otherwise proprietary manufacturing drawings for hydraulically relevant geometries. Second, where accessible, measurements were taken on the impeller contour directly and third, the impeller was imaged

using the technique of Neutron Radiography. Figure 3.6 shows the neutronographic image and 3.7 the impeller drawing.

Figure 3.6: Neutron Radiography Image of Pump Impeller

In table 3.1 the measurements for all three techniques are compared.

Obviously, there exist large discrepancies between actual dimensions and drawings. This might be due to

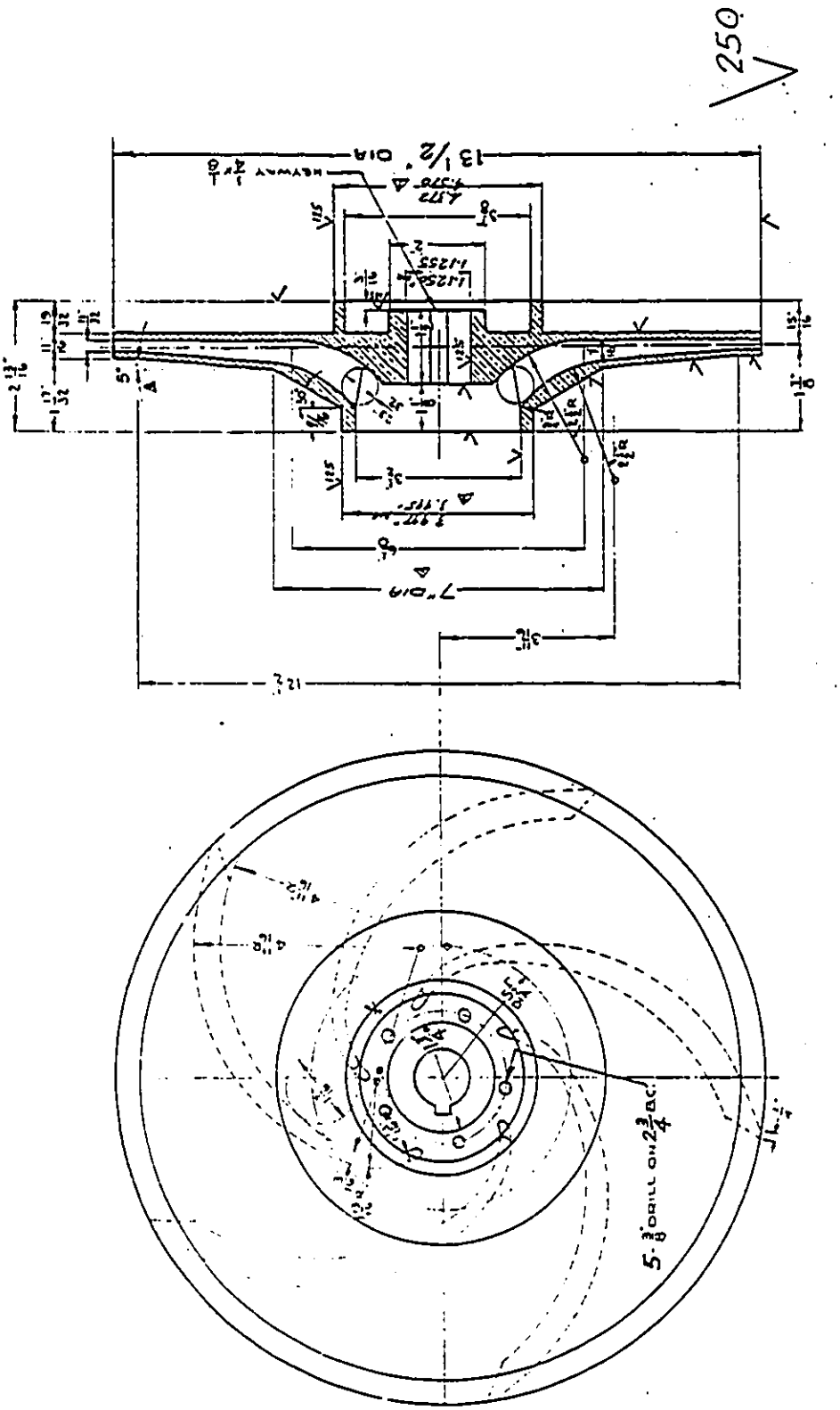

Figure 3.7: Manufacturer's Drawings of Pump Impeller

Table 3.1: Comparison of Pump Impeller Dimensions Obtained by Different Measurement Sources

		Measurement			
		Direct	Drawing	X-Ray	
Inlet					
	Diameter, D_1	89	89	89	mm
	Angle, β_1	n/a	42	35	°
	Passage Width, b_1	20	18	n/a	mm
	Blade Thickness, t_1	4	5	7	mm
Outlet					
	Diameter, D_2	343	343	346	mm
	Angle, β_2	26	32	21	°
	Passage Width, b_2	9	9	n/a	mm
	Blade Thickness, t_2	35	6	33	mm

alteration of cast models without updating the drawing (last amendment to drawing 1973). The inlet angle of the blade could not be accessed by direct measurement and measurement on the exit angle was complicated by irregular surface and narrow passage. Therefore, the radiographic measurement is probably the most reliable source of information on angles. For linear dimensions a very accurate measurement could be made directly except for the inlet blade thickness.

3.3.2 Pump Casing

Similarly to the impeller, the casing drawings were made available by the pump manufacturer. Because of better accessibility, the important features could be measured directly eliminating the need for a radiographic examination. Figure 3.8 shows the drawing and in table 3.2 the dimensions are tabulated.

Table 3.2: Comparison of Pump Casing Dimensions Obtained by Different Measurement Sources

	Measurement Direct	Drawing
Casing Width, b_3	40	38 mm
Casing Cut-Water at Centre Line		
Base Diameter, D_3	363	353 mm extrapolated from spiral radii 203 mm @ 0° 195 mm @ 90° 186 mm @ 180° 181 mm @ 270° Tongue @ 56°
Tongue Angle, α_V	38	34°
Tongue Radius, R_T	1.6	n/a

The dimensions for base diameter of volute and outlet diameter of the impeller yield a impeller-tip volute-tongue clearance $(D_3-D_2)/D_2$ of 5.8 % (again giving preference to the actual, measured dimensions) or a gap of 10 mm radial.

The volute cut water (figure 3.9) is a three-dimensional contour resulting from the intersection of the torus-like spiral and the conical discharge pipe. It is

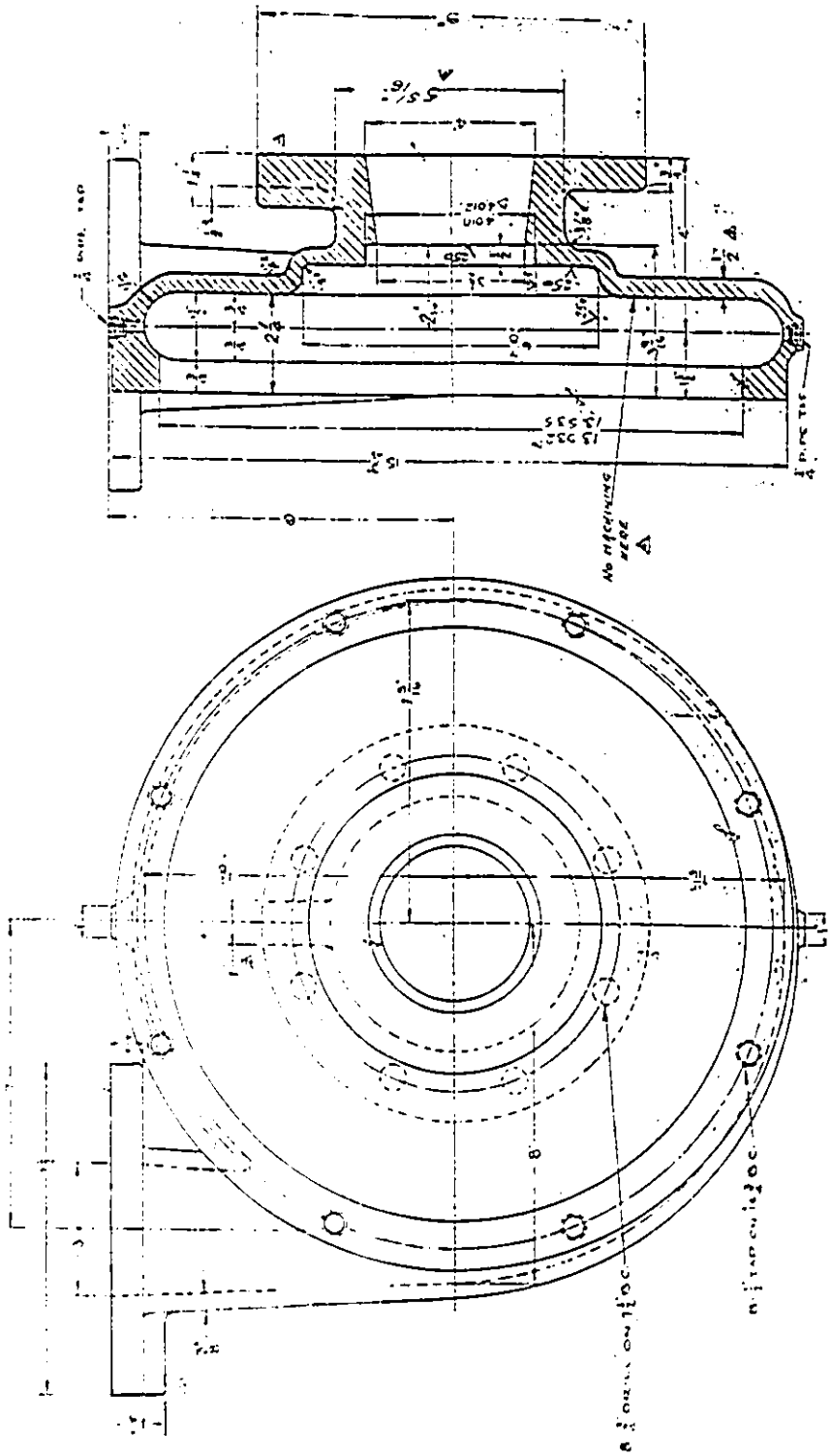

Figure 3.8: Manufacturer's Drawing of Pump Casing

symmetric to the casing centre line and not smooth there. Instead it rather resembles a "gothic arch". Information regarding the reason for this peculiar form could not be obtained, but is probably based on manufacturing considerations rather than hydraulic ones.

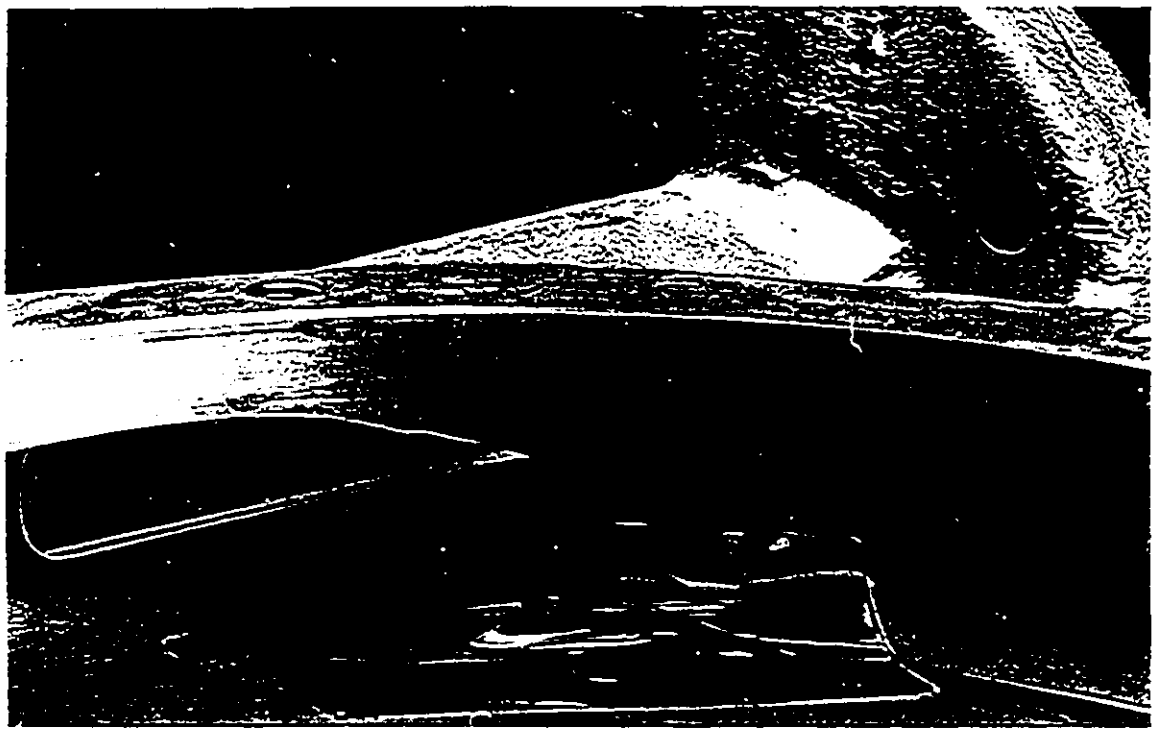

Figure 3.9: Photograph of Pump Casing with Illumination and Viewing Window (Three-Dimensional)

An acrylic [ag] side window for illumination was placed into the discharge part of the casing and, initially, so was another acrylic window which was intended to allow viewing access from the suction side into the cut-water region. The windows replaced the original casing. Their contours were internally matched identical to the original shape including the cut-water of the casing down to the casing centre line.

This volute configuration is hence referred to as volute A.

In a subsequent experimental stage the cut water was two-dimensionalized by replacing the "gothic arch" by a straight edge 20 mm on either side of the centre line. The prism now forming the cut-water has an identical centre-line shape to the original three-dimensional cut-water. A modular design of the cut-water wedge permitted experimentation with a controlled variation in cut-water tip radius R_T. Obviously, a transition had to be faired into the casing to avoid flow discontinuities. Figure 3.10 depicts the orthographic projection of the three two-dimensional cut-water geometries (referred to as volute B to D) featuring B a sharp edge, C a radius R_T equal to 2.5 mm and D a radius R_T of 5 mm. It is noteworthy that the clearance was not altered by the change of radius due to the circular arc at the recirculation side of the tongue.

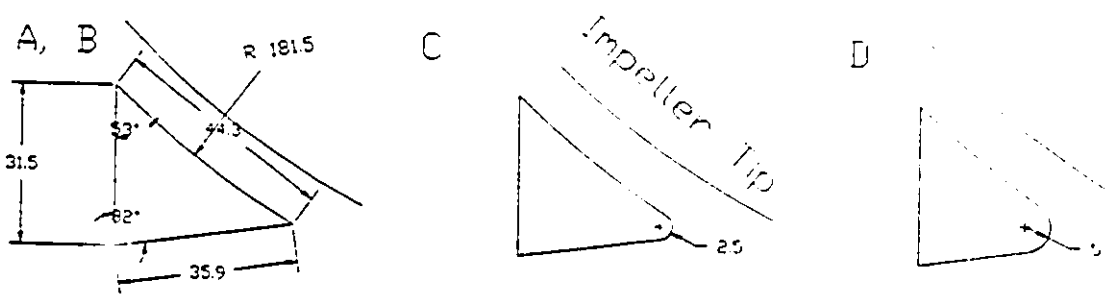

Figure 3.10: Cut-Water Geometry Alternatives

3.4 Instrumentation

3.4.1 Instrumentation for Static Measurements

Static measurements refer to those physical quantities that are only of interest in their mean value and not their fluctuating or dynamic components.

Ambient temperature and atmospheric pressure are monitored by a mercury thermometer and standard wall mounted barometer respectively. These measurements do not enter any of the experimental correlations, but are only consulted in the case of data inconsistencies.

Fluid temperature is measured by a thermocouple [o] in the flow about 2 diameters upstream of the pump suction flange. Initial measurement using the Cold Junction Compensation CJC of the A/D board of the computer [y] was replaced by the use of a reference thermocouple in a ice bucket at 0°C. The water temperature ranged from 13 to 16°C for the measurements reported and does not correlate with fluctuating pressure measurements.

Flow rate is measured by a magnetic inductive flow meter [l] located in the 4" suction line upstream of the pump. The unit is factory calibrated and its current signal is processed by the computer data acquisition system. Repeatability of measurements with this device was better then

1 % of the actual measurement except in the case of flow rates below 3 m/s as shown where the non-repeatability of measurements still never exceeded 3 %. The data on repeatability was obtained by repeating a measurement 100 times, taken over 10 s at 10 Hz, and plotting the ratio of standard deviation over the arithmetic average versus the average flow rate. Figure 3.11 shows repeatability for measurement of both flow rate and corresponding head at nominal flows.

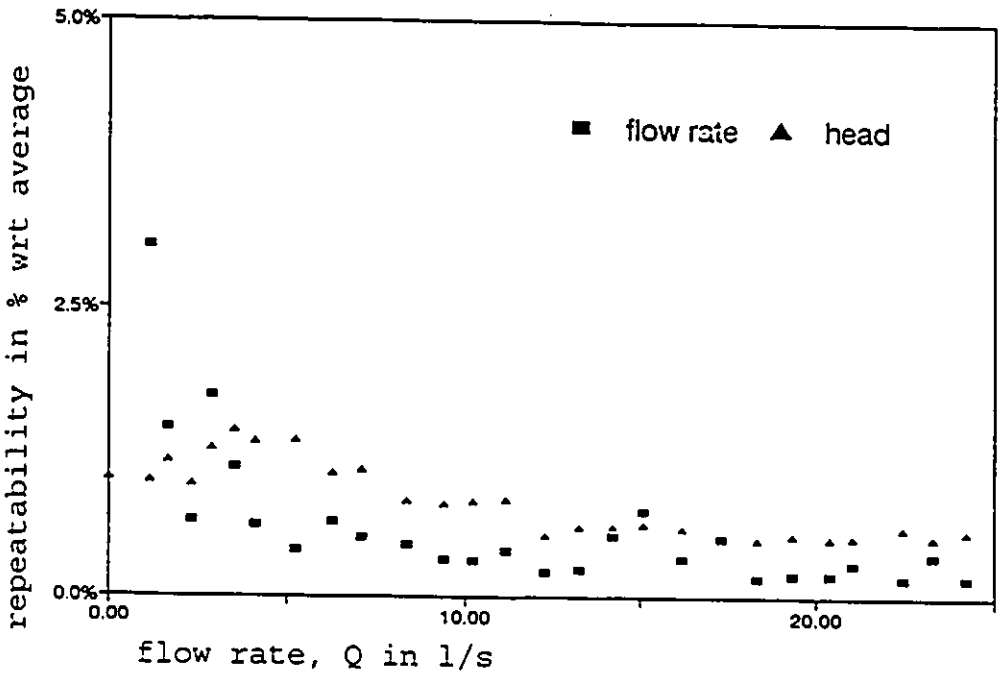

Figure 3.11: Repeatability for Head and Flow Measurements

The pump head across the pump is measured by a differential pressure gauge [j] giving an electrical voltage

signal that is processed in the computer. The repeatability for head in figure 3.11 is slightly higher than that for the flow rate at intermediate flows, but does not show the same increase at low flows. Repeatability remains at all times better than 1.5 % and above 8 m/s below 1 %.

The pump shaft speed is determined by digitally counting teeth of a 10-tooth-wheel with a proximity sensor [m] connected to counter 1 of the A/D board. The shaft speed resolution for the counting time used of 20 s is 0.3 rpm (or 25 mHz for the BPF).

3.4.2 Instrumentation for Dynamic Measurements

The physical quantity for which the dynamically fluctuating component and its transform into the frequency domain are of interest is the pressure. Measurements are taken at equally spaced locations along the loop.

Initially, strain gauge type pressure transducers [n] had been utilized, but after obtaining comparison with piezo electric transducers [k] it was discovered that the frequency response for the strain gauge transducers is only constant up to about 50 Hz and drops thereafter in a non-linear fashion. All measurements reported were carried out with the piezo electric transducers in a signal processing chain as shown in figure 3.12.

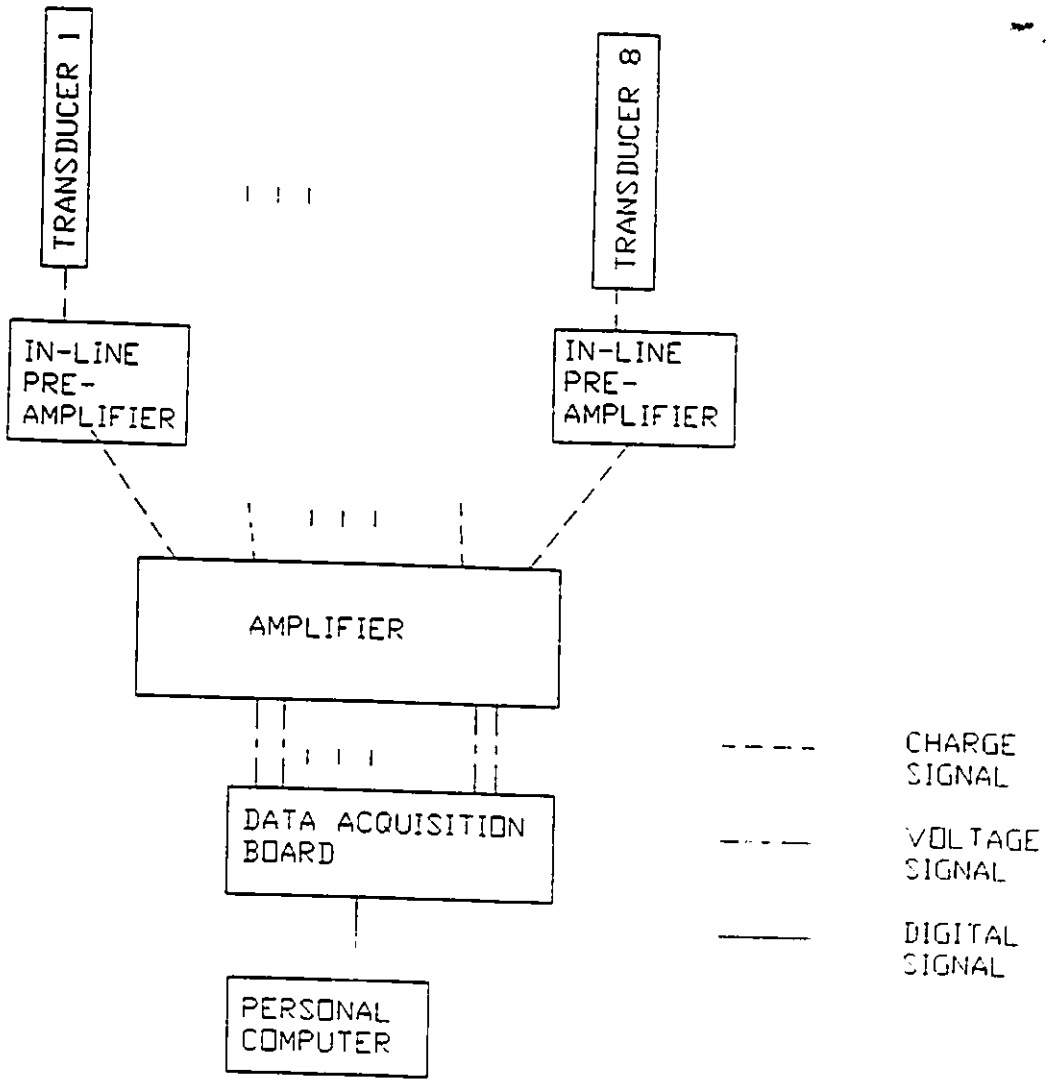

Figure 3.12: Signal Processing for Dynamic Pressure Measurements

The use of preamplifiers [w] close to the transducer is necessary to avoid the undue introduction of electronic noise into the low level charge signal. The amplifier [x] transforms the charge into a voltage signal that is further amplified by the A/D board. All signal lines including the individual in-line preamplifier, the amplifier channel, cables and connectors were electronically calibrated in the Ontario Hydro

Technology (OHT) laboratories by means of highly accurate capacitors discharging a known charge signal. As well, the amplification settings were locked by the lock dials of the amplifier channels. This calibration was done without the actual transducers, but by relying on manufacturer's data. Therefore, it was felt necessary to calibrate physically the signal line including the transducer. Transducer 4 served as a reference and calibration was done for two symmetrically arranged transducers (transducer 4 and device under test) on an air piston excited at 50 Hz and an amplitude of about 10 mbar. This calibration is reflected in the gain factor of the Global Lab software.

Table 3.3: Gains of Piezoelectric Pressure Transducers

Transducer	Gain
1	489.7
2	512,8
3	488.4
4	500.0
5	515.2
6	504.7
7	547.8
8	447.1

Repeatability of the calibration procedure was better than 1 % for all transducers. From Table 3.3 it can also be seen that relying on the merely electronic calibration without the transducer would have resulted in errors of up to 10 %. Since transducer 4 was selected arbitrarily as a reference, the level of pressure fluctuations might still be off by as

much as 10 %, but the relative amplitudes important for acoustic mode shape determination are considered to be within 1 % repeatability.

CHAPTER 4: SEPARATION OF HYDRAULIC FROM ACOUSTIC PRESSURE FLUCTUATIONS

"We are usually convinced more easily by reasons we have found ourselves than by those which have occurred to others."
Blaise Pascal, 1670

Dynamic pressure measurements, in a pipeline excited by a pump as an acoustic source, need interpretation to become meaningful. As briefly explained in chapter 1, the type of pressure fluctuations measured can be classified either as hydraulic or acoustic according to the underlying fluid mechanics.

Knowing the spatial functional relationship of the acoustic contribution to the pressure fluctuations from theoretical principles, and knowing also the spatial behaviour of hydraulic pulsations, a semi-empirical model can be constructed. This model is linearly parametric in the normalized amplitudes for both contributing terms. The acoustic part depends non-linearly on the relative source location, the acoustically relevant system length and the Helmholtz number. The hydraulic part of the model depends on the source location and the decay rate. Given the spatial behaviour of acoustic and hydraulic pressure, a numerical fit

of the model to experimental data renders physically descriptive parameters. Experimental data refers in this context to the peak at BPF of the measured pressure spectra.

This chapter is devoted to describing a semi-empirical model which permits separation of the two sources of pressure fluctuations. In section 4.1 the solution for the one-dimensional homogeneous acoustic wave equation without friction and open-open ended boundary conditions is presented. Section 4.2 covers the model term for the decay of the hydraulic pressure fluctuations in space and in section 4.3 results from the application of the combined hydraulic-acoustic model to measured data, focusing on the hydraulic part of the model, are presented. The behaviour of the acoustic pressures is the object of chapter 5.

4.1 Green's Function Solution for One-Dimensional Acoustic Boundary Value Problem

The governing equation for the problem of a one-dimensional acoustic system was derived in chapter 2 (equations 2.1 to 2.5) and resulted in the homogenous wave equation:

$$\frac{\partial^2 p'}{\partial t^2} - c^2 \nabla^2 p' = \Box p' = 0 \qquad (4.1)$$

This equation is completely analogous to the equation presented for a vibrating string by Morse and Ingard [24] where a more detailed treatment of the general solution technique by Green's functions can be found.

The major underlying modelling simplifications are the one-dimensionality of the wave propagation and the absence of friction and mean flow: One-dimensionality is appropriate due to the large difference in length scale between longitudinal and transverse modes. The neglect of friction is justified by the large Reynolds number. It can also be shown that including a small amount of acoustic damping does not change the acoustic mode shapes noticeably. (However, amplitudes and phase shifts are modified but the model does not utilize either information.) Finally, the effect of ignoring the mean flow velocity can be illustrated by calculating a Mach number

$$Ma = \frac{v}{c} = \frac{\omega D_2}{2c} \leq 0.02 \tag{4.2}$$

based on a maximum shaft speed of 1200 rpm and the measured sound speed of about 1339 m/s. Hence, Doppler effects in the flow are certainly negligible.

To obtain a complete model of the system, boundary conditions have to be prescribed. At a pipe end discharging into semi-infinite half-space the pressure is determined by the ambient conditions, and, in the absence of externally imposed fluctuations, no pressure fluctuations can be

sustained. The real situation where a pipe discharges into a tank departs somewhat from this ideal case and the effect of the local transition from a one-dimensional wave propagation to a hemispherical radiation into a half-space is typically considered by adding an end correction to the geometric pipe length to obtain an acoustically relevant pipe length. This end correction typically amounts only to fractions of a pipe diameter and is negligible in comparison to the pipe length. The effect of mean flow out of the pipe end on the transition from one-dimensional to three-dimensional wave propagation can only be speculated upon and is, therefore, not included in the model.

The source location is assumed to be an acoustic point monopole or pressure source of infinitely small geometric extension. The latter assumption can be made due to the comparably small size of the cut-water region of the pump versus the system length. Passages in the pump were developed into a one-dimensional channel because pump internal acoustic modes are again to be found at much higher frequencies than the forcing BPF.

The non-homogeneous equation for the solution g with a normalized non-homogeneous harmonic source term is thus

$$\frac{\partial^2 g}{\partial x^2} + \left(\frac{\omega}{c}\right)^2 g = -\delta(x - x_0) \tag{4.3}$$

The solution g must satisfy the corresponding

homogeneous equation everywhere except at $x = x_0$ where it still must be continuous and the boundary conditions are

$$g(0/x_0) = g(L/x_0) = 0 \tag{4.4}$$

The Green's function provides a steady state solution (sufficient time of excitation has passed to go through the transition) that assumes the form

$$G(x/x_p) = \frac{L}{\pi f_r \sin(\pi f_r)} \begin{cases} \sin\left(\frac{\pi f_r (L - x_p)}{L}\right)\sin\left(\frac{\pi f_r x}{L}\right) & x \in [0, x_p[\\ \sin\left(\frac{\pi f_r x_p}{L}\right)\sin\left(\frac{\pi f_r (L - x)}{L}\right) & x \in]x_p, L] \end{cases} \tag{4.5}$$

where x_p is the pump location, f_r the ratio of BPF over first acoustic natural frequency, $f_{ac,1}$, L the acoustically relevant length of the system and x a location.

This solution is normalized with the absolute maximum occurring in either of the intervals $[0, x_p[$ or $]x_p, L]$ to make the linear factor for the acoustic pressure term comparable independently of the other parameters. Additionally, to reflect the Fourier transformation the amplitudes of the measured pressure fluctuations are always taken as positive. Figure 4.1 shows the shape of the curves described by equation 4.5 for different frequency ratios and for the source location at $x_p/L = 0.101$.

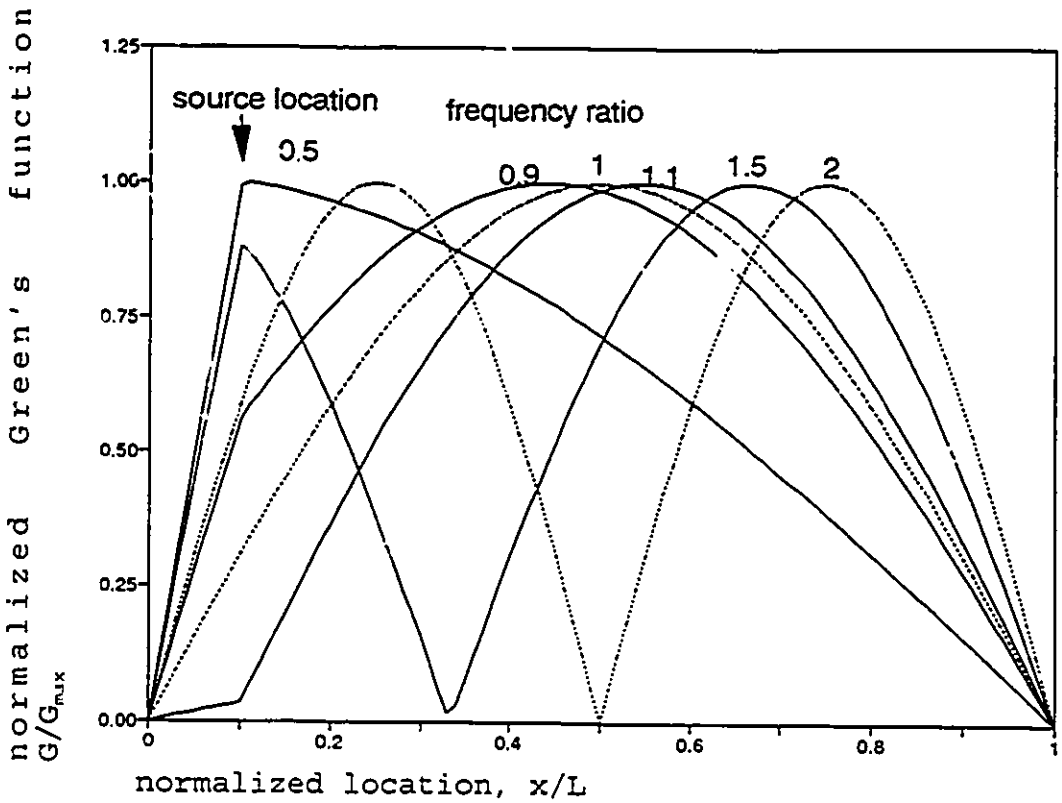

Figure 4.1: Green's Function (equation 4.5) for Open-Open Ended One-Dimensional Acoustical Boundary Value Problem. (x_p/L = 0.101)

It may be noted that the Green's function solution becomes singular at an integer frequency ratio f_r = 1,2,..., i.e. resonance condition, because of the absence of friction in the model. This definition gap can sensibly be closed by including in the numerical model the equation

$$G(x/x_p) = \sin(\pi f_r \frac{x}{L}) \qquad f_r = 1,2,... \tag{4.6}$$

that describes the resonant mode shapes.

4.2 Models for Hydraulic Pressure Fluctuations

Close to the sound source the acoustic pressure fluctuations have a component superimposed that is of a local, hydraulic nature only, and occurs at identical frequency. Initially, an approach had been taken where observations close to the pump had been assigned lower weights to account for their lower reliability. In the framework of a purely acoustic model this seemed a practical option. Subsequently however, this approach was revised in view of the intention to get as much information about the physical behaviour of the system into the model as possible. A superior modelling approach was designed to include the hydraulic component of the pressure fluctuations in the form of a separate hydraulic decay function.

As stated above, the generation of sound is related to vortex structures transversing the mean flow streamlines and resulting in far field acoustic pressure pulsations. The imposed frequency at which these vortices are emitted is related to the BPF. These coherent vortex structures create local pressure fluctuations due to momentum exchange at a discrete frequency which are designated hydraulic pressure fluctuations. A local pressure transducer measures the superimposed acoustic and hydraulic oscillations. The question arises: What happens to those coherent flow structures as they travel downstream? From turbulence models large scale

structures transfer their energy to smaller scale ones and at the smallest length scale viscous action dissipates the energy into heat. This implies is a spatial decay of the hydraulic part of the pressure fluctuations away from the source.

A functional relationship which describes this spatial decay was needed to enter the numerical model. Reader-Harris [59] developed for decay of swirl in a pipe (from a order-of-magnitude analysis on the Navier-Stokes equation combined with a simple constant eddy-viscosity turbulence-model) an exponential decay formulation with a decay rate proportionally related to the pipe friction factor (determined from the Moody diagram or computed from the Colebrook-White equation).

This formulation was adapted for the present purposes:

$$p_{hyd} = e^{k\frac{(x-x_p)}{L}} \tag{4.7}$$

where k is an exponential decay factor that assumes a negative value and the downstream distance $x-x_p$ is normalized with respect to the overall system length L.

A functional sensitivity analysis of the model for various forms of decay functions (linear, parabolic, hyperbolic and exponential) was conducted. A comparison between the four different hydraulic models showed only small variations in physical parameters resulting from application of the model to sets of experimental data. Since the numerical advantages of a simpler model are only modest the exponential

decay function which based on physical grounds was applied in the numerical non-linear curve fit.

4.3 Evaluation of Combined Acoustic-Hydraulic Model

The combined acoustic-hydraulic model consists of a linear superposition of the Green's function solution to the acoustic boundary value problem and the hydraulic decay model. This model was fitted to observations of experimental data from eight spatially equally distributed measurement locations along the loop as shown in figure 3.1. The experimental data was obtained from the frequency spectra of eight simultaneously measured pressure signals. The root mean square (rms) amplitude at BPF of each spectrum served as an observation for a numerical non-linear curve fit based on a least square approach. The software used was derived from a public domain FORTRAN program called VARPRO written by John Bolstad at Stanford University that uses a Marquardt-Levenberg iteration algorithm for the non-linear parameters followed by a direct matrix solver for the linear parameters.

The model contained initially six parameters: acoustic and hydraulic pressure amplitude, frequency ratio, source location, acoustically equivalent length and decay rate. The algorithm relies on the analytical presence of the partial derivatives with respect to the non-linear parameters in the

function definition subroutines. The necessary partial derivatives are given with respect to source location x_p,

$$\frac{\partial G}{\partial x_p} = \frac{-1}{\sin(\pi f_z)} \begin{cases} \cos\left(\frac{\pi f_z (L - x_p)}{L}\right) \sin\left(\frac{\pi f_z x}{L}\right) & x \in [0, x_p] \\ \cos\left(\frac{\pi f_z x_p}{L}\right) \sin\left(\frac{\pi f_z (-L + x)}{L}\right) & x \in]x_p, L] \end{cases} \tag{4.8}$$

$$= 0 \quad f_z = 1, 2, \ldots$$

with respect to the acoustically relevant length L,

$$\frac{\partial G}{\partial L} = \frac{1}{\pi f_z \sin(\pi f_z)\, L} \begin{cases} L \sin\left(\frac{\pi f_z (L - x_p)}{L}\right) \sin\left(\frac{\pi f_z x}{L}\right) \\ + \cos\left(\frac{\pi f_z (L - x_p)}{L}\right) x_p \sin\left(\frac{\pi f_z x}{L}\right) \\ \cdot \pi f_z \\ - \sin\left(\frac{\pi f_z (L - x_p)}{L}\right) \cos\left(\frac{\pi f_z x}{L}\right) \\ \cdot x \pi f_z \quad for \quad x \in [0, x_p[\\ - L \sin\left(\frac{\pi f_z x_p}{L}\right) \sin\left(\frac{\pi f_z (-L + x)}{L}\right) \\ + \cos\left(\frac{\pi f_z x_p}{L}\right) x_p \sin\left(\frac{\pi f_z (-L + x)}{L}\right) \\ \cdot \pi f_z \\ + \sin\left(\frac{\pi f_z x_p}{L}\right) \cos\left(\frac{\pi f_z (-L + x)}{L}\right) \\ \cdot x \pi f_z \quad for \quad x \in]x_p, L] \end{cases} \tag{4.9}$$

$$= -\frac{\pi f_z x}{L^2} \cos\left(\pi f_z \frac{x}{L}\right) \quad for \quad f_z = 1, 2, \ldots$$

and with respect to the frequency ratio f_r

$$
\frac{\partial G}{\partial f_r} = \frac{1}{\pi f_r^2(-1+\cos^2(\pi f_r)}
\begin{cases}
L \sin\left(\frac{\pi f_r (L - x_p)}{L}\right) \sin\left(\frac{\pi f_r x}{L}\right) \\
\quad \cdot \sin(\pi f_r) \\
+ L \sin\left(\frac{\pi f_r (L - x_p)}{L}\right) \sin\left(\frac{\pi f_r x}{L}\right) \\
\quad \cdot \cos(\pi f_r)\, \pi f_r \\
- \cos\left(\frac{\pi f_r (L - x_p)}{L}\right) \sin\left(\frac{\pi f_r x}{L}\right) \\
\quad \cdot \pi f_r \sin(\pi f_r)\, L \\
+ \cos\left(\frac{\pi f_r (L - x_p)}{L}\right) \sin\left(\frac{\pi f_r x}{L}\right) \\
\quad \cdot \pi f_r \sin(\pi f_r)\, x_p \\
- \sin\left(\pi f_r \frac{(L - x_p)}{L}\right) \cos\left(\frac{\pi f_r x}{L}\right) \\
\quad \cdot x \pi f_r \sin(\pi f_r) \\
\textit{for } x \in [0, x_p[\\
\\
- L \sin\left(\frac{\pi f_r x_p}{L}\right) \sin\left(\frac{\pi f_r (-L + x)}{L}\right) \\
\quad \cdot \sin(\pi f_r) \\
- L \sin\left(\frac{\pi f_r x_p}{L}\right) \sin\left(\frac{\pi f_r (-L + x)}{L}\right) \\
\quad \cdot \cos(\pi f_r)\, \pi f_r \\
+ \cos\left(\frac{\pi f_r x_p}{L}\right) x_p \sin\left(\frac{\pi f_r (-L + x)}{L}\right) \\
\quad \cdot \pi f_r \sin(\pi f_r) \\
- \sin\left(\frac{\pi f_r x_p}{L}\right) \cos\left(\frac{\pi f_r (-L + x)}{L}\right) \\
\quad \cdot \pi f_r \sin(\pi f_r)\, L \\
+ \sin\left(\frac{\pi f_r x_p}{L}\right) \cos\left(\frac{\pi f_r (-L + x)}{L}\right) \\
\quad \cdot \pi f_r \sin(\pi f_r)\, x \\
\textit{for } x \in]x_p, L]
\end{cases}
$$

$$
= \pi \frac{x}{L} \cos\left(\pi f_r \frac{x}{L}\right) \quad \textit{for } f_r = 1, 2, \ldots
$$

(4.10)

Given the large potential of arithmetic error for derivation by hand the symbolic algebra software MAPLE was used to manipulate the equations and the feature of exporting the resulting terms into FORTRAN syntax was used to minimize chances of a programming error.

An initial approach was to subject all model parameters to the numerical optimization of the residual error, R. This residual is the sum of the deviation between model and experimental observation,

$$R = \sum_{i=1}^{8} (x_i - x_{M,i})^2 \tag{4.11}$$

with x_i being the observation and $x_{M,i}$ the value calculated based on model parameters, i.e. it has the meaning of an average deviation between model and observation. Numerical difficulties (ill-conditioning and convergence failure) as well as numerically stable but physically absurd solutions were encountered. Further, the model was overly sensitive to initial guesses for the non-linear parameters due to an abundance of local minima of the least square residual that the algorithm minimizes.

A reduction in adjustable model parameters remedied the situation greatly. The acoustically relevant length L is known to deviate only minutely from the geometric length. Hence, a value of unity was assigned to the length L and all independent variables (the measurement locations x) as well as

the source location x_p were normalized by the geometrical system length of 13.102 m ($x_p/L = 0.101$). This source location was also held fixed at its geometrical value. Therefore, the model actually utilized consisted of four parameters that needed to be optimized for a minimum residual. These were the two linear parameters hydraulic and acoustic pressure amplitude (p_{hyd} and p_{ac}) and the two non-linear parameters frequency ratio f_r and decay rate k. The algorithm required initial guesses for the non-linear parameters only. The initial guess for the frequency ratio was determined by the BPF and for the decay factor a wide range of negative values could be used. In both cases the choice of initial guess, chosen within reasonable limits, gave identical results for the model parameters; only the time for numerical convergence to a solution varied somewhat.

Figure 4.2 depicts a series of data sets for four different frequency ratios or Helmholtz numbers (equal to loop length, L, over wave length, λ, based on BPF). The evident goodness of fit between experimental data and model is substantiated by the statistical measure of an average model deviation (1/8 times the square root of the residual R as defined above) which is lower than 1.5 % of the measured maximum pressure fluctuation in all instances.

In figure 4.2 a) the Helmholtz number is low (0.2), i.e. the driving frequency, the BPF, is well below the first acoustic resonance of the system. The pump is located in a

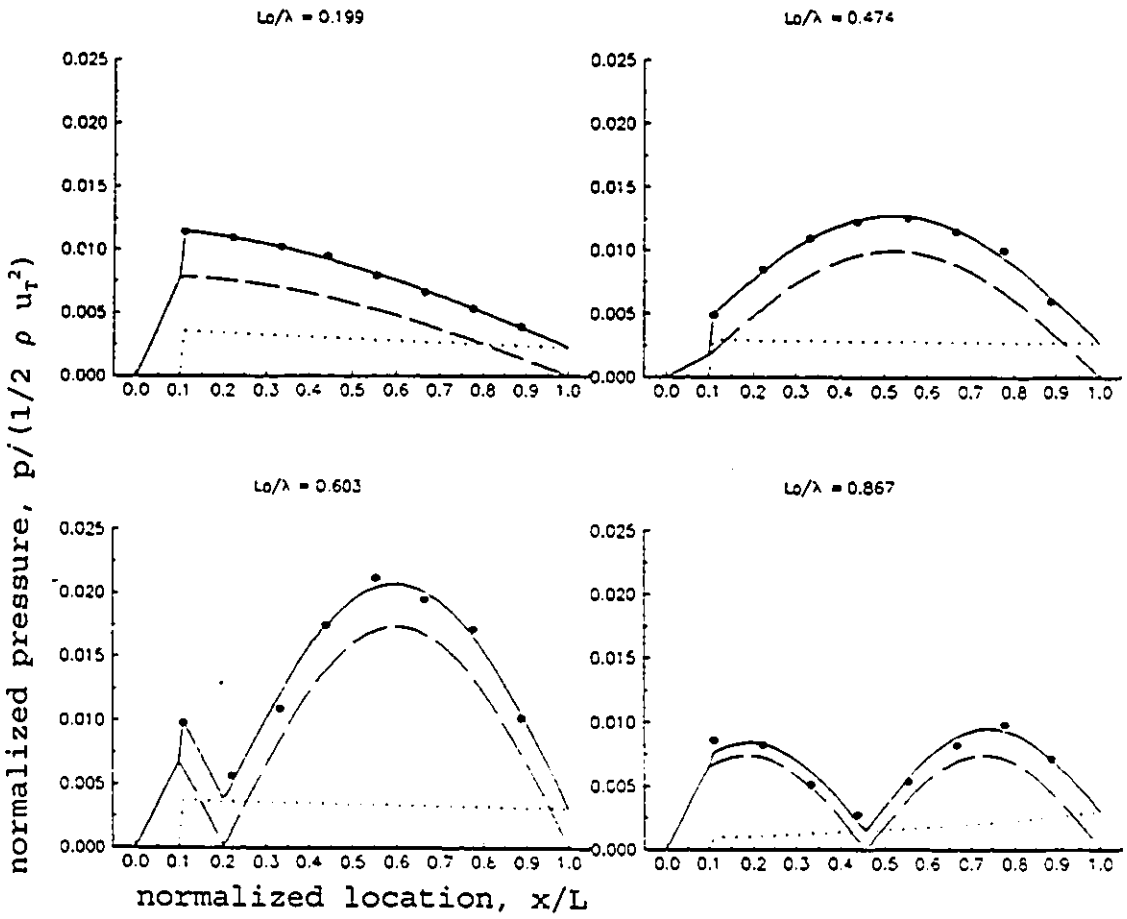

Figure 4.2: Combined Model Applied to Experimental Data at Different Helmholtz Numbers

pressure antinode. The solid line depicts the combined acoustic-hydraulic model while the hydraulic component is represented by a dotted line and the acoustic component by a dashed one. The camber of the acoustic dashed curve decreases as the Helmholtz number gets smaller. This shape results in an increasing ambiguity as the Helmholtz numbers decreases. The shape of the graph for the acoustic pressure approaches that of a hydraulic decay function more and more which means that

the model can no longer distinguish very clearly between the two. This, in combination with the low pressure amplitudes, that at very low Helmholtz numbers approach the transducer sensitivity limits, causes a reduced reliability of the model in the region below a Helmholtz number of about 0.3. To remedy the numerical problems in that region, the model had to be reduced at times to a purely acoustical one to achieve convergence. The scatter of acoustic pressure amplitudes in this low Helmholtz number region is further amplified when normalized with the static hydrodynamic head which is necessary to compare data over a range of Helmholtz numbers.

Figure 4.2 b) shows the behaviour just below the first acoustic resonance at a Helmholtz numbers of 0.47. The acoustic term clearly dominates the behaviour in the region close to resonance and above (above a Helmholtz number of about 0.45), and the hydraulic contribution is set in the background. The hydraulic term is only important immediately downstream of the pump. The acoustic mode shape is a half sine wave with pressure nodes at either end of the loop at the tank inlet and outlet.

Between a Helmholtz number of about 0.5 and 0.6 the upstream pressure node shifts from the upstream tank inlet to the location of the pump. This behaviour can be interpreted as a change of source type of the pump from the modelled monopole to a dipole type source. An alternate interpretation is that the volume expansion of the pump imposes an acoustic open end

boundary condition on the system and continues to act as a monopole source only with a coincidence of source location and boundary (an analytically singular condition). The acoustic resonance occurs in this region at 0.57 to 0.59, as discussed in chapter 5, and no phase shift between pressures upstream and downstream of the pump takes place. Both facts are evidence for the latter interpretation, i.e the acoustic mode shape results from a strong partial reflection at the pump while the source remains of the monopole type.

However, independent of which interpretation is appropriate, the model is well capable of capturing the acoustic mode shape of a half-sine wave between pump and downstream tank outlet. Therefore, the extracted acoustic and hydraulic pressure amplitudes retain their pertinence.

Figure 4.2 c) shows the behaviour at a Helmholtz number of 0.6. The acoustic pressure node has now moved from the pump slightly downstream and in figure 4.2 d) at a Helmholtz number of 0.9 it is almost at loop midpoint. The second acoustic resonance at a Helmholtz number of 1 is approached.

Note that in figure 4.2 d) the hydraulic decay factor k is positive, the hydraulic pressure term gets bigger with distance from the pump. This, obviously, can no longer be explained based on the hydraulic vortex structures from the pump being convected and breaking down in the cascade of turbulence. However, in the region of high Helmholtz numbers, since the driving frequency is linked to the shaft speed and

that in turn proportional to the flow rate, additional sound sources arise in the form of flow noise from fittings and valves. In particular, the control globe valve when operated in a partially closed position, obscured the picture somewhat, as is described in the following.

Focusing at this point mainly on the hydraulic contribution it can be expected that the hydraulic pressure amplitude will rise approximately quadratically with the Helmholtz number ($He \alpha f_{BP} \alpha rpm \alpha u_T$, $p \alpha u_T^2 \Rightarrow p \alpha He^2$). Figure 4.3 shows the hydraulic pressure amplitude versus the Helmholtz number for all geometries tested.

Below a Helmholtz number of approximately 0.8 (corresponding to a pump shaft speed of about 1000 rpm and 17l/s flow rate) a quadratic dimensional relation approximates the data reasonably well. It can be cast in the form of a dimensional equation based on a least square average of data for all four geometries investigated to

$$p_{[mbar]} = 8.6\ mbar \cdot He^2 \tag{4.12}$$

The dimensional coefficient of 8.6 mbar has a standard deviation of about 63 % and normalized with the dynamic head based on the tip speed p_u,

$$p_u = \frac{1}{2}\rho u_T^2 \tag{4.13}$$

the average ratio of hydraulic pressure over dynamic head p_{hyd}/p_u in this region amounts to about 0.35 %.

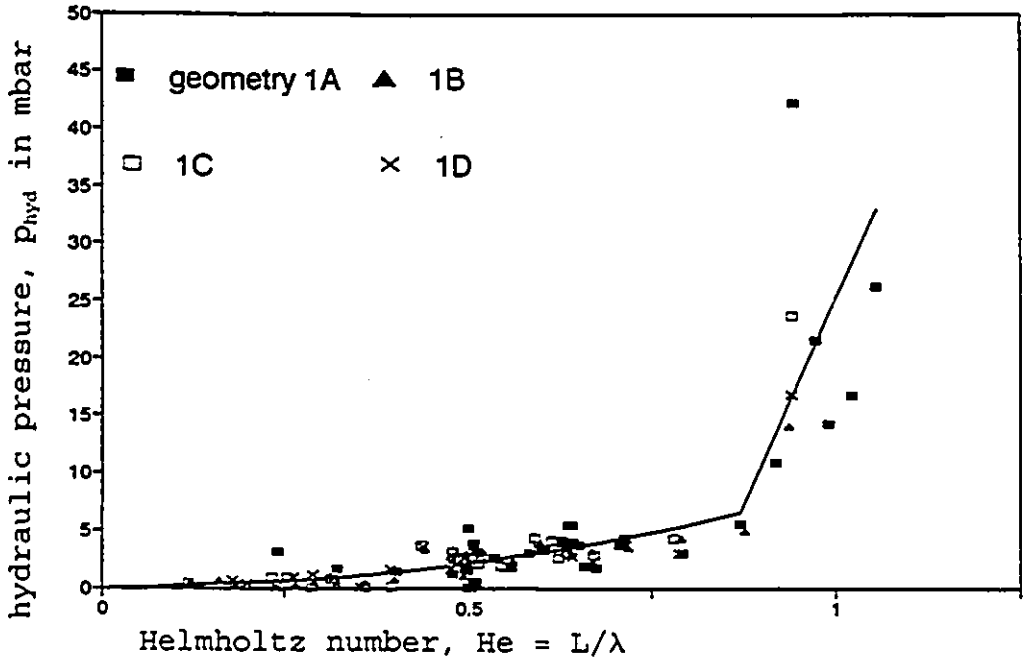

Figure 4.3: Hydraulic Pressure as a Function of Helmholtz Number for All Four Geometry Variations at 100% Flow

The quadratic relationship ceases to hold true above a Helmholtz number of about 0.8. In this context, it is noteworthy that at a shaft speed of about 800 rpm (Helmholtz number of about 0.64) the onset of cavitation in the control valve is audible. This second sound source, in addition to flow noises, raises the general noise level. This can provide an explanation for the steep slope in the region beyond a Helmholtz number of about 0.8 when cavitation, presumably, has developed sufficiently to produce significant fluid born noise. Since this phenomenon seems to be peculiar to our test

rig and not of generic interest, further investigation was not conducted in that region.

In conclusion, figure 4.3 does not suggest a significant influence of the cut-water geometry on the hydraulic term in the model.

The relative flow rate dependency of the hydraulic pressures is depicted in figure 4.4 for the geometry 1B.

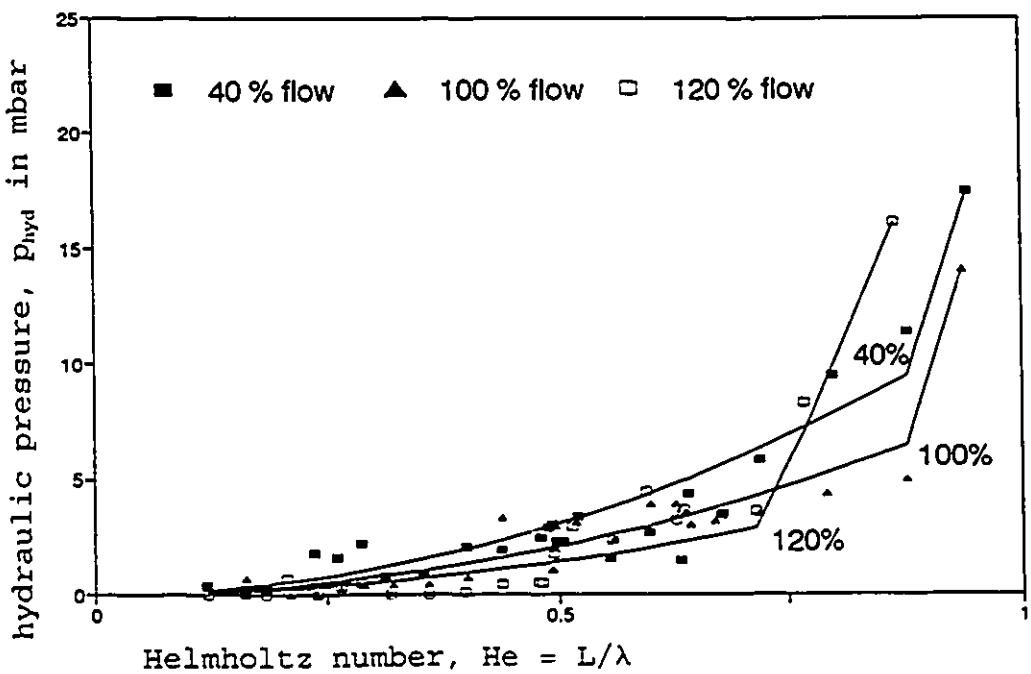

Figure 4.4: Hydraulic Pressure as a Function of Helmholtz Number for Variations in Flow Rate, Geometry B

In the quadratic region of each curve higher hydraulic pressure fluctuation is encountered with lower flow rate as represented by the dimensional coefficients: 40 % flow - 12.3 mbar, 100 % flow - 8.4 mbar, 120 % flow - 5.7 mbar. This is

probably related to a stronger recirculating flow inside the impeller at lower mean flow rates resulting in more hydraulic noise. All three curves display a sudden steep slope in the region of higher Helmholtz numbers as seen previously in figure 4.3. While for 40 % flow and 100 % flow this kink occurs at a Helmholtz number of about 0.85 it occurs earlier for 120 % flow (around 0.7). This substantiates the argument of a cavitating control valve because at higher flow rates the inclination to cavitate increases. Higher local velocities produce local pressures low enough to go below the vapour (or critical) pressure and cause cavitation.

The hydraulic decay rate, k, displays a much larger variability than the hydraulic pressure amplitude. In an attempt to obtain a meaningful average of this parameter a credibility measure had to be established. Therefore, a decay rate average was determined by entering the credibility of each observation into the averaging equation. As a measure for credibility of a value of k the ratio of hydraulic over acoustic pressure amplitude p_{hyd}/p_{ac} was used, i.e. the weight of an observation for calculating the average was determined by how large a portion of the overall measured pressure signal was of a hydraulic nature. This resulted in an equation for the average decay rate of

$$\overline{k} = \overline{\left(\frac{p_{ac}}{p_{hyd}}\right)} \sum_{i=1}^{n} k_i \left(\frac{p_{hyd}}{p_{ac}}\right)_i \qquad (4.14)$$

where overscores stand for an arithmetic average.

Computed average decay rates for different geometries ranged from -0.42 to -3.81 (100 % flow - geometry A: -0.42, geometry B: -3.60, geometry C: -3.81, geometry D: -1.05). The variations are obviously large and can be considered statistical variations rather than reliable information about physical correlations.

In summary, the procedure of separating acoustic from hydraulic pressure fluctuations is based on a linear superposition of an analytical solution to the acoustic boundary value problem and a hydraulic exponential decay function. The number of possible model parameters was reduced, based on geometric conditions, to include acoustic and hydraulic pressure amplitude, frequency ratio and decay rate. This model was numerically fitted to a set of eight spatially distributed experimental observations of pressure fluctuations at BPF. The model was able to represent the experimental observations well. Limits of the model were encountered at very low Helmholtz numbers (below 0.3) because there the shape of the hydraulic and acoustic functions approached each other. This made a separation into acoustic and hydraulic term less reliable. At high Helmholtz numbers (beyond 0.8) the model did not represent the physical behaviour of the system well any longer because a second sound source (cavitating valve) started to make a noticeable contribution to the noise level. Evaluating the parameters of the hydraulic part of the model,

it was found that while the hydraulic pressure amplitude showed clearly explainable trends the decay rate behaved somewhat erratically. None of the experimentally determined parameters were used to lower the degrees of freedom of the model to avoid over constraining the solution.

In conclusion, the model is a reliable tool to separate acoustic from hydraulic pressure fluctuations in a Helmholtz number range of about 0.3 to 0.8. Below a Helmholtz number of 0.3 the application of a merely acoustic model to extract mode shape and amplitude is a workable solution as long as electronic signal noise is not the limiting factor. The upper boundary of the range is a result of increasing background noise and can possibly be extended if the acoustic pressure amplitude is of primary interest relative to the hydraulic part of the model.

CHAPTER 5: ACOUSTIC PRESSURE FLUCTUATIONS

"Everything should be made as simple as possible, but not simpler"
Albert Einstein, 1916

This chapter is dedicated to the effects that driving frequency, pump operating point and a selected feature of the cut-water geometry, the tip radius, have on the acoustic pressure fluctuations in a pipe circuit. What is meant specifically by the acoustic pressure fluctuations has been presented in the previous chapter which developed a semi-empirical model to separate hydraulic and acoustic pressure fluctuations. In short, it is that part of the pressure fluctuations that displays acoustic features, i.e. travelling waves at the speed of sound to form an acoustic standing wave pattern described by a Green's function solution of the wave equation with the appropriate boundary conditions.

A further separation of the acoustic pressure fluctuations into a pure source term and acoustic loop amplification could not be achieved. This problem is closely related to a reliable method of determining acoustic damping in the system. Methods like wave decomposition or reflection factor determination failed due to unreliable and non-repeatable phase information of cross-spectra. A statistical

averaging to suppress signal noise would only be possible with a large variety of different loop impedances upstream and downstream of the pump to filter out system related signal noise. This flexibility was not designed into the test apparatus and was found rather difficult to retrofit.

The first part of this chapter deals with the acoustical description of the loop, namely, the acoustic natural frequency. Subsequently, an attempt is made to illustrate the effects of Helmholtz number, normalized flow rate and geometry in separate sections. However, these parameters do not act separated from one another. Instead, various interactions take place. Therefore, while a subdivision is somewhat artificial it is intended to help clarify the presented data. In this context the following chapter 6 on flow visualization will be a useful tool to complement the picture.

5.1 Acoustic Natural Frequency of Loop

How critical a good knowledge of the exact acoustical natural frequency is can well be illustrated by an analogy to a simple mechanical single-degree-of-freedom system under forced vibration. Suppose we are interested in the vibration amplitude in the damping controlled region close to resonant frequency of a lightly damped system (5 % of critical). The

forcing function is normalized to unity so figure 5.1 shows the system admittance. Because of the sharpness of the resonance peak, a small uncertainty in the frequency ratio of +/- 0.5 % at a value of 0.98 is associated with an amplitude uncertainty of about +/- 3 %, a magnification of the uncertainty by a factor 6. Of course, this amplification gets worse with lower damping and the closer it is to resonance.

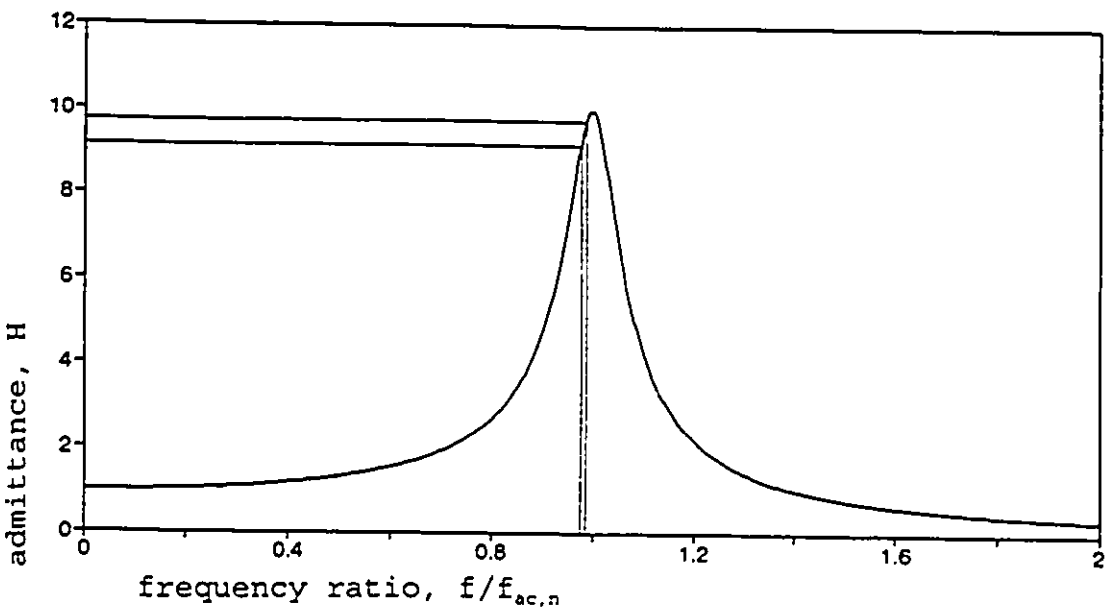

Figure 5.1: Admittance of Harmonic Oscillator at a Damping of 5 % of Critical

In the mechanical system the natural frequency can reasonably be assumed to be fixed. Opposed to that, in the acoustical system the acoustic natural frequency can very well change with time due to minor changes in temperature, pressure, and foremost, aeration properties of the water used in the loop. For this reason a very accurate and, especially,

repeatable methodology for measurement of natural frequency is required.

5.1.1 Theoretical Prediction of Acoustic Natural Frequency

In theory, the prediction of the natural frequencies of a simple one-dimensional system with open-open boundary conditions is a straightforward task. From the eigenvalues of the governing equation the natural frequencies are determined to be

$$f_{ac,n} = n \frac{c}{2L} \tag{5.1}$$

where the integer number, n, denotes the order of the acoustic natural frequency, and L, the overall length of the system. In other words, a resonance occurs when the Helmholtz number He = L/λ is equal to an integer multiple of 0.5. The wave length λ is of course dependent on the driving frequency which is the BPF f_{BP}. So a condition for resonance can also be formulated as $f_{BP}/f_{ac,n} = n$.

Crucial in either formulation is an accurate knowledge of the sound speed c. In chapter 2 the theoretical background for calculating the actual sound speed from the one in an infinite volume of water as a base value, and modifying it for the elasticity of the pipe for a specified material, pipe

geometry and structural boundary conditions was presented. The design value obtained for the sound speed was 1339 m/s.

The technique developed to measure the sound speed is a transient one and is depicted in figure 5.2 schematically.

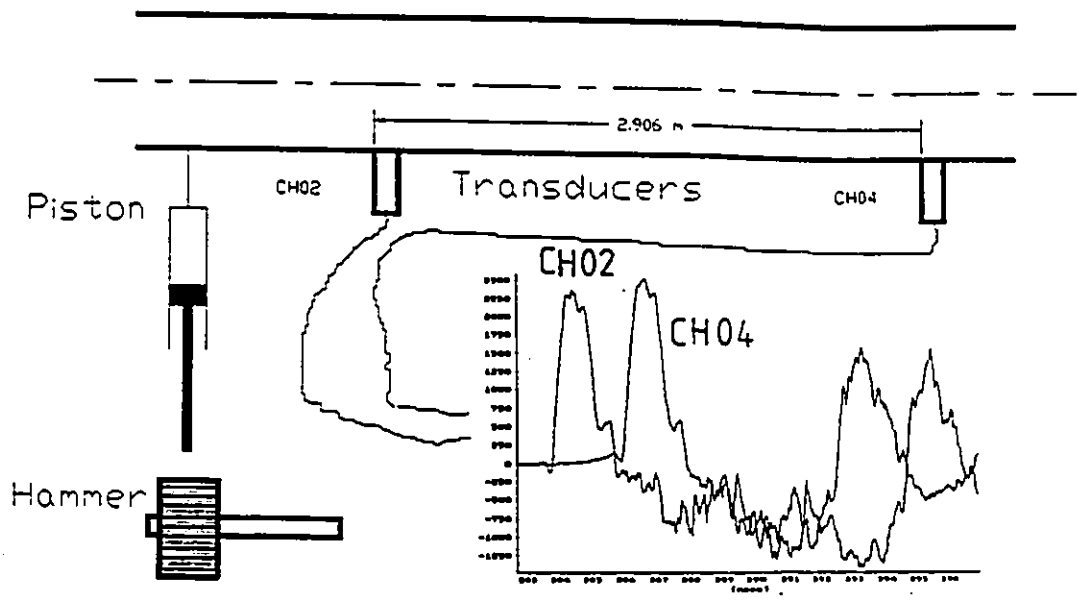

Figure 5.2: Schematic of Transient Sound Speed Measurement

The transient is produced by manually impacting a side branch 1" diameter piston with a hammer. This impact generates (at least as part of the effect) an acoustical pressure signal of about 2 bar peak amplitude that travels at the speed of sound in the loop. The measurement concept is to determine the elapsed time that it takes for the supposedly "frozen" pressure pulse to travel a known distance between two transducers.

The accumulated random error of this measurement

technique relies on the accuracy with which the transducer distance and the elapsed time can be measured.

$$\Delta c = \frac{\Delta x_{ij}}{t_{ij}} + \frac{x_{ij}\Delta t_{ij}}{t_{ij}^2} \tag{5.2}$$

where Δ stands for the absolute error in the quantity, and the subscript ij means from transducer i to transducer j. Theoretically, a large spacing between transducers and a high resolution (small discretization interval, high sampling frequency) of the time measurement yield the smallest error in sound speed.

However, a practical upper limit for the spacing of the transducer is posed by the requirement that the signal remain "frozen" or, in other words, that it correlates with itself, measured at a different location, well enough to be able to determine accurately a time constant for signal travel time. Since a better accuracy is achievable for measuring the distance between transducers along a straight line (rather then a sound path in a bend or elbow) the transducer locations 2 and 4, spaced a distance x_{24} = 2.906 m (Δx_{24} = 0.002 m) apart, were selected as the measurement locations. The 2 mm error in transducer spacing seems high for a geometrical quantity but is realistic considering that the measurement was taken with a tape measure because no large enough calliper was available. It is a measurement error and does not reflect a variation of this distance. Consequently, this error becomes

systematic and does not affect the repeatability of the sound speed measurement.

The pressure signal was recorded using the PC based data acquisition system at its maximum sampling rate of 50 000 Hz (with two channels in use 25 000 Hz per channel) which translates into a time resolution of 0.04 ms. In this context the concept of time skewing became important and needed to be considered in the calculations. Time skewing results from a sequential data acquisition of the different channels and, hence requires a constant time correction by the inverse of the maximum sampling frequency ($1/f_{sample}$ = 0.02 ms). To determine the travelling time between transducers, the crosscorrelation, defined to be

$$R_{24}(\tau) = \frac{\overline{p_2(t)p_4(t+\tau)}}{\overline{p_2(t)p_4(t)}} \tag{5.3}$$

(with p_2 and p_4 standing for the pressure signal at transducer 2 and 4, t the time and τ the time lag), was computed in a direct method (as opposed to the computationally more efficient method via Fourier transforms that, however, experienced aliasing problems). The resulting discretization of the correlation corresponding to the sampling frequency of 0.04 ms was further refined by fitting a parabola to the peak of the crosscorrelation and computing the delay time τ at the apex of this parabola. By this measure, the error for the sound speed could be reduced to the repeatability error and is

no longer limited by the time discretization. The QuickBasic routine CROSS (see also Appendix B) contains the necessary steps for calculation of the elapsed time τ from an ASCII file containing the time history of the pressure signal of the two transducers.

The time window found to be most reliable and repeatable for determining the crosscorrelation is a window of about 10 ms width containing just the pressure peaks of both transducer time histories. The time calculations were found to be insensitive to the exact time window location as long as the window contained the peaks from both transducer signals. Repeatability of this methodology was found to be within 0.5% for the sound speed regardless of the exact amplitude of the signal (produced by a manual, not amplitude controlled, hammer impact) as long as the data acquisition system did not saturate.

An attempt to expand the method to measurements under flow conditions in the loop dropped repeatability to less than 3 % and was consequently discarded.

Sound speeds measured during the experiments ranged from 1355 to 1390 m/s and agreed to within 1 to 4 % with the predicted design sound speed of 1339 m/s. This range is a result of the different ambient temperature and barometric pressure conditions for experimentation at different times. Aeration properties of the loop water may also have experienced a drift due to the refill with fresh tap water or

the stagnant de-aeration of the water over extended periods of time.

Given the length of the whole loop from tank outlet to tank inlet of L = 13.102 m a first natural frequency of 51.7 to 53 Hz results for the complete system. Experimental results from direct methods of measurement of the natural frequency showed that partial reflections in the loop are present. It can be asserted that the most likely cause for partial reflections is the impedance change at the pump (elastic modulus and wall thickness of material and, most importantly, hydraulic cross sectional area change). The associated length from pump discharge to tank inlet of 11.781 m yields a first acoustic natural frequency of 57.5 to 59 Hz. (The frequency of the partial system upstream of the pump is with about 520 Hz, to far removed from the exciting BPF to be of interest.)

5.1.2 Measurement of Acoustic Natural Frequency by Reflection Time Method

The method of measuring the natural frequency by a reflection time is similar to the previously described method for measuring the sound speed in that transient pressure signals are generated and evaluated. Rather than determining the sound speed and calculating the natural frequencies the acoustic natural frequency is measured directly from the time

it takes the pressure transient to be reflected at the open pipe ends and pass a single stationary transducer a second time with the same shape and direction as the original pulse.

Figure 5.3 shows a schematic of the measurement technique as well as a sequence of instantaneous pictures of the travelling waves.

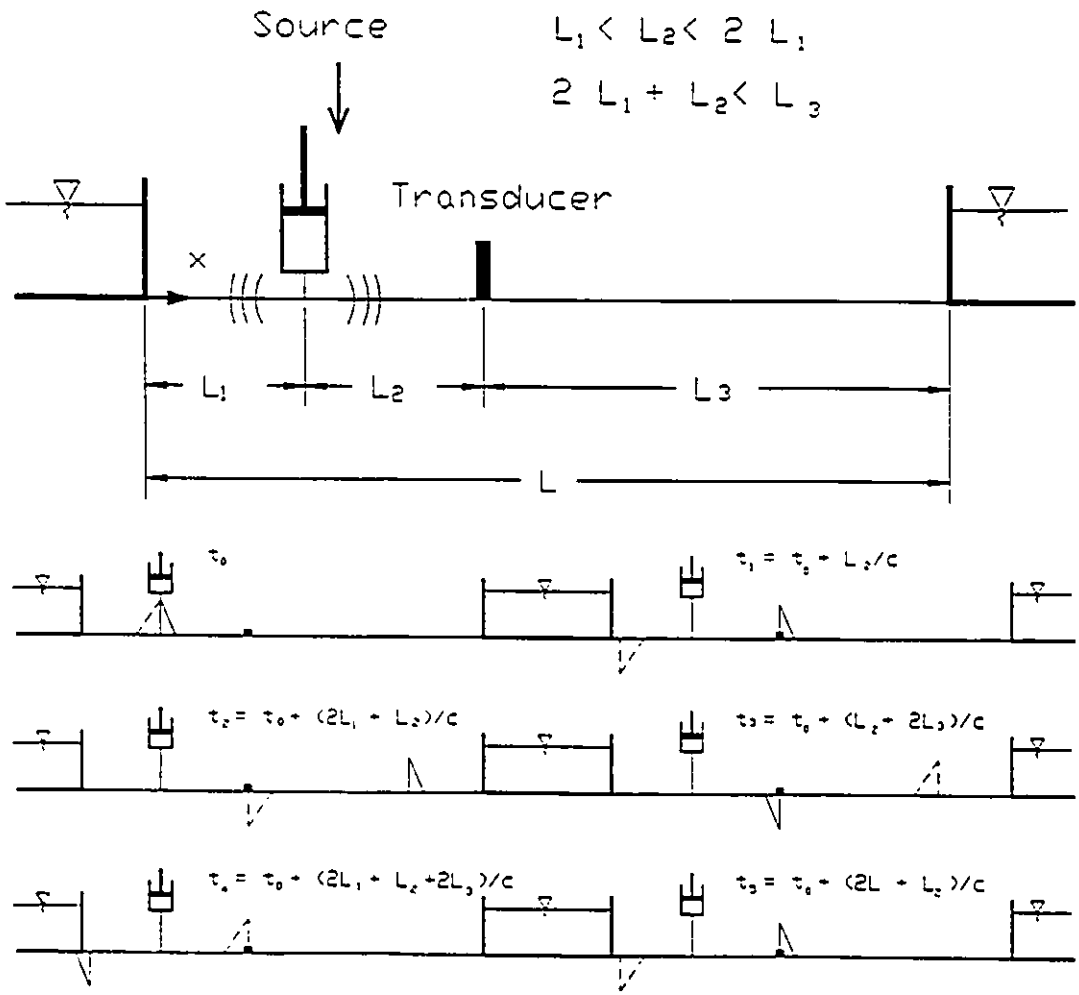

Figure 5.3: Reflection Time Measurement Technique and Sequence of Travelling Waves

At $t = t_0$ the impact on the piston generates an

acoustic pressure wave which travels in positive w^+ as well as in negative w^- x-direction (in figure 5.3 w^+ is depicted as solid line, w^-dashed). For the assumed geometric ratios the transducer is passed first by the wave w^+ at the time $t_1 = t_0 + L_2/c$ and only afterwards by the wave w^-. It is reflected, i.e a change in travelling direction and a inversion of the positive pressure peak into a negative one, at the open end at the time $t_0 + L_1/c$ and arrives at the transducer at $t_2 = t_0 + (2\ L_1 + L_2)/c$. At t_3 the reflected wave w^+ and at t_5 the second reflection of w^- passes the transducer again. Notably, at t_5, the configuration resembles the one at t_1 (friction losses would be reflected in a smaller amplitude and a "smearing" out of the details of the shape of the initially very well defined pressure pulse and are not depicted). From the sequence of reflections shown in figure 5.3 it can be seen that the pressure signal observed by the transducer repeats itself (almost) exactly after the reflection time

$$T_R = \frac{2\ L}{c} \tag{5.4}$$

Regardless of the geometric distribution of source and transducer in the loop, an autocorrelation computed for the signal at the transducer according to

$$R_{22}(\tau) = \frac{\overline{p_2(t)\,p_2(t+\tau)}}{\overline{p_2(t)^2}} \tag{5.5}$$

will show a peak at a time that corresponds to that self repetition of the time history. Minor peaks also show up for times corresponding to small partial reflections and may be a propagation of vorticity produced by the injection of fluid from a side branch when the piston is impacted.

Figure 5.4 shows the autocorrelation measured according to the described method.

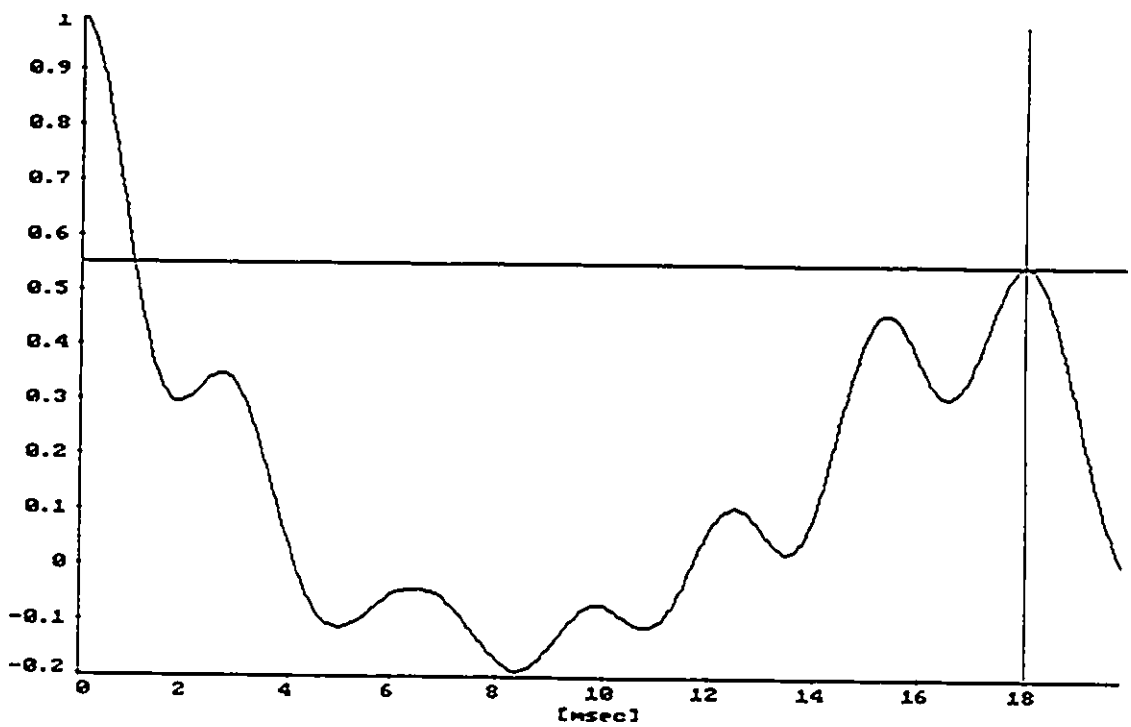

Figure 5.4: Autocorrelation of Pressure Signal at Transducer 2 after Impact on Piston

Visible in figure 5.4 is the sequence of two maxima of the autocorrelation at times of 15.36 and 18 ms. The peak at 18 ms corresponds according to

$$f_{ac,1} = \frac{1}{T_R} \tag{5.6}$$

to a natural frequency of 55.6 Hz. The other peak yields a frequency of 65.1 Hz. The higher frequency must be associated with a partial reflection in the system. The ratio of the geometric length from pump discharge to downstream tank outlet of 11.871 m over the complete system length of 13.102 m gives a value of 0.91. The ratio of the above two frequencies of 0.85 suggests again a partial reflection at the pump. Autocorrelation coefficients of similar magnitude (0.55 and 0.48) suggest also that the pump can about equally well reflect a pressure wave as let it pass through, a result that will be discussed later in this chapter.

5.1.3 Measurement of Acoustic Natural Frequency by Externally Forced Acoustics

Another method of measuring the acoustic natural frequency is an external forcing device that excites the system at variable frequency to produce directly the admittance function of the system and from that the resonant frequency. The ways in which the external excitation can be provided are numerous. Experimental harmonic forcing in a linearly and logarithmically swept sine fashion, square wave forms and white noise were used as input signals to an electromagnetic shaker connected to a hydraulic piston. Both were mounted together in a rigid frame. The side branch piston

was connected to the main line alternatively by a instrumentation line of 3.2 mm (1/8") diameter and about 0.3 mm length (first natural frequency about 2250 Hz) or mounted directly to the main pipe. Multiple impacting of a steel mass, attached to the shaker diaphragm, onto the piston rod provided the best amplification of the pressure signal measured inside the piston. The impacting was periodic with a linearly swept frequency between 20 and 70 Hz.

Figure 5.5 shows an experimentally obtained linear trace of the pressure ratio of a signal from a transducer mounted at the midpoint of the loop (transducer 4) where the first mode shows a pressure antinode over the pressure measured inside the hydraulic piston.

The low amplification factor of 0.5 is immediately apparent and corresponds by no means to reasonable acoustic damping values (which would lead one to expect an amplification in the neighbourhood of 10). A possible explanation for this experimental difficulty (that could not be resolved) is as follows: The pressures measured inside the pistons serving as the reference are hydrodynamically produced by motion of the piston in its cylinder. A major part of the pressure potential is used to pump fluid from the piston into the main pipeline, i.e. overcome friction losses in the instrumentation line and discharge orifice and mixing of the submerged jet. Only a minor part of this pressure will compress the fluid and originate acoustic pressure pulsations.

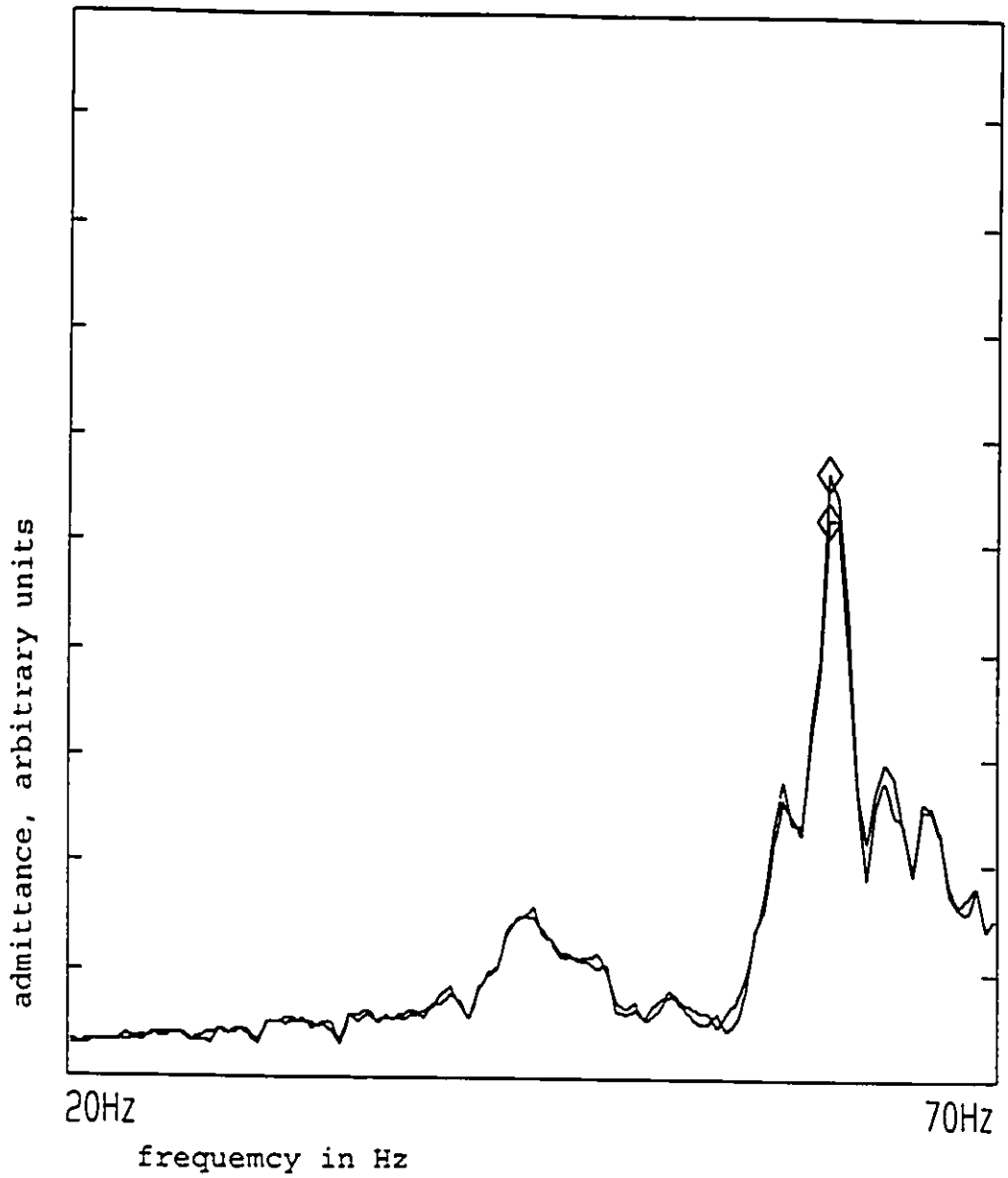

Figure 5.5: System Admittance Measured by Excitation with External Sound Source

Only this small part will excite the system, experience acoustic amplification in the loop and be reflected in the measurement at the loop transducer. This puts the use of the

piston internal pressure as a reference for the source term in question. However, no better reference pressure than that inside the piston can anywhere be found that relates in a more direct way to the acoustic source term.

Natural frequencies found by this method unfortunately depend on the particularities (piston size, instrumentation line length, location of excitation in the loop, signal form and amplitude) of the experimental arrangement in such a wide range that results from this method can not be considered very helpful.

5.1.4 Measurement of Acoustic Natural Frequency by Order Trekking of Pump Spectrum

Order trekking is a process of dynamically accelerating the pump shaft speed along a speed ramp of constant slope and observing the amplitude of a fixed multiple of the shaft speed (a fixed order) in each spectrum measured. The process is somewhat comparable to a swept sine excitation except, rather than computing the average of a spectrum over the whole duration of the sweeping process, the time history (equivalent to a graph of amplitude versus shaft speed) is recorded. Further, the excitation is not provided by an external source but by the pump itself. This mixes source and loop amplification effects together.

For the present experiments the shaft speed was ramped from 300 to 1300 rpm (BPF of 25 to 108 Hz) in a rpm triggered fashion with increasing and decreasing speed. The spectrum was calculated for 20 orders (100 Hz for 300 rpm to 433 Hz for 1300 rpm) with a frequency resolution of 0.1 orders (0.5 to 2.2 Hz). The critical information extracted from this data is the sampling time T_{sample}

$$T_{sample} = \frac{1}{\Delta f} \tag{5.7}$$

which amounts to 10 order^{-1} (2 to 0.5 s) or 10 over the shaft speed, n. With the number of cycles, n_c, given in a time interval by

$$n_c = T\, n\, n_B \tag{5.8}$$

This translates into 10 revolutions of the shaft per sample or with the number of blades, n_B, equal to 5 into 50 cycles per spectrum sample.

The minimal ramping rate that the controller hardware allowed for was 2 rpm/s so that a complete ramping process lasted about 500 s.

Figure 5.6 shows the order trekking trace obtained under the previously mentioned parameters.

Each of the traces shown in figure 5.6 for increasing and decreasing shaft speed show only one maximum. A second maximum corresponding tc a complete system resonance could not be detected, possibly because of the low number of cycles not

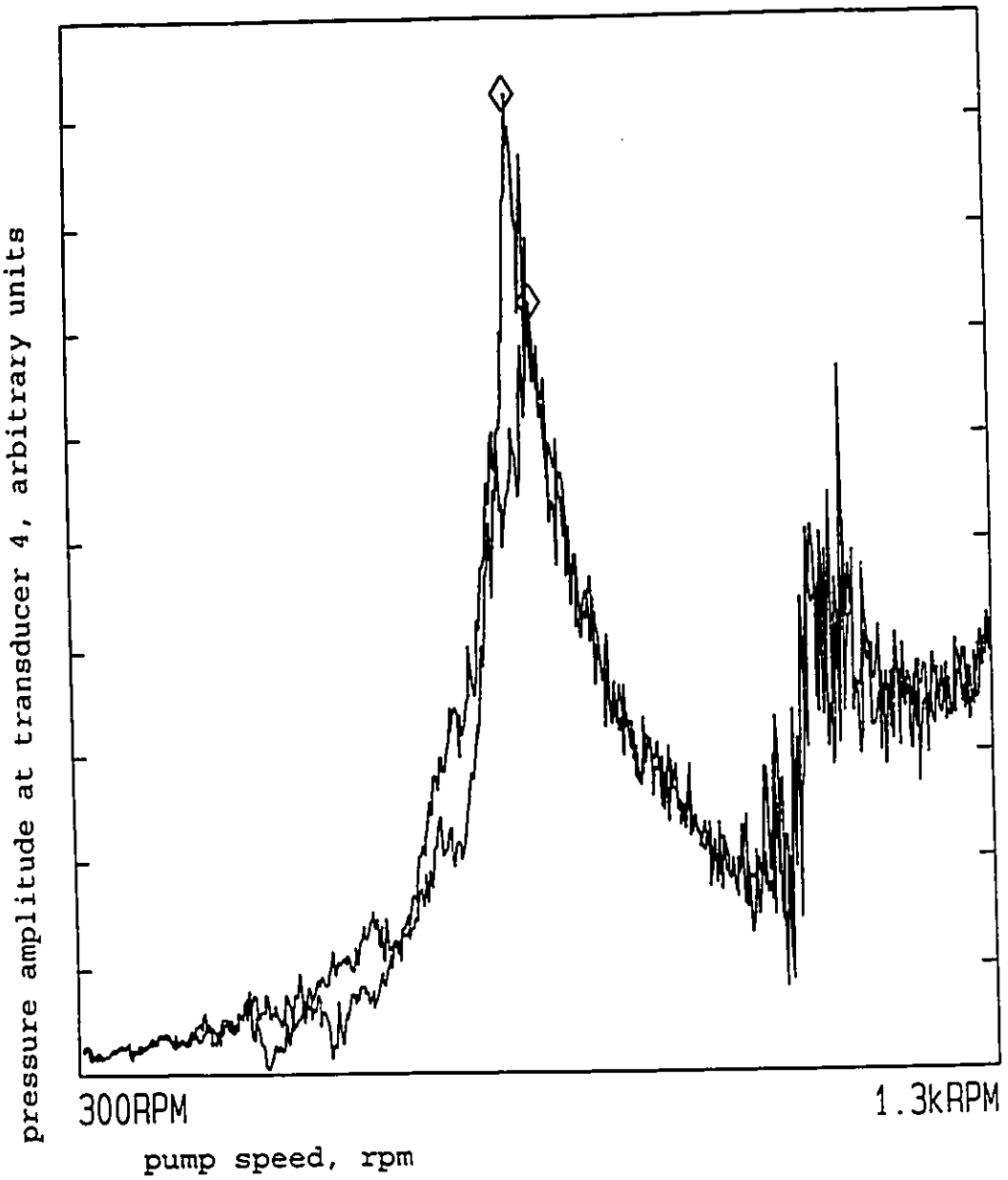

Figure 5.6: Order Trekking of Fifth Order (BPF) for Increasing and Decreasing Speed Ramping

being able to attain resonant amplitude. In the case of increasing shaft speed this maximum was at 804 rpm (BPF of 67Hz) and for decreasing shaft speed at 780 rpm (BPF of 65Hz).

The slight discrepancy in the resonant frequency was probably a result of the pump operation time of about 8 minutes between passing the resonance frequency with increasing and decreasing speed. In other experiments it was also observed that extended operation of the pump could cause a shift in natural frequencies. This occurred, especially, at higher flow rates where operation is associated with slight control valve cavitation and, where, therefore, fluid acoustic properties can change. As a consequence of this observation, a rigid scheme for conducting acoustic measurements on this test apparatus (short operation and defined down time) had to be established to ensure comparable and repeatable test data.

5.1.5 Comparison for Various Measurements of Acoustic Natural Frequency and Measurement Repeatability

The four different methods described for determining the acoustic natural frequencies show some discrepancy with respect to their results. Table 5.1 summarizes those results

To assess the reliability of each method their underlying assumptions need to be examined.

For the method by measurement of sound speed, the acoustically relevant pipe length of the system must be known which, in turn, depends on knowledge of the acoustic boundary conditions. These conditions might be slightly obscured by the

Table 5.1: Comparison of Methods to Obtain Acoustic Natural Frequency

	Complete System	Partial System	Ratio
Sound Speed (5.1.1)	51.7-53 Hz	57.5-59 Hz	0.90
Reflection Time (5.1.2)	55.6 Hz	65.1 Hz	0.85
External Excitation (5.1.3)	(45 Hz)	61 Hz	(0.74)
Order Trekking (5.1.4)	-	65-67 Hz	-

geometric details of transition from pipe to tank which takes place in steps from pipe diameter of 75 or 100 mm respectively to 150 mm and then by the dimensions of the tank bottom (about 1 by 7 m rectangular) and a free surface about 1 m above this transition. This geometry is due to a sliding seal design requirement on the pipe - tank transition for ease of assembly. The one-dimensional equivalent length or acoustic path length inside the pump is also only approximated by cartesian dimensions. However, the acoustical relevant pipe length is not considered to differ significantly from that length measured geometrically.

The reflection time method agrees well in the ratio between the partial and complete system response. So in that respect it supports the previous method. However, the frequencies are about 6 to 8 % higher, suggesting an

acoustically relevant pipe length of 12.360 to 12.131 m. A shortening of the acoustically relevant length from the measured length by 0.8 m is hard to justify on physical grounds.

The problem with externally excited acoustics is the wide range of frequencies that could be measured depending on the specific experimental parameters. This renders the method less useful for accurate calibration of pressure measurements.

Order trekking, requires some time and permits a shift in acoustic properties of the fluid during the extended operation period of the pump. Further, the controller ramping limitation produced a rather rapid sweep past resonance which could cause too few cycles at resonance frequency to produce steady state resonance amplitudes. This combined with the fact that the source location is coincident with the location of partial reflection of the system, might account for the absence of the complete system's resonance frequency in the spectrum.

The conclusion to be drawn from this discussionis that the sound speed measurement method (which is also supported by the reflection time method) is used as a calibration tool in ensuring the reliability of the Helmholtz number, the independent parameter of primary importance for the experimental work that follows.

5.2 Overview of Pressure Fluctuations

To obtain an overview of the behaviour of pressure fluctuations in the parameter domain of Helmholtz number versus relative flow rate, a single transducer method utilizing order trekking at finely discretized relative flow rates was employed. Since only pressure fluctuations from one transducer (transducer 4, located at the loop midpoint to reflect first mode resonance) were evaluated, no separation of hydraulic and acoustic components is possible with this method. Nevertheless, the method possesses the advantage of generating a large amount of data with a reasonable effort (in terms of acquisition and post processing time). To produce the same amount of information with the more refined procedure described in the subsequent section a time factor of about 50 to 60 is applicable, i.e. to produce the information content of figure 5.7 continuous data acquisition over a period of about 2 weeks (50 hours per week) would be necessary. During such an extended period major shifts in laboratory conditions could take place which would put the comparability of data in question.

Recognizing the limitations of the following figure, namely, the non-separability of hydraulic and acoustic pressure fluctuation and the drawbacks of a transient method described in the previous section, its chief merit is providing an overview over the trends in pressure fluctuation

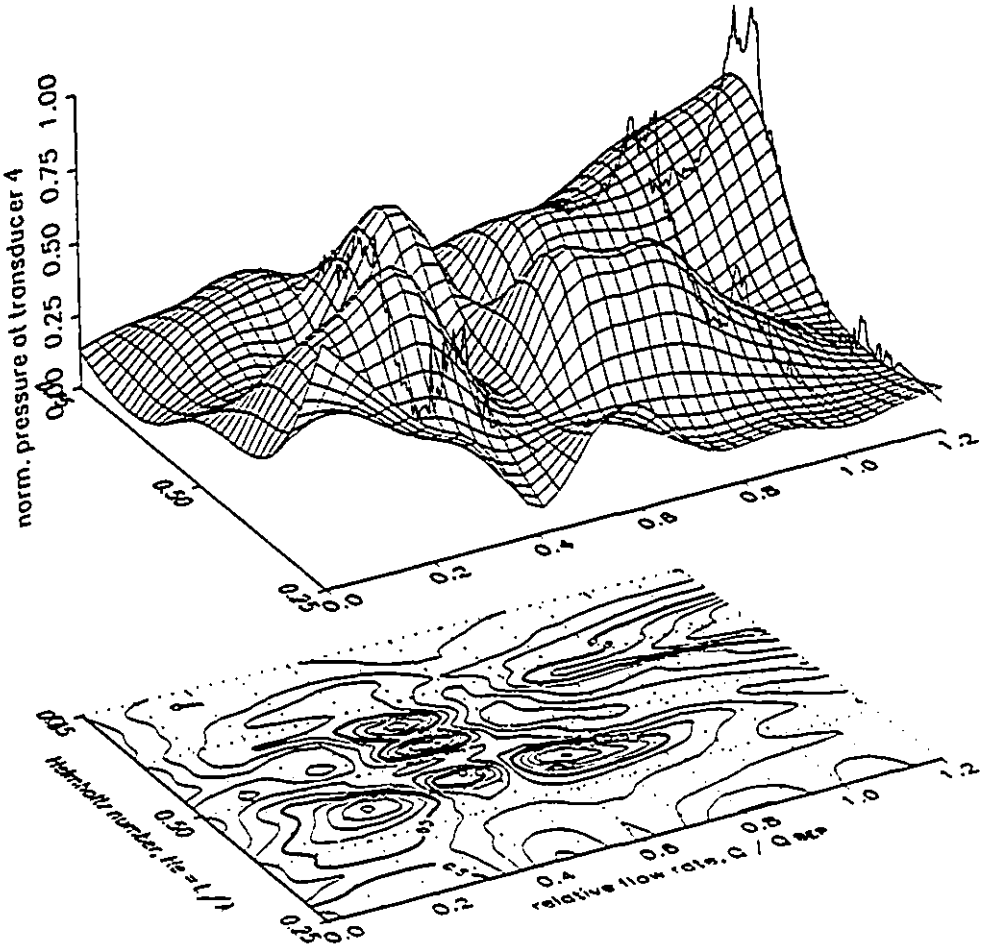

Figure 5.7: Overview of Pressure Fluctuations with Single Transducer Method

behaviour.

The upper graph in figure 5.7 shows the topography of pressure fluctuations in the flow rate - Helmholtz number domain where the lower graph translates the same data into a contour plot showing a projection of equal pressure fluctuation magnitude. Pressures are normalized with respect to the maximum occurring in the domain. The parameter

boundaries of the domain are, in the case of the relative flow rate, given by the test rig limits. The loop friction losses at fully open control valve allow for a maximum flow of about 125 % of nominal. The limit for the Helmholtz number range is determined by the consideration that the mid loop transducer only gives meaningful information about the maximum pressure encountered in the loop in the vicinity of a Helmholtz number equal to 0.5 where the first acoustic resonant mode shape is reasonably well approximated. As the Helmholtz number comes closer to unity the second resonant mode features a pressure node at this transducer and so the reading there looses its representative status for the maximum pressure encountered in the loop. Therefore, the parameter boundaries are chosen from 0.25 to 0.75 for the Helmholtz number.

Figure 5.7 reveals a complicated topography with multiple local pressure maxima and minima. The absolute maximum, occurs at the highest obtainable flow rate and a Helmholtz number of about 0.62. It seems fair to speculate that a further increase in pressure fluctuations would occur for flow rates higher than the relative flow of 125 % obtainable in the test loop (e.g. if the loop had lower friction or a negative elevation between a suction and a discharge reservoir supporting the flow). The other peaks present in the domain occur at Helmholtz numbers of about 0.42 and flow of 25 %, a forked peak at 0.57 and 0.52 and 45 % flow and another single peak at 0.44 and 65 % flow. The pattern

seems to alternate between a Helmholtz number of about 0.4 and 0.6 with increasing flow rate. The Helmholtz number of about 0.6 is consistent with the resonance of a partial system between pump and downstream tank. The peaks just above 0.4 do not come close enough to the value of 0.5, which would indicate a complete system resonance, to create high confidence in this explanation of their existence. Furthermore, no peaks in the Helmholtz number range around 0.4 showed up subsequently during more carefully controlled experiments. Therefore, the repeatability of such peaks has to be seriously questioned.

Cutting imaginary slices through the domain parallel to the Helmholtz number axis at, a relative flow of 40 %, 100 % and 120 % (corresponding to the more detailed investigation to follow in this chapter) shows pressure peaks for different Helmholtz numbers in each case. The measured traces at these flow rates are highlighted in the topology. At the low flow of 40 % one pressure fluctuation peak is encountered around a Helmholtz number of 0.52 to 0.57 and a second one, slightly lower in amplitude, below 0.5 at about 0.42. The first peak is consistent with a resonance of the partial system between pump and tank. The second peak of the trace seems to be the root of a mountain whose peak occurs at a Helmholtz number of about 0.42 and relative flow rate of about 25 %. Neither peak was observed in the more detailed measurements to follow (figure 5.9 a), but there the behaviour was dominated by a strong peak

at 0.25. However, the peak at the higher Helmholtz number is consistent with behaviour observed at higher flow rates. This discrepancy in behaviour may be due to a shift of fluid properties caused by the transient nature of the measuring technique. The difficulty in controlling the fluid acoustic properties during extended operation periods of the pump is the same as for the order trekking measurements mentioned in a previous section. Therefore, no further confidence in the presence of the peak at 0.42 (and the one at similar Helmholtz number of 0.44 and a flow of about 60 % to 80 %) could be gained by the more refined measurements.

The trace at nominal flow again features two peaks. Here, clearly, the one around 0.6 is dominant, a dominance of the partial system resonance. This observation will be later confirmed.

At the high flow of 120 % only a single peak at about a Helmholtz number of about 0.62 exists. This is the peak dominating the whole domain. Now, only a partial system resonance takes place and a second peak persists.

Slicing the topography parallel to the flow axis reveals pressure fluctuation behaviour as a function of relative flow rate. Expectations from conventional wisdom suggest a minimum of the pressure fluctuations at nominal flow rate or best efficiency point (BEP). This point of view is questioned by the data in figure 5.7. For different Helmholtz numbers the flow of least noise generation was found anywhere

between 80 % and 120 % of nominal flow with local minima sometimes as low as 20 % to 40 % flow.

As a matter of fact, a strict coincidence between nominal flow and a minimum in sound generation can not necessarily be expected because the acoustic power generation is not related in a direct way to the hydrodynamic pump loss. To illustrate this fact, the hydraulic power of the pump flow is compared with the acoustic power at nominal flow and resonance for the geometry 1B. The hydraulic power P_{hyd} based on a flow rate Q of 12.73 l/s and a hydraulic head Δp of 651mbar is given to

$$P_{hyd} = \rho g Q H = Q\,\Delta p \approx 830W \tag{5.9}$$

and the acoustic power P_{ac} with an acoustic pressure fluctuation p_{ac}' of 18 mbar, a sound speed c of 1353 m/s and a cross sectional area of the pipe A of 4.42e-3 m^2 as the product of intensity I and cross sectional area A to

$$P_{ac} = I\,A = \frac{p_{ac}'^{\,2}}{\rho c}\,A \approx 10.6mW \tag{5.10}$$

Now it becomes evident that, when the pump efficiency is in the neighbourhood of 70 % and the acoustic power constitutes only 0.0013 % of the hydraulic power, the acoustic power is a negligible fraction of the pump power. Nevertheless, an inefficient pump can be expected to be noisier due to the reliance of the acoustic far field on the generating region of the near field (in particular the cut-water region). So the

noise generated can be seen as an indication for losses, though it is not a major loss factor. Since no linear relation between energy losses and generated noise can be expected the coincidence of minimum loss (maximum efficiency) and minimum noise is only a likely not a necessary coincidence.

In summary, not all information extracted from figure 5.7 was confirmed by the more carefully controlled experiments and by the subsequent evaluations of acoustic mode shapes reported in the following sections. However, the potential for fundamentally different behaviour at different relative flow rate was demonstrated by the presented experimental data and could be substantiated by further experiments. The results shown in figure 5.7 draw one's attention to the fact that a potential of multiple resonant peaks exists for some flow rates and emphasize how complicated the topography can be. Further, the conventional assumption of least sound generation at nominal flow conditions needs further examination.

5.3 Influence of Excitation Frequency on Acoustic Pressures

In principle, the influence of varying frequency on the acoustic pressure fluctuation amplitude can be obtained by a cross sectional slice through the previous topography.

However, to obtain a clearer picture of the purely acoustic pressures without the contamination by the

fluctuations of hydraulic nature a multi-step method had to be applied. A pressure spectrum was obtained by Fast Fourier Transform (FFT) from a pressure time history. The data acquisition parameters were 60 s sampling time and 512 Hz sampling frequency resulting in a spectrum averaged over 60 FFTs of 1024 lines from 0 to 200 Hz and a resolution of 0.5Hz. The need for analog filtering of the signal was investigated but it was found that over sampling provided sufficient safeguard for aliasing problems. Then the pressure peak at BPF was extracted. Through application of the semi-empirical numerical model of spatial distribution an acoustical pressure amplitude was obtained. This acoustic pressure was normalized with the maximum amplitude of the acoustic mode shape and, hence, represents the maximum acoustic pressure encountered in the piping system. For meaningful plots, a normalization by the hydrodynamic head

$$p_u = 1/2\ \rho\ u_T^2 \tag{5.11}$$

based on the impeller tip speed u_T was necessary because a change in the Helmholtz number was automatically coupled to the pump head or pressure level. This is so since the loop length as well as the sound speed are kept constant while the BPF, the means of tuning the loop, is obviously directly proportional to the shaft speed. Preference was given to the impeller tip speed as a velocity scale over, for example, the mean flow velocity in the pipe because it probably relates

better to the velocities in the local flow field that generates the sound.

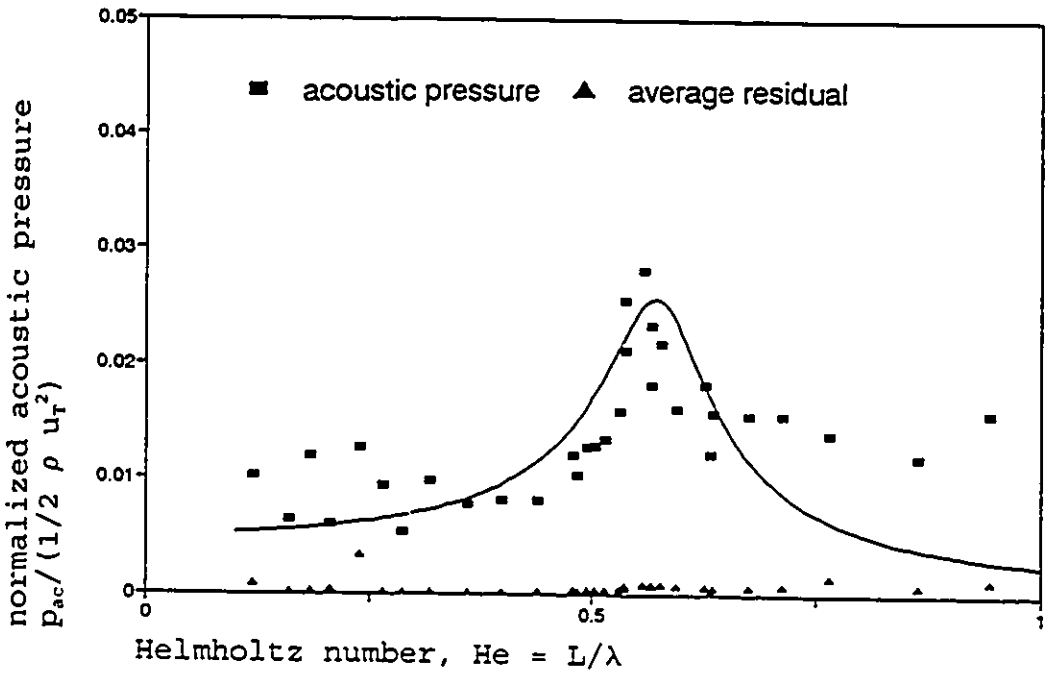

Figure 5.8: Dependency of Acoustic Pressure on Helmholtz Number for Two-Dimensional Geometry 1B at 120% Flow

Figure 5.8 shows the relation of the acoustic pressures obtained by this method versus the Helmholtz number for the case of a sharp tipped two-dimensional geometry at 120 % flow (filled squares).

Filled triangles represent the average residual of the numerical model applied to extract the acoustic - hydraulic separation which is also normalized by the hydrodynamic head p_u. The residual can be seen to be rather insignificant and

only assume slightly larger values in the higher Helmholtz number range beyond 0.75. This also coincides with the somewhat erratic behaviour of the acoustic pressures. The grounds for this behaviour lay in the cavitation of the control valve. Cavitation is characterised by sound generation through bubble collapse. This raises the overall noise floor and contributes to pressure fluctuations measured at all transducers. Residuals rise because the model, obviously, does not include a second sound source located downstream of the pump at the control valve close to the tank inlet. Therefore, the model fits the data less well.

To emphasize the resonant Helmholtz number a curve corresponding to the admittance of a simple harmonic oscillator is graphed in figure 5.8 (solid line). Of course, the assumption is not that this system should behave exactly like a harmonic oscillator but only that this class of functions can serve well to illustrate the resonant behaviour. This line should not be viewed as anything more than a visual aid helping interpret the data. Only the resonant Helmholtz number from this numerical least square curve fit is of interest.

The resonant peak found for this set of data is at a Helmholtz number of about 0.57 not 0.5 as would result from a resonance of the whole system. The larger Helmholtz number corresponds to a shorter length of pipe or a higher natural frequency. The ratio of the two associated natural frequencies

is 0.88 and corresponds, as seen in the previous sections to the ratio between the natural frequencies of whole and partial acoustic systems. The partial system is then characterised by the pump acting as a volume expansion, a pressure release surface or a pressure antinode. This is confirmed by the spatial distribution of the fluctuating pressures and the good fit of the acoustic - hydraulic model.

5.4 Influence of Pump Flow Rate on Acoustic Pressures

In this section the influence of flow rate on the acoustic pressure fluctuations is illustrated by comparing data for relative flow of 40 % of nominal, nominal and 120 % flow. The pump geometry selected is the two-dimensional cut-water with sharp tip, 1B, because the sensitivity of the acoustic pressure to a change in flow rate is most significant for a sharp tipped cut-water geometry. There the point of separation is distinctly defined. No separation point movement with instantaneous blade position takes place and the separated region switches from the discharge to the recirculation side of the pump cut-water for a change in relative flow. This behaviour will be further discussed in the following chapter on flow visualization.

Figure 5.9 shows acoustic pressure plotted against Helmholtz number for three different flow rates. Data in each

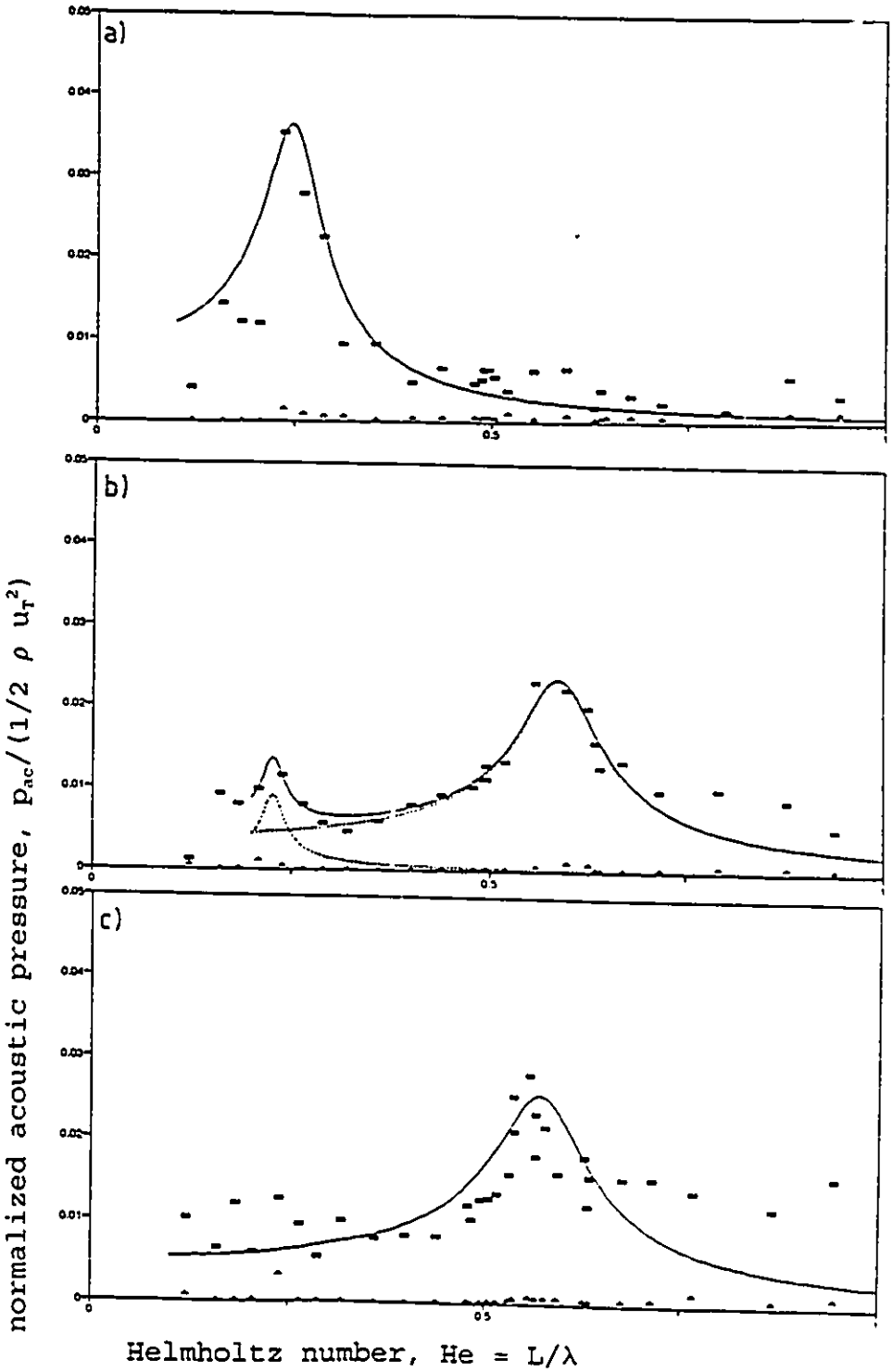

Figure 5.9: Dependency of Acoustic Pressure on Flow Rate: a) 40 % Flow, b) 100 % Flow, c) 120 % Flow

graph is presented in the same form as figure 5.8 and was obtained in an identical manner.

Figure 5.9 c) was discussed in the previous section as figure 5.8. The main feature of the graph is a single peak at a Helmholtz number of 0.57 that stands for a partial system resonance.

Figure 5.9 b) was obtained under the condition of nominal flow rate. The peak indicating a partial reflection at the pump is also dominating the picture and occurs at about 0.59. This value is also in reasonable agreement with the interpretation of a partial system resonance and the range of 0.57 to 0.59 remains typical for all measurements with two-dimensional geometries.

An interesting feature of the graphs for nominal and 40% flow is the existence of a peak at the Helmholtz number of 0.25. This peak even dominates the picture (p_{ac}/p_u = 0.036) for 40 % flow while it is present to a lesser degree for nominal flow. As seen before, at the high flow rate of 120 % the 1/4 wave length peak does not appear at all and only the one peak typical for partial system resonance persists.

The following is an attempt to explain this peculiar behaviour. First the argument is presented why the explanation can not be based purely on acoustic amplification. Then the possibility of a source change is discussed.

What makes this 1/4 wave peak an abnormality is that in the theoretical framework of acoustic amplification by a one-

dimensional system its presence could only be permitted by a combination of closed and open - end boundary conditions for the system. Either the downstream, the upstream tank inlet, or the pump would need to assume acoustically the role of a closed end. The resonant Helmholtz numbers change only under these mixed boundary conditions to

$$He_n = (2n - 1)\ \frac{1}{4},\ n = 1,\ 2,\ 3,\ \ldots \tag{5.12}$$

Considering, that the associated acoustic mode shape for the first resonance would also change from a half sine to a quarter sine wave with a pressure antinode at the closed end and a pressure node at the open end, we are left with two possible explanations. Either the downstream end or the pump must act as a closed end with a pressure antinode.

It is known from no-flow experiments that the partial closing of the control valve, that is necessary to decrease the flow to 40 %, does not change the type of acoustic boundary condition from open to closed. So this element is not a likely location for a closed end condition or pressure node which leaves the pump as a potential pressure antinode.

The observed spatial pressure distribution (figure 5.10) at the Helmholtz number of 0.25, corresponding to 40 % flow, is an almost perfect half sine with certainly no pressure antinode at the pump.

The train of thought presented so far excludes an

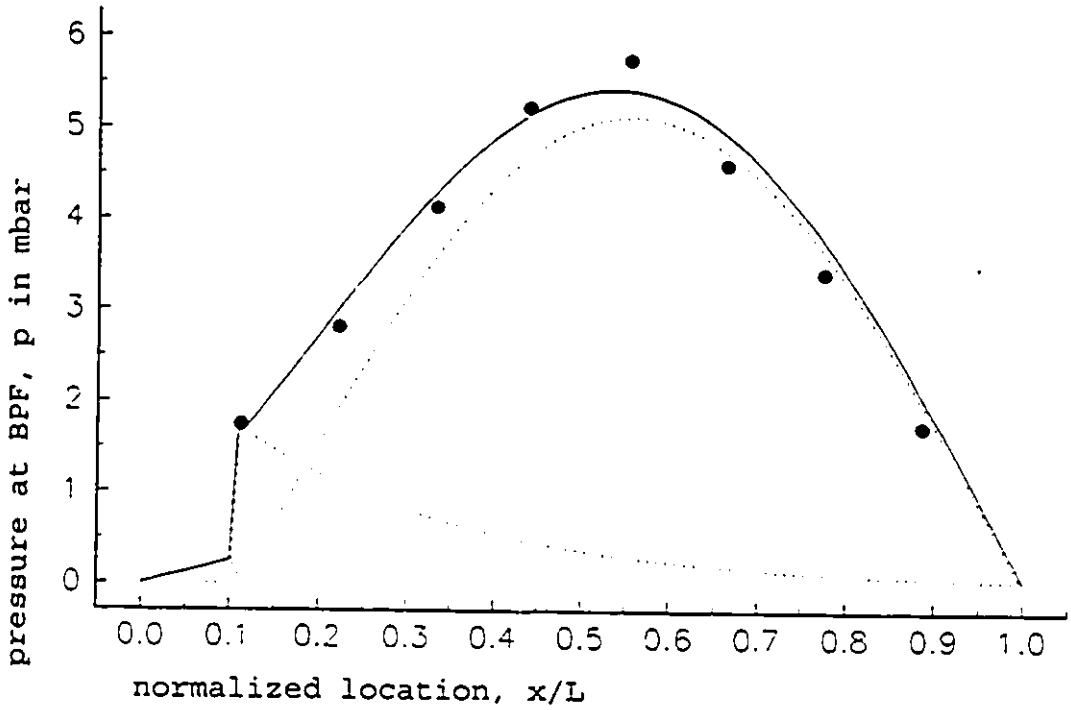

Figure 5.10: Spatial Pressure Distribution for Two-Dimensional Geometry 1B with 40 % Flow at Helmholtz Number of 1/4

explanation based on a purely acoustic amplification. Therefore, explanation has to be sought in a change of source type and strength as the cause for the peak in the presented data. The hypothesis follows that follows from this is that the pump acts as a velocity source (pressure node, acoustic dipole) at low relative flow rates. The peak at a Helmholtz number of about 1/4 is no acoustic resonance. Rather, to produce a peak in this Helmholtz number range a strengthening of the acoustic source term has to take place (under the assertion that the acoustic damping of the system does not

change).

The presented acoustic - hydraulic model is, strictly speaking, not designed to capture the source behaviour of a dipole. Nevertheless, the observed mode shape can be captured by the model because no limitations are imposed on the frequency parameter and the observed mode shape is very similar to one that occurs normally (model with pressure antinode at source) at a Helmholtz number slightly beyond resonance (0.5). Of course, the frequency parameter of the model is no longer meaningful because the natural frequencies now occur at different values than for a system with a pressure node at the pump. However, the acoustic pressure amplitude retains its validity.

At higher relative flow rates the pump again acts increasingly as a pressure source (pressure antinode, acoustic monopole) and in combination with the high degree of reflection at the pump the peak at a Helmholtz number of 0.57 to 0.59 dominates the graph. At intermediate flow rates (up to about nominal flow) a mixed source behaviour is observed with both resonant peaks present.

The argument presented so far is conclusively pointing to a dipole source type at low flows when a 1/4 wave peak is encountered. Additional experimental evidence for a dipole source would be a 180° phase shift between pressure measurements upstream and downstream of the pump (while monopole pressure are expected to be in phase). Unfortunately,

measurements just upstream and downstream of the suction and discharge flange of the pump respectively produced in the whole Helmholtz number range only in-phase behaviour. However, considering that for the 40 % flow case the acoustic pressures at the pump feature a pressure node, while the mean flow being so far off nominal produces a lot of hydraulic noise, it is not too surprising that the phase measurements were not successful.

Therefore, in spite of not being able to produce the final evidence of phase shift, the acoustic mode shape is viewed as sufficient confirmation of the hypothesis that a source change from a monopole to a dipole takes place at low flow rates for the sharp tipped cut-water geometry.

Figure 5.11 summarizes the flow rate dependency of the acoustic pressure peaks. As described the dominant peak of a graph shifts from a peak at a quarter wave length for low flow to a one at a Helmholtz number of 0.57 to 0.59 representing partial reflection at the pump for high flow. The combined behaviour shows a decrease in acoustic pressure generation from a value of about 3.6 % of the hydrodynamic head at 40 % flow to 1.4 % at nominal flow followed by another increase to 2.8 % at 120 % flow.

Obviously, the acoustic pressure generation needs to be supplied with energy which must be associated with hydraulic losses in the pump. This general trend, that a minimum in acoustic noise occurs close to an efficiency maximum, which is

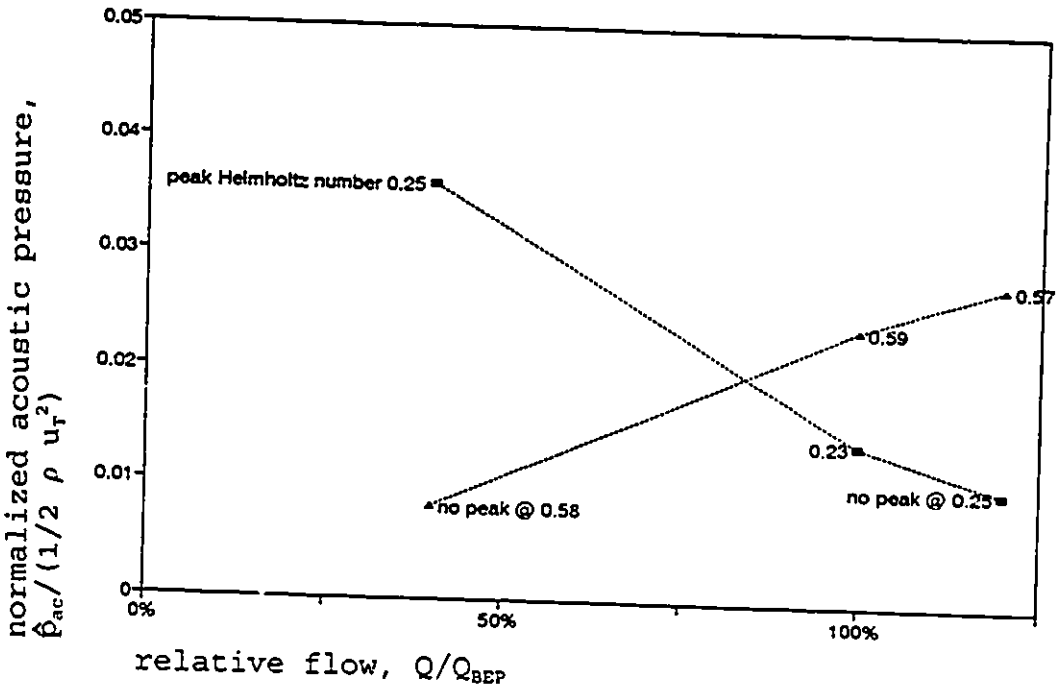

Figure 5.11: Dependency of Acoustic Pressure on Flow Rate for Two-Dimensional Geometry 1B

again close to the nominal operating point, is confirmed by the data. This demonstrates the argument that there is a high likelihood of coincidence between BEP and point of minimum sound generation.

5.5 Influence of Cut-Water Geometry

In the following section the dependency of acoustic pressure pulsations on cut-water geometry is presented. The cut-water geometry was selected for modification because of its great potential for significantly influencing sound

generation. Notably, the tip radius of the cut-water could be altered without changing the gap between the impeller tip and the cut-water. Hence, the effect of changing the cut-water radius may be determined independently of the impeller tip to cut-water gap, another important design parameter. The latter has been studied previously and changing the acoustic performance by increasing the impeller gap must be paid for by significant hydraulic performance alteration. As a matter of fact "trimming" the impeller without changing the casing is common practice in generating, with minimum effort, a modular series of pumps with different hydraulic characteristics (and efficiencies).

The first section deals with a comparison of hydraulic head versus flow rate curves measured for the different geometries, followed by a section that summarizes the geometry effects on the acoustic pressure fluctuations.

5.5.1 Influence of Cut-Water Geometry on Hydraulic Characteristic

Figure 5.12 shows for the investigated geometries the hydraulic characteristic of head coefficient

$$\Psi = \frac{\Delta p}{1/2\ \rho u_T^2} \tag{5.13}$$

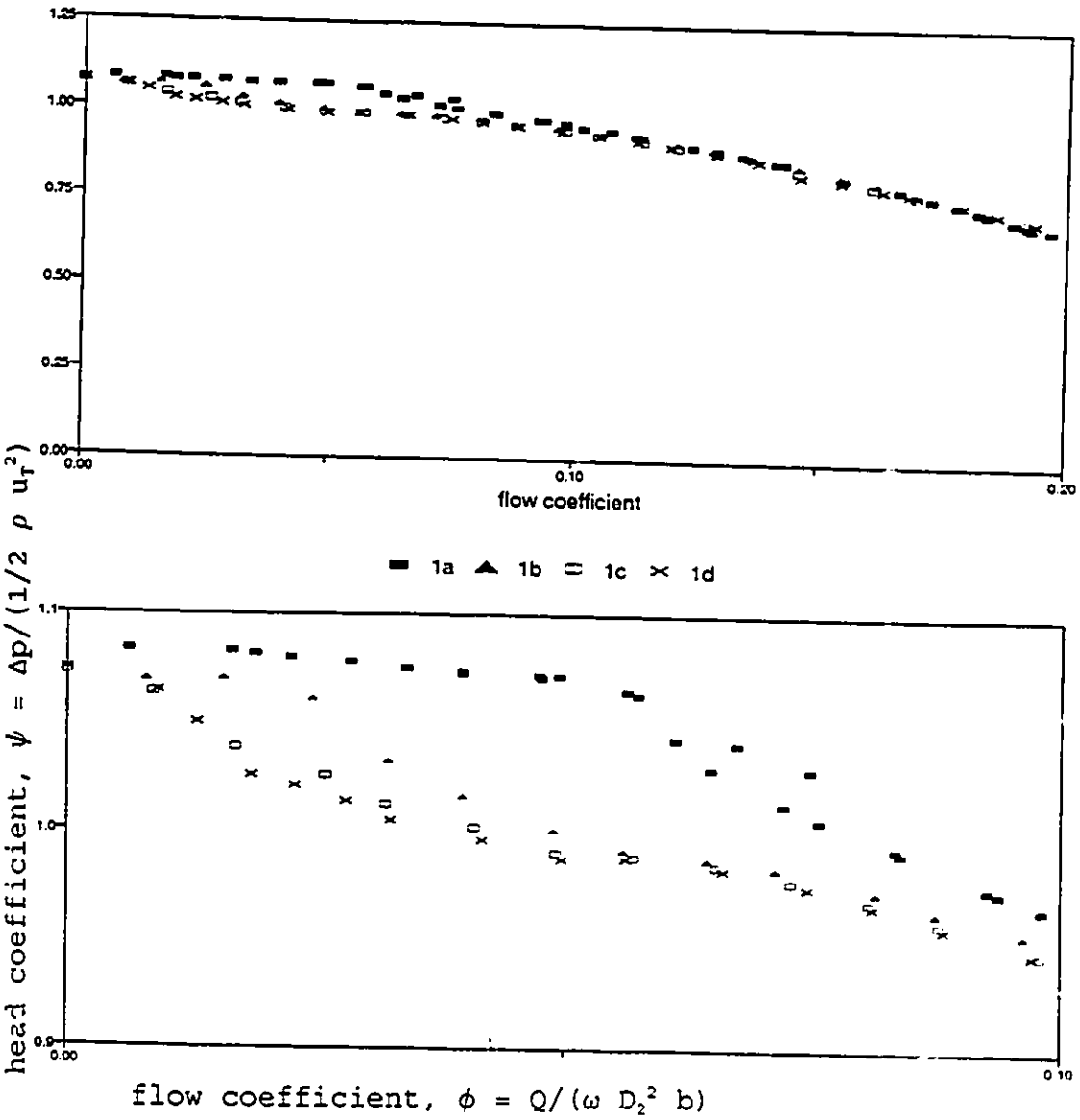

Figure 5.12: Hydraulic Characteristic for Different Cut-Water Geometries: 1A - Original Shape, 1B - Sharp Tip, 1C - 2.5 mm Tip Radius, 1D - 5 mm Tip Radius

versus flow rate coefficient

$$\Phi = \frac{Q}{\omega D_2^2 \, b} \tag{5.14}$$

where Q is the flow rate, ω the shaft speed, D_2 the impeller exit diameter, b the impeller passage width at exit, Δp the pump head corrected for pressure tap elevation and difference between flow speed in suction and discharge pipe, ρ the fluid density and u_T the circumferential speed of the impeller tip. The upper graph gives the overview in the whole parameter domain while the lower graph zooms in on the low flow rate region.

The change in tip radius and even the two-dimensionalization of the cut-water region shows a very small effect on the hydraulic characteristic. The latter is, on first sight, surprising since the flow transition to a two-dimensional cross section is typically associated with more hydrodynamic losses due to a greater potential for flow separation. However, it should be noted that the original three-dimensional volute shape seemed to be optimized not at all for hydraulic performance or smooth transition. So it may be that the two-dimensional cut-water shape in combination with a careful fairing of the transition is producing less potential for flow separation and hydraulic losses. Furthermore, the effect of machining part of the spiral casing is to produce a smoother surface finish as opposed to the original rough cast surface. Especially around the nominal operating point, the changes to the characteristic are insignificant to a point where they are not distinguishable from the measurement uncertainty.

In the low flow rate region it can be observed that the original characteristic features a slight discontinuity, called a "hook" around a flow coefficient of 0.055. For this pump, the hook is of very minor magnitude. Generally, these hooks are undesirable since they lend themselves, in connection with certain hydraulic system characteristics, to pumping instability, i.e. low frequency, large flow rate oscillations. The hooks in the two-dimensionalized geometry characteristics are all found at substantially lower flow coefficients and shift even more towards low flows with increasing tip radius. This behaviour was not investigated further.

5.5.2 Influence of Cut-Water Geometry on Acoustic Pressures

The modification from a three-dimensional pump casing to a two-dimensional one has, opposed to initial expectations, lowered the observed maximum sound levels somewhat. An explanation for this is based on the initial shape not being hydraulically optimized and then being replaced by a carefully faired two-dimensional cut-water shape. Additionally, the smoother wall surface produced by machining the casing partly contributed to a quieter pump.

In the representation of acoustic pressure versus Helmholtz number for the three investigated two-dimensional

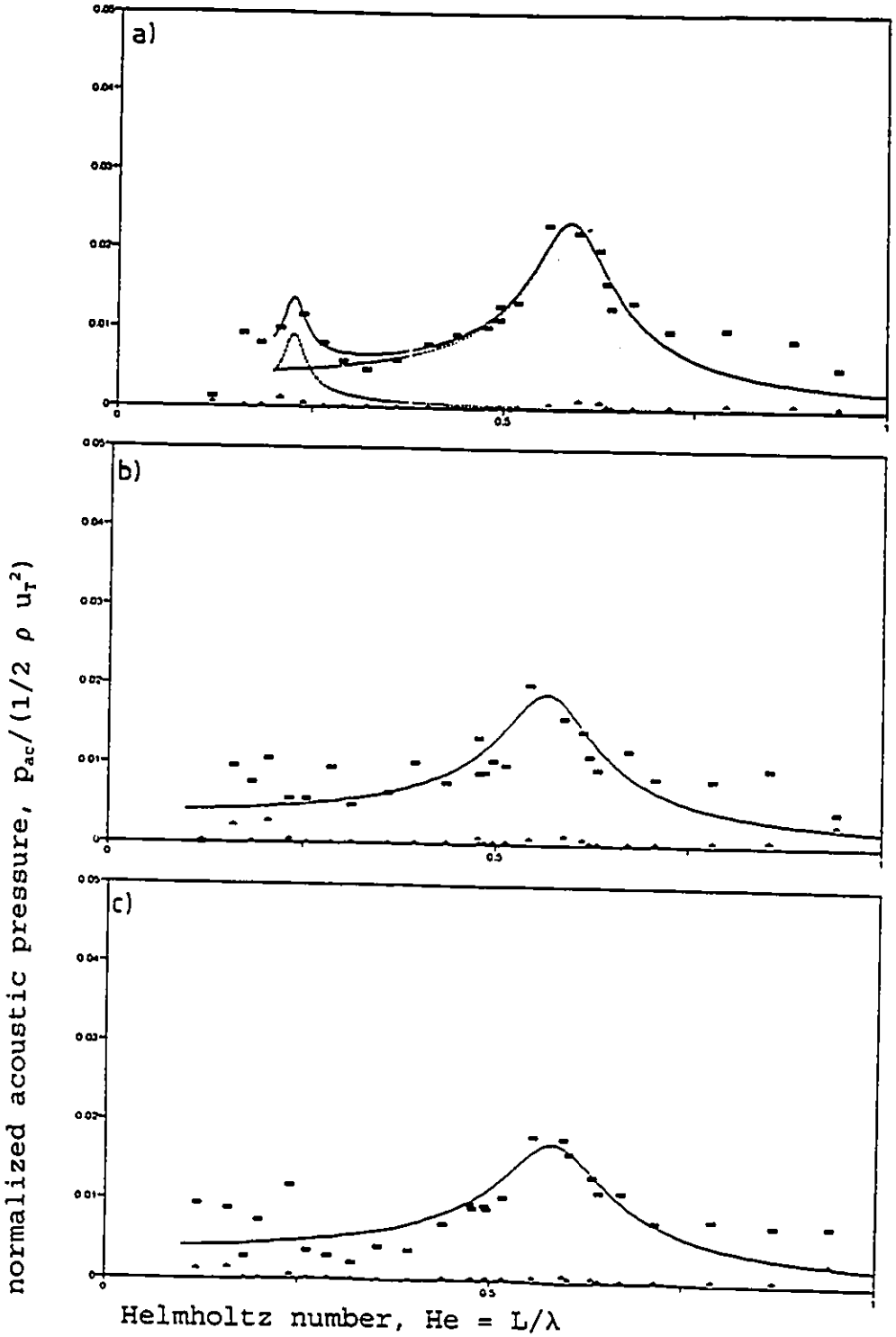

Figure 5.13: Dependency of Acoustic Pressure on Geometry: a) 1B - Sharp Tip, b) 1C - 2.5 mm Tip Radius, c) 1D - 5 mm Tip Radius

geometries (figure 5.13) at nominal flow the occurrence of multiple peaks was most pronounced for (and possibly exclusive to) the sharp nosed geometry. (Certainly no other geometry except the sharp tipped one displayed a dominant 1/4 wave length peak at any flow conditions) However, in all cases the peak produced by partial reflection at the pump was the dominant one of the spectrum and occurred between a Helmholtz number of 0.57 and 0.59. The peak amplitude decreased from 2.4% of the hydrodynamic stagnation pressure at the impeller tip for the sharp cut-water tip to 1.9 % for the 2.5 mm radius and further to 1.7 % for the bluntest tip of 5 mm radius.

In terms of fluid mechanics, the meaning of a sharp tip is a clearly defined point of flow separation while a blunter nose allows for a moving of the stagnation and separation points. The mean position of the stagnation point on a rounded cut-water tip is determined by the relative flow rate. Additionally, it also changes during each cycle, i.e. the passing of an impeller vane past the tip, due to impeller casing interaction. Furthermore, the presence of the sharp nose is more prone to flow separation in the first place in the case of only slight discrepancies of flow field and geometric boundary.

Hence, the concept of flow separation, vortex growth and shedding as the mechanism for generation of blade pass noise is consistent with the observation of stronger acoustic pressure fluctuations for a sharper cut-water tip radius.

Table 5.2: Summary of Acoustic Pressure Peak Amplitude for Various Flow Rates and Geometries

Flow	Geometry 1B	1C	1D
40 %	3.6% @ 0.25*)	-	1.6% @ 0.23 1.5% @ 0.53
100 %	1.4% @ 0.23 2.4% @ 0.59	1.9% @ 0.57	1.7% @ 0.59
120 %	2.8% @ 0.57	n/a	n/a

*) reads: maximum acoustic pressure in spectrum is 3.6 % of hydrodynamic head based on impeller tip speed at a Helmholtz number of 0.25

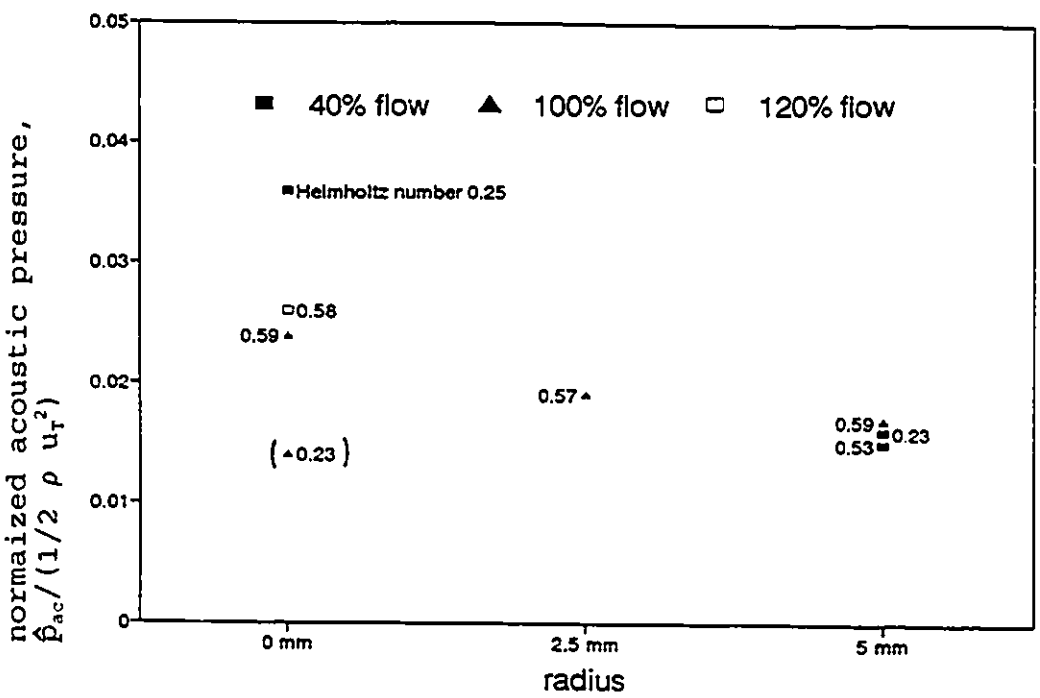

Figure 5.14: Summary of Acoustic Pressure Peak Amplitude for Various Flow Rates and Geometries

From the summary of measured acoustic pressure peak amplitudes two principal conclusions can be drawn.

First, for a sharp cut-water tip the sensitivity to flow rate changes is stronger then for blunter noses expressing itself in a wider band width (from 1.4% to 3.6%) of possible acoustic pressure amplitudes. The Helmholtz numbers associated with the peaks are either that of a partial reflection or that corresponding to a source change at 0.25. Considering only the absolute maximum of each spectrum and so eliminating the lowest shown peak value for geometry 1B (1.4% at a Helmholtz number of 0.23 for nominal flow) the range is still from 2.4 % to 3.6 %. Opposed to this large span for the bluntest nose of 5 mm radius (geometry 1D) it is reduced to 1.5 % to 1.7 % demonstrating a much lesser dependency of acoustic pressure on flow rate.

Second, a trend to lower acoustical pressures for a blunter nose is observed at all flow rates. In a comparison of three geometries at nominal flow the acoustic pressure decreases from 2.4 % to 1.7 % and in the 40 % flow case even as much as from 3.6 % to 1.6 %.

CHAPTER 6: FLOW VISUALIZATION IN CUT-WATER REGION OF PUMP

"God could cause us considerable embarrassment by revealing all the secrets of nature to us: we should not know what to do for sheer apathy and boredom."
Johann Wolfgang v. Goethe, early 19th century

Visualization of the flow in the cut-water region of the pump is a major tool to link the flow regime in the hydrodynamic near field to the pressure fluctuations in the far field reported in the previous chapter. In particular, the observation of cyclic vortex formation and motion, including information on size and phase of the eddies, in the source region inside the pump is the goal of flow visualization in the context of this research.

This chapter starts by describing in section 6.1 the methodology used for flow visualization. In section 6.2 the flow field below nominal flow is described, followed by a flow field description at higher than nominal flows in section 6.3. In section 6.4 the correlation between flow observations and acoustic pressures at various resonance conditions is provided. Finally, in section 6.5 the influence of a larger cut-water tip radius on the flow field is discussed.

6.1 Methodology of Flow Visualization

Flow visualization is a technique successfully employed for centuries, particularly for flows of low Reynolds numbers where the detailed flow structures of vortices can easily be seen forming and shedding.

Flow visualization consists mainly of three components: the lighting, the tracer to make the flow visible and the recording to preserve images for documentation.

Higher Reynolds number flows (i.e. flows that are typically highly turbulent where flow processes happen rapidly and vortex behaviour gets more complicated) encounter problems with all three components: First, a short exposure time of photographic devices requires high light intensity and good reflection from the tracer. Second, the tracer, especially liquid dyes, experiences fast diffusion in the flow with an associated decrease in concentration and light scattering. And third, the recording system needs to allow for high shutter speed or frame rate of the camera to catch the rapid sequence of events.

For lighting purposes the initial attempt to collimate light from a 1500 W halogen lamp by means of an optical system of cylindrical plano convex lenses into a thin light sheet was soon abandoned because of the poor emission characteristics of the source. Instead, two 300 W projector light bulbs in

combination with two slotted (1.6 mm and 3.2 mm) sheet metal screens were used. The resulting light sheet (1.6 mm and 3.2 mm thickness at inlet) was introduced through an acrylic window to illuminate the centre plane of the cut-water region. A light intensity deficit necessitated a widening of the slits to obtain presentable images.

The casing inside and impeller face were coated in matt black to reduce background light scatter. To have an indication of the instantaneous impeller blade position a segment of the top shroud corresponding to the blade exit thickness was made reflective with an aluminium paint. A second light source from the top was used to make the shroud reflection visible, but had to be screened out from the flow field region to avoid undesirable reflections.

The light reflections due to the curvature of the original three-dimensional viewing window did not allow for flow observation close to the cut-water wall. Therefore, a two-dimensionalization of the cut-water region was undertaken. Figure 6.1 shows the assembly of the two-dimensionalized casing.

In the context of a coloured liquid flow tracer there are three parameters of importance: fluid type, bleed location and bleed rate. For the fluid the relevant criteria are visibility (even more so for the recording system than for the naked eye) and, in this work due to high turbulence levels, the diffusivity of the dye. Regular drawing ink [ae] was first

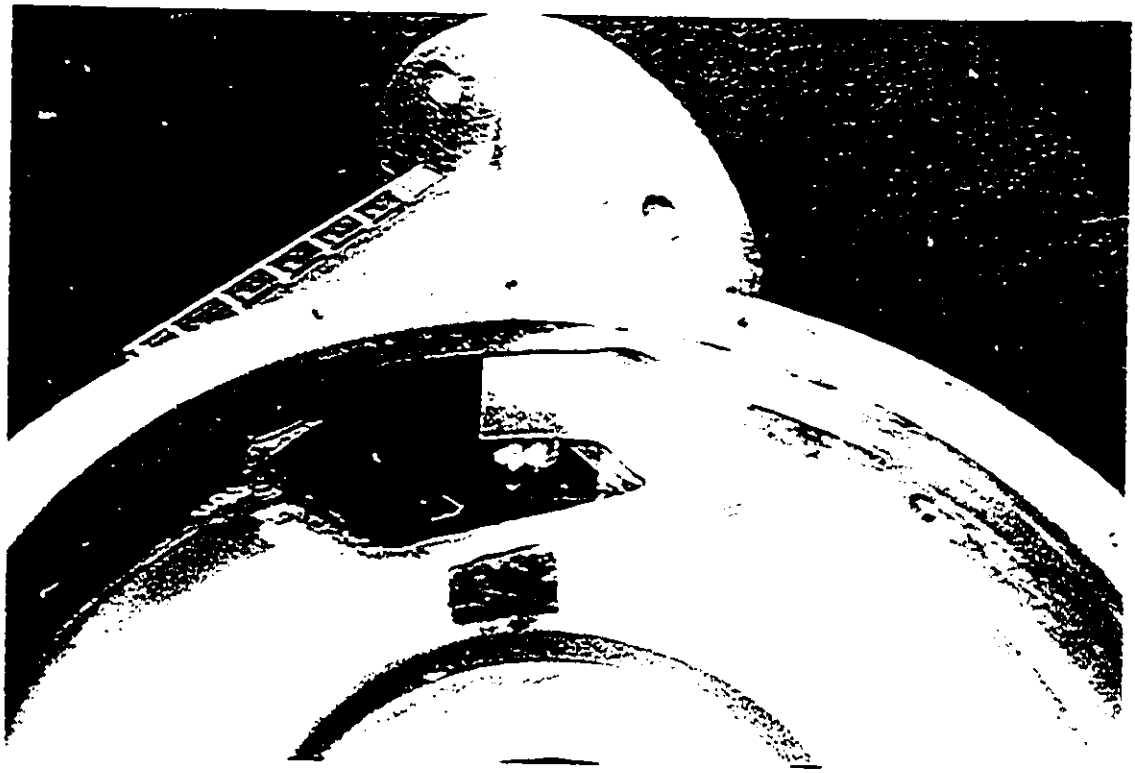

Figure 6.1: Photograph of Two-Dimensionalized Casing

attempted, but proved to disperse to quickly and provided only a poor contrast. Successful visualization was achieved with a mixture of 10 % water solution of fluorescein [ad], a green fluorescent dye, and 90 % milk ("half-and-half-cream") that suppressed the dispersion sufficiently. However, due to practical concerns regarding contamination and fouling leading to the plugging of the fine bleeding nozzle and to deposits on the pump casing walls, a different solvent for the flourescein was needed. Walker, in a paper on flow rate measurement (by an optical concentration method [85]) reported the strong ph-dependent properties of flourescein. He cited an optimum fluorescence at ph 8.5 and above. For this reason a water

solution of sodium carbonate and sodium hydrogen carbonate was used to buffer the tracer fluid at ph 10. Diffusivity was slightly compromised in comparison with the milk solution, but organic fouling was averted thereby.

The bleed location for the sharp edged geometry B was chosen as the tip of the tongue. This bleed location coincides with a well defined separation point. For manufacturing reasons a small flat of 1.6 mm diameter had to be milled before the bleeding hole of 0.46 mm diameter (number 77 drill) could be drilled. This bleeding nozzle connects to a feeding channel of 3.2 mm diameter. This, in turn, was connected with a medical LUER-LOK fitting and hypodermic tubing to a medical syringe of 30 ml volume. This syringe was expressed at a constant flow rate by a mechanical spindle driven by a small, speed controlled, geared down dc motor. The compromise necessary in optimizing the feed rate consists in not disturbing or altering the original flow while bleeding enough tracer into the flow to make it visible. Once the best bleed rate was found for one pump operating speed it was scaled with respect to the pump flow rate to maintain a fixed ratio of feed rate over flow rate. Otherwise changes in the appearance of the flow picture could artificially be introduced by a change in relative bleed flow.

The recording system was a Kodak Ektapro black and white high speed video camera system [ab] and motion analyzer system with a maximum frame rate of 1000 frames per second

(fps) of full size. Memory capabilities were installed for 409 frames (0.409 s maximum recording time at full speed).

The sensitivity to coloured light of the system is highest in the green spectral range (see Appendix A) providing for a good compatibility of flourescein as tracer pigment and the recording system. Figure 6.2 shows the video signal path.

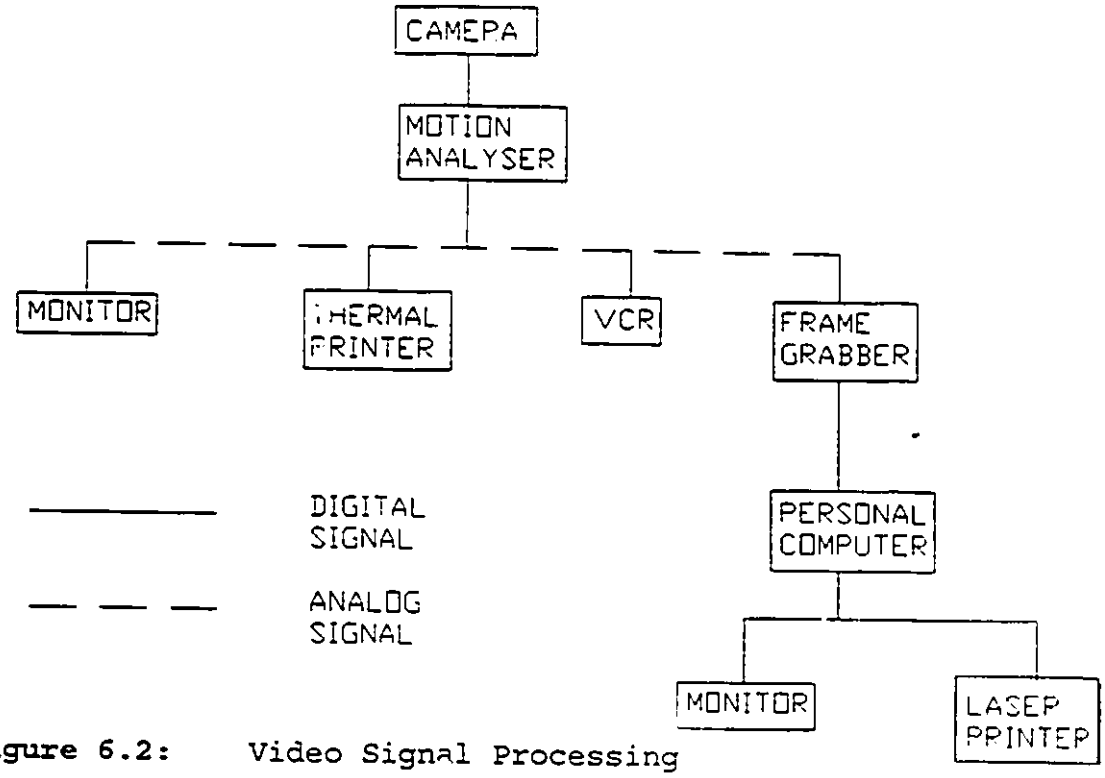

Figure 6.2: Video Signal Processing

The digital signal from the camera is transformed in the motion analyzer into a analog video signal that can be used to store pictures on a SuperVHS video recorder and be printed on a thermal printer.

Since light intensity was the limiting factor for picture quality at the frame rates utilized, and the resolution of the picture was rather poor with a thermal

printer, an alternative for hard copy reproduction of the video images had to be found. Reproduction by a laser printer, after redigitizing the analog signal from the motion analyzer with a video frame grabber card in the Personal Computer (PC) has proven to be the most satisfactory method. Additionally, digital picture enhancing techniques could be used to manipulate the images to show flow structures more clearly.

6.2 Flow Field Below Nominal Flow Conditions

A flow field classification according to the pump mean flow rate stands for the most significant changes in flow patterns. Changing shaft speed, i.e. Helmholtz number or resonant conditions, while maintaining constant relative flow, resulted only in subtle changes of the flow field and will be reported in section 6.4.

Generally, it should be noted that the evaluation of flow images from the video tapes requires a high degree of judgement and experience in discriminating the relevant flow structures and their repeatability over each cycle. The evaluator has to carefully observe a large number of cycles to then select one that represents the typical flow field features under the given conditions. Inherently, such a process contains some subjectivity and, thus, a potential for inaccuracy. The following results need to be understood in

light of this fact.

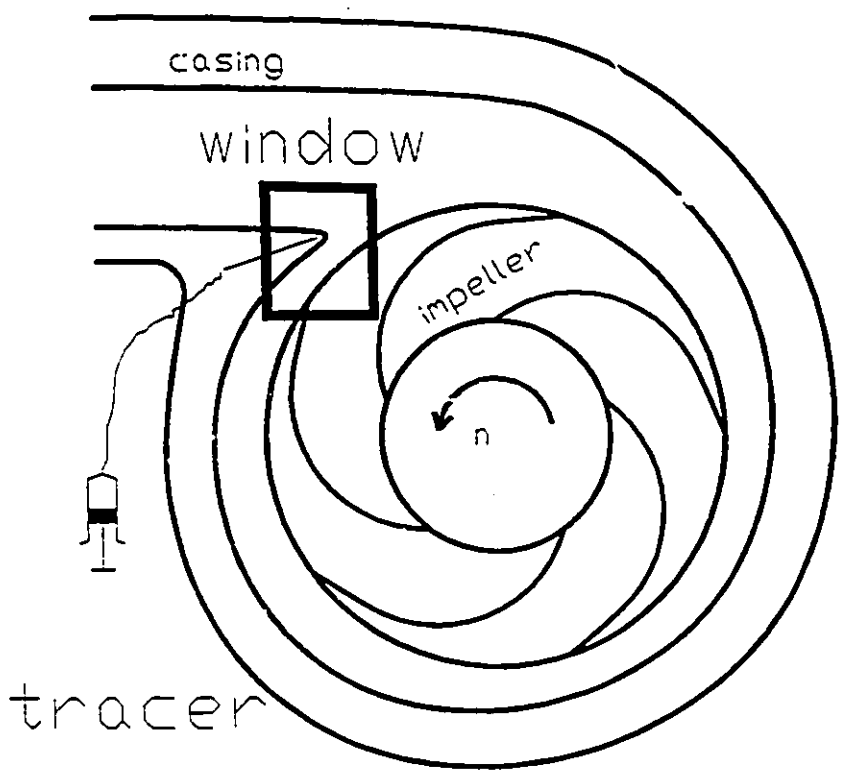

Figure 6.3: Sketch of Pump Casing

To clarify the following sequences of flow pictures figure 6.3 depicts the sketch of a cross section through the pump casing. The window of observation and the bleed location are also marked.

Figure 6.4 shows the evolution of a flow field over a complete period T of 24 ms at 40 % flow and a Helmholtz number of 0.4 (500 rpm) which is off-resonance. The duration of a

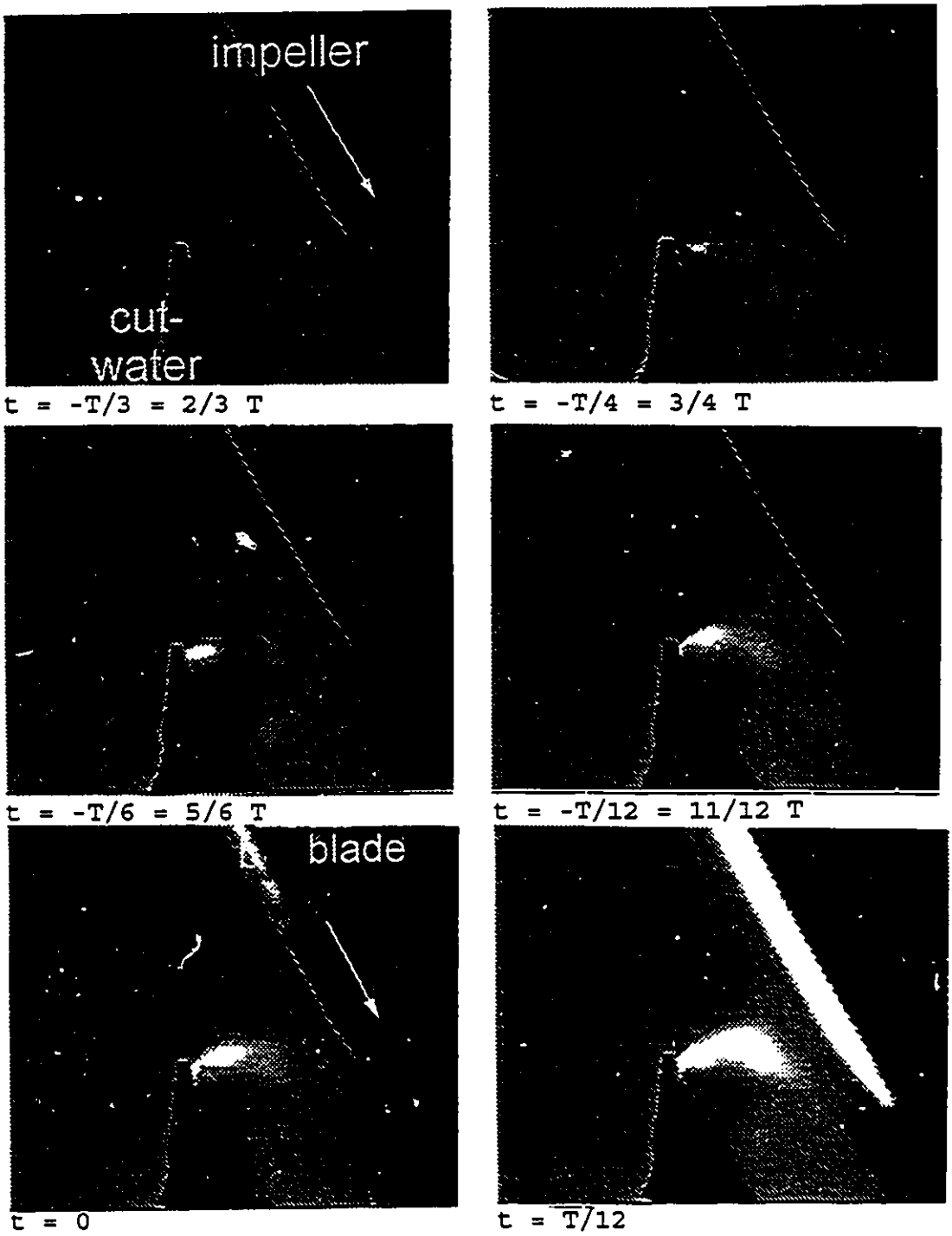

Figure 6.4: Flow Images at 40 % Flow and He=0.4 (500 rpm)

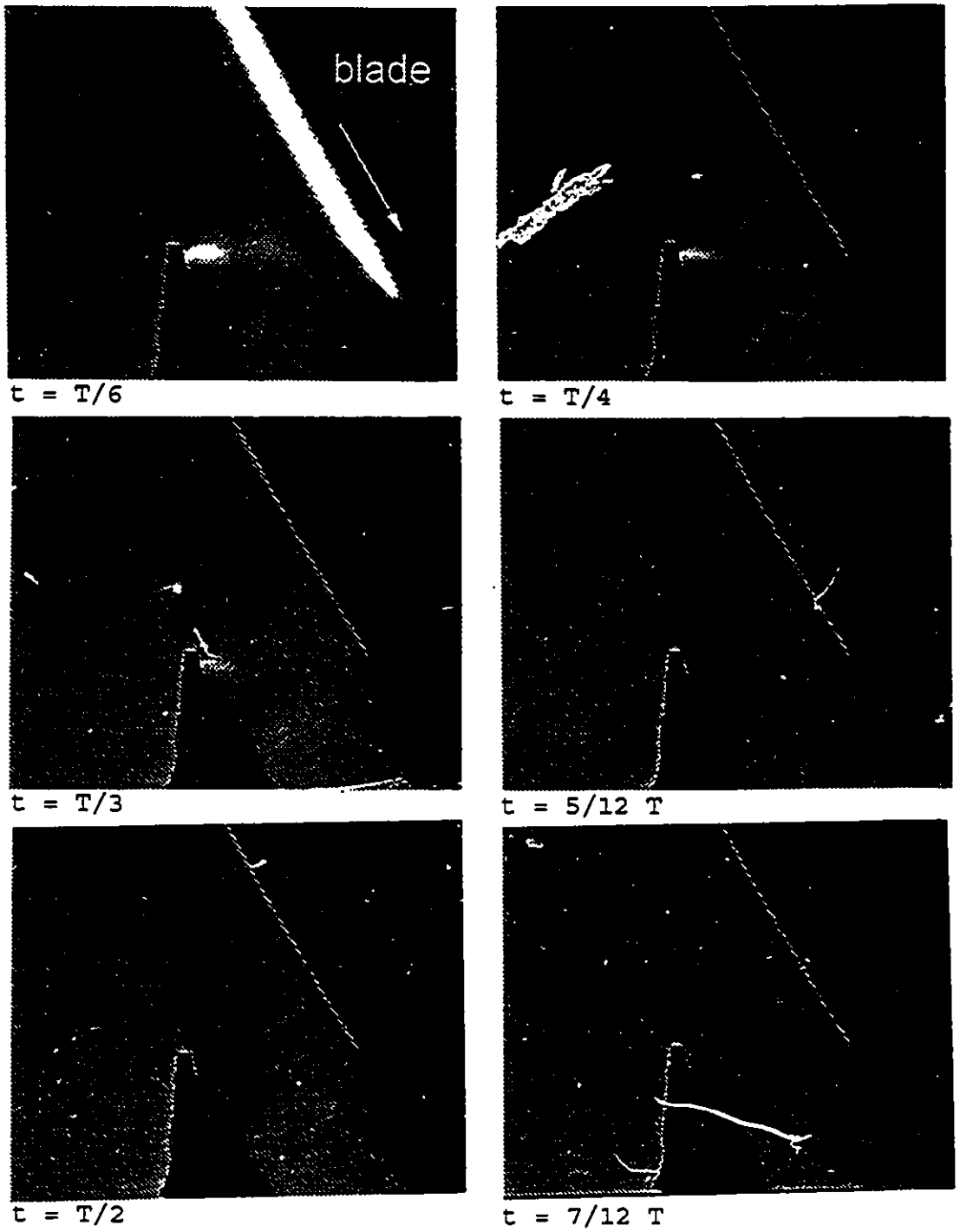

Figure 6.4: Flow Images at 40 % Flow and He=0.4 (500 rpm), Continued

blade passing a fixed stationary point results from the impeller geometry being about one sixth of a period and can, therefore, be seen in two to three consecutive frames. The instant of time when the pressure face of the impeller lines up with the cut-water tip is by definition the time t = 0 and was rounded to the frame rate resolution of 2 ms.

An obvious and important flow feature is the shedding of the vortex into the recirculation channel of the pump scroll casing at below nominal flows (as sketched in figure

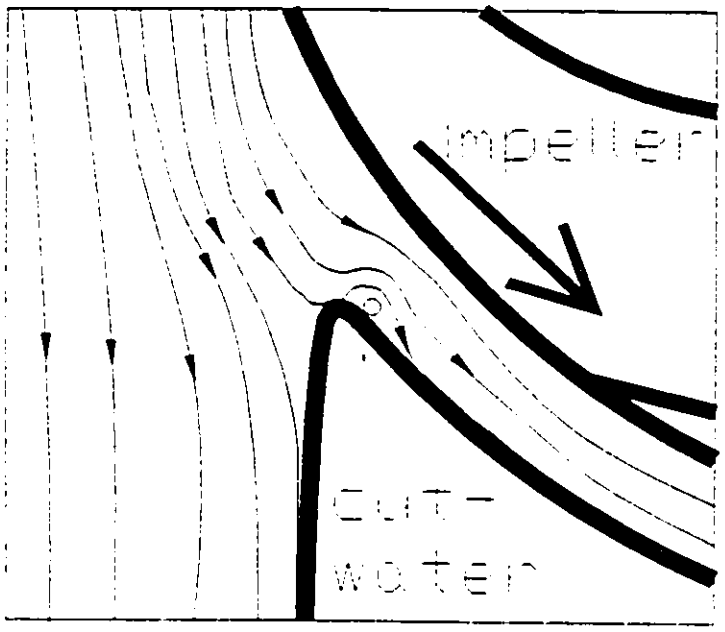

Figure 6.5: Sketch of Flow Field at 40 % Flow

6.5). This means that the stagnation point on the cut-water tip moves to the outside of the tongue, away from the impeller, an observation consistent with those of other researchers. A significant portion of the flow emerging from the impeller then recirculates in the casing, interacts with

the impeller flow and raises turbulent back ground noise. Additionally, the low mean flow leaving the pump, with most fluid being recirculated inside the casing, leads to the problem of excessive accumulation of tracer fluid. That fluid is now approaching the cut-water, mixed in with the mean flow instead of coming from the bleed nozzle. This makes flow observations even more difficult.

The maximum size of the eddy fills about 80 % of the gap between impeller tip and cut-water (10 mm) based on a streamline envisaged to go along the contour of the tracer cloud on the outside of the vortex. The occurrence of the maximum separation size coincides approximately with the blade being positioned at the cut-water. The vortex growth starts to emerge at about one third of a period earlier. This can be interpreted as the impeller jet (in the moving reference frame of the impeller) starting the vortex growth. As the wake, coinciding with the blade location, sweeps past the cut water the velocity component in the stationary frame becomes almost purely tangential to the impeller and carries the vortex into the recirculation channel.

From the geometric dimensions of the pump casing and the timing of the vortex evolution an average growth rate g_v of the vortex can be determined by the ratio of maximum separation size s_v (8 mm) and the time lag between "birth" of the vortex and occurrence of the maximum size Δt_v (T/3 = 8 ms)

$$g_v = \frac{s_v}{\Delta t_v} \tag{6.1}$$

Subsequently, the idea emerged to formulate a dimensionless number that could be representative of the flow field with respect to sound generation. Based on the growth rate g_v (in this instance 1 m/s), which is essentially a velocity and the sound speed in the medium c, a vortex Mach number Ma_v can be formulated as

$$Ma_v = \frac{g_v}{c} \tag{6.2}$$

This non-dimensional number can be seen as representative of the magnitude of compressible effects in the hydraulic near field of sound generation.

In the sense of Powell's vortex sound theory the growth rate can serve as a velocity scale for the vorticity travelling perpendicular to streamlines of the mean flow. Therefore, this growth rate must be related to the sound generated in the near field around the pump cut-water and can constitute a quantitative parameter of sound generation.

The correlation of the growth rate, or equivalently the vortex Mach number, with the acoustic pressures measured can allow an assessment of the presence of self-excitation. If self-excitation is a dominant mechanism the vortex Mach number must experience a significant increase for resonant conditions. Otherwise it seems a safe assumption that self-

excitation does not play a major role, but that the sound amplification is purely acoustical without any source changes.

6.3 Flow Field Above Nominal Flow Conditions

Flow visualization at nominal flow was impossible to record with the employed methodology due to very shallow separation zones and strongly stretched out vortices. By the use of stroboscopic lighting that allowed for halting the picture (and by means of a delay circuit changing the instantaneous blade position observed) the flow field could be inspected visually. The impression was gained that the tracer filled, very shallow, separated vortex is split to both sides of the cut-water. More likely than an actual splitting, is the notion that it is an intermittent process that only, through the visual averaging by stroboscopic lighting, appears to be happening simultaneously. The vortex could be shed randomly either into the recirculation channel or into the discharge pipe caused by small changes in the turbulence structure of the flow leaving the impeller.

Figure 6.6 shows the vortex development for a relative flow of 120 %. Opposed to the flow images reported at lower than nominal flow, the vortex is not swept into the recirculation channel, but consistently travels down the discharge pipe. This causes less problems with recirculating

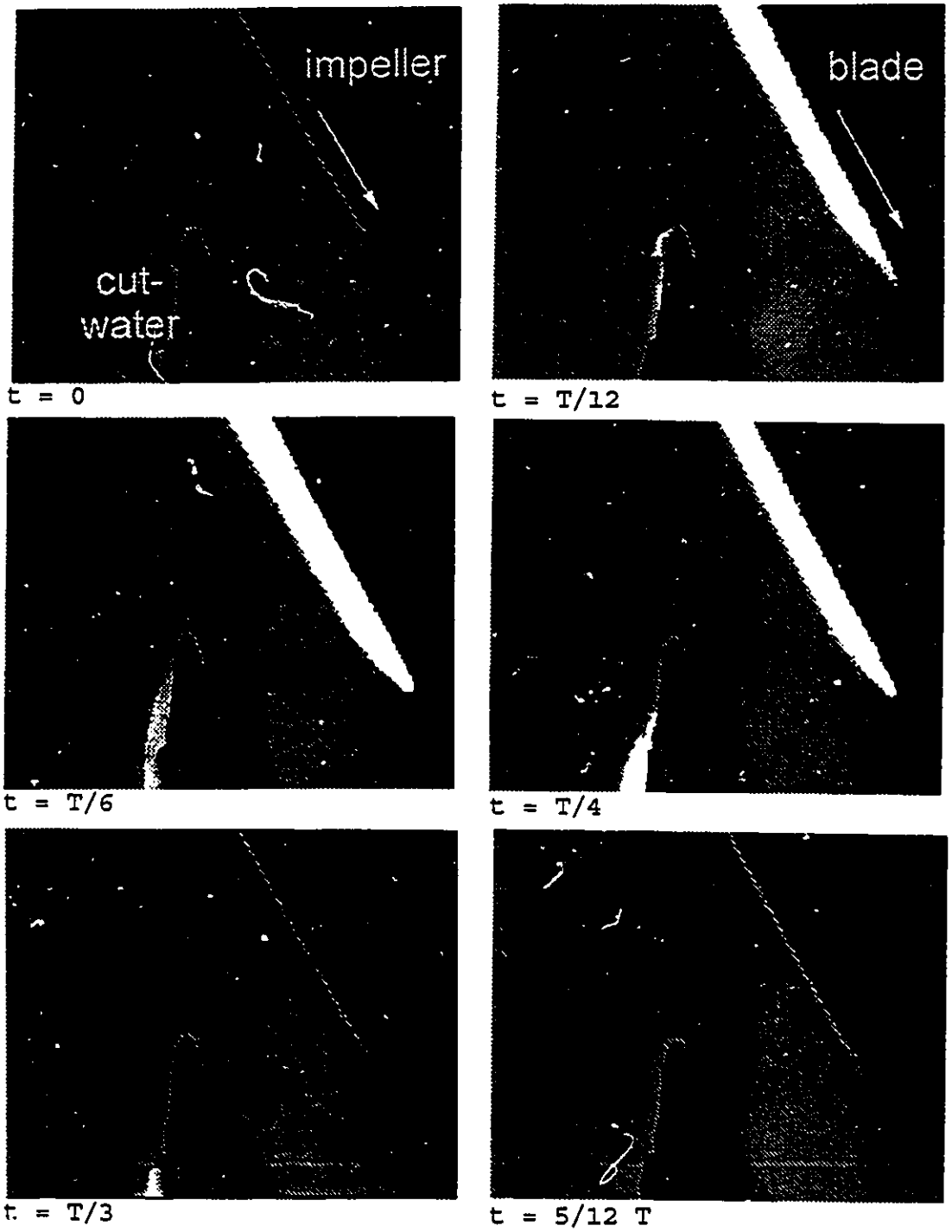

Figure 6.6: Flow Images at 120 % Flow and He=0.4 (500 rpm)

tracer that otherwise increasingly blurs the background. The timing between start of tracer bleeding and the start of recording becomes less critical.

Phasing of the vortex evolution is such that the birth of the vortex is repeatable at just the instant when the impeller blade arrives at the cut-water tip. The vortex then, almost immediately, starts shedding down the discharge side of the cut-water. An extended growth process can barely be observed. Only the feathering out of the vortex trail as it travels down the wall gives an indication of its location.

The size of the vortex is much more random than in the case of low flow . Variations go from about 3 mm maximum thickness to virtually no visible vortex. Therefore, the vortex size cannot be considered a characteristic that could reliably be evaluated as a quantitative measure to determine a velocity scale of the flow field.

Rather than using the vortex growth from its first occurrence to maximum size as a velocity scale, the velocity can more reliably be defined by the time a vortex takes to travel a fixed distance in the image frame. This again allows for the definition of a velocity scale as the ratio of distance travelled (10 mm from cut-water tip to edge of frame) and time needed to travel that distance. This velocity scale can again be expressed in the form of a vortex Mach number to represent the sound generation in the near field. A major draw back with respect to the vortex sound theory is that the

vortex velocity includes only a small, unknown angle with the mean flow velocity. This means that it is less clear what portion of the velocity contributes to the sound generation. This makes the vortex Mach number for above nominal flows less valuable. Furthermore, the vortex Mach number is not quantitatively comparable to that of the 40 % flow.

6.4 Correlation between Flow Field and Acoustic Pressure Fluctuations at Various Helmholtz Numbers

As [illegible] in the previous section, the correlation [illegible] pressure [illegible] in the absence of an [illegible] flow [illegible] the acoustic [illegible] of the system, the [illegible] with the [illegible] of self excitation [illegible]

[illegible]

side for high mean flow, remained unaffected. Likewise, did the timing with respect to the blade position, described in the previous two sections, not change with Helmholtz number variations.

Therefore, if present at all, the changes in flow field must be of a more subtle nature. They can only be recognized by the vortex size, velocity of growth and the convection speed of the flow structures, not by their fundamental features.

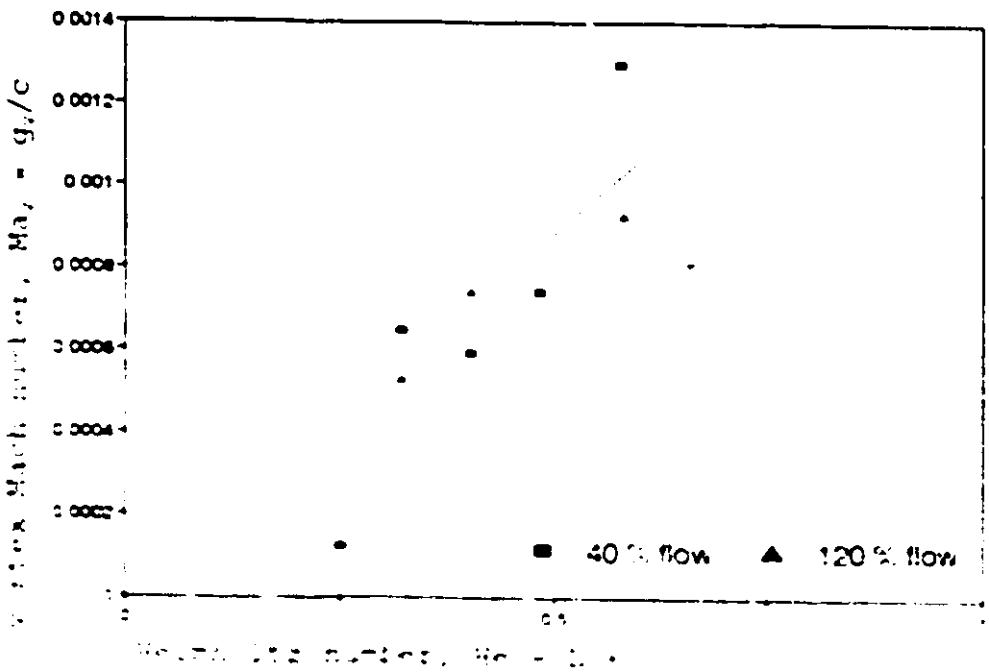

Figure 6.7: [illegible]

[illegible] shows the [illegible] between the vortex [illegible] and the [illegible] number. The [illegible]

adjusted by varying the pump shaft speed to obtain a different BPF and therefore a different relevant wave length. The graph contains data from flow evaluation at 40 % flow (filled squares) and five different velocities, as well as 120 % flow (filled triangles) and four different velocities. A collapsing of the two sets of data can naturally not be expected because of the different definition of the vortex Mach numbers, which are based in each case on the different features of the flow field (see sections 6.2 and 6.3 respectively). However, the trend for increasing Helmholtz number is close to a linear rise in Mach number and collapses reasonably well after all. This can be expressed in an empirical equation

$$Ma_v = 1.78 \cdot 10^{-3} \cdot He \qquad (6.3)$$

with a standard deviation of 14 % for the factor.

The essential meaning of this behaviour is that the separation eddy grows or sheds at a rate that directly depends on the mean velocity of the flow (Helmholtz number is directly proportional to the pump flow rate because it is controlled by the shaft speed). This leads to the conclusion that an acoustic feedback modifying the local flow field is absent.

Figure 6.8 represents an attempt to relate the acoustic pressure at BPF (normalized by the hydrodynamic stagnation pressure at impeller tip) to the vortex Mach number. At almost identical vortex Mach number a large bandwidth of acoustic pressures can occur. Largely different vortex Mach numbers can

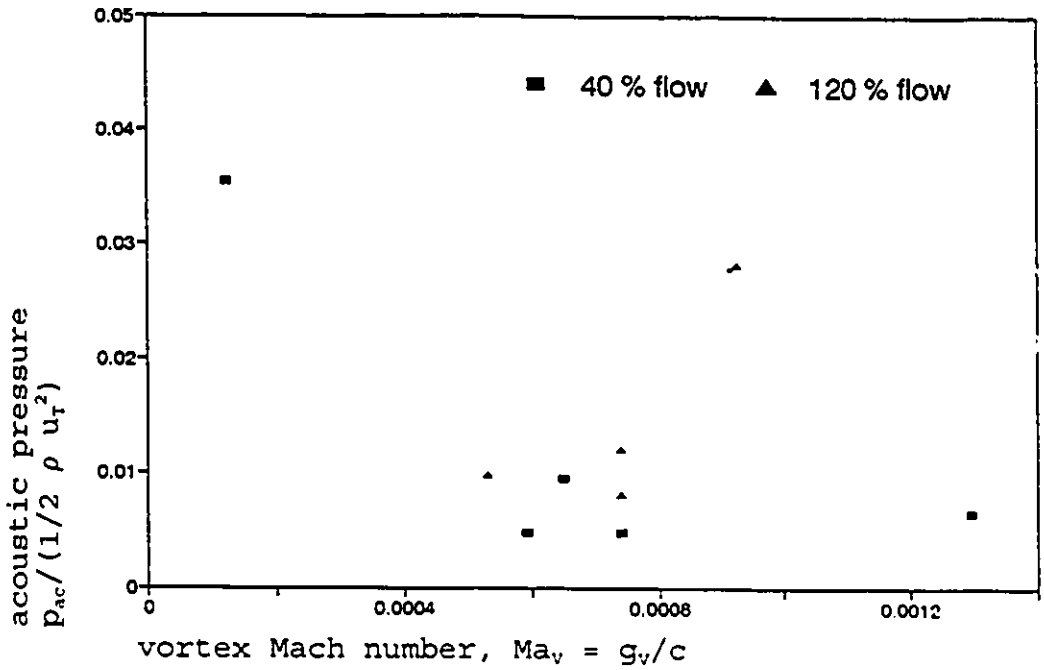

Figure 6.8: Correlation of Acoustic Pressure and Vortex Mach number, Geometry B - sharp tip, 40% and 120% Flow

produce similar acoustic pressures. There appears to be a trend for the 40 % data to feature a decreasing acoustic pressure with increasing vortex Mach number. This is not a likely behaviour because it would essentially say that as the source strength (its measure being the vortex Mach number) decreases the acoustic pressure increases. For the data at 120% flow the opposite trend of increasing acoustic pressure with increasing Mach number appears to be present. Not having a consistent explanation that holds true for all data it is felt that the apparent trends are a coincidence and really

only the acoustic loop amplification creates the variety of acoustic pressures observed.

The conclusion to be drawn from the flow behaviour observed is that for the investigated pump under the investigated conditions no dominant feedback takes place. No evidence points to a significant source enhancement through acoustic self-excitation. The mechanism of pressure amplification is therefore of a simpler, merely acoustic nature.

6.5 Effect of Cut-Water Tip Rounding on Flow Field

In chapter 5 it was concluded that the geometry of the cut-water has a strong effect on the sound generation by the pump. Rounding the cut-water from a sharp tip to a 5 mm radius about halves the encountered maximum acoustic pressures at BPF. Under the new insight learned from the previous sections of this chapter, namely that a resonance does not change the flow field noticeably, the change in sound generation properties of a pump with rounded cut-water tip can be seen to be exclusively an effect of a change in source strength.

Figure 6.9 shows the evolution of a vortex for a cut-water tip rounded to a radius of 5 mm for a 40 % of nominal flow at an off-resonant Helmholtz number of 0.4 (500 rpm). The vortex starts emerging at about 5/12 of the period T (24 ms)

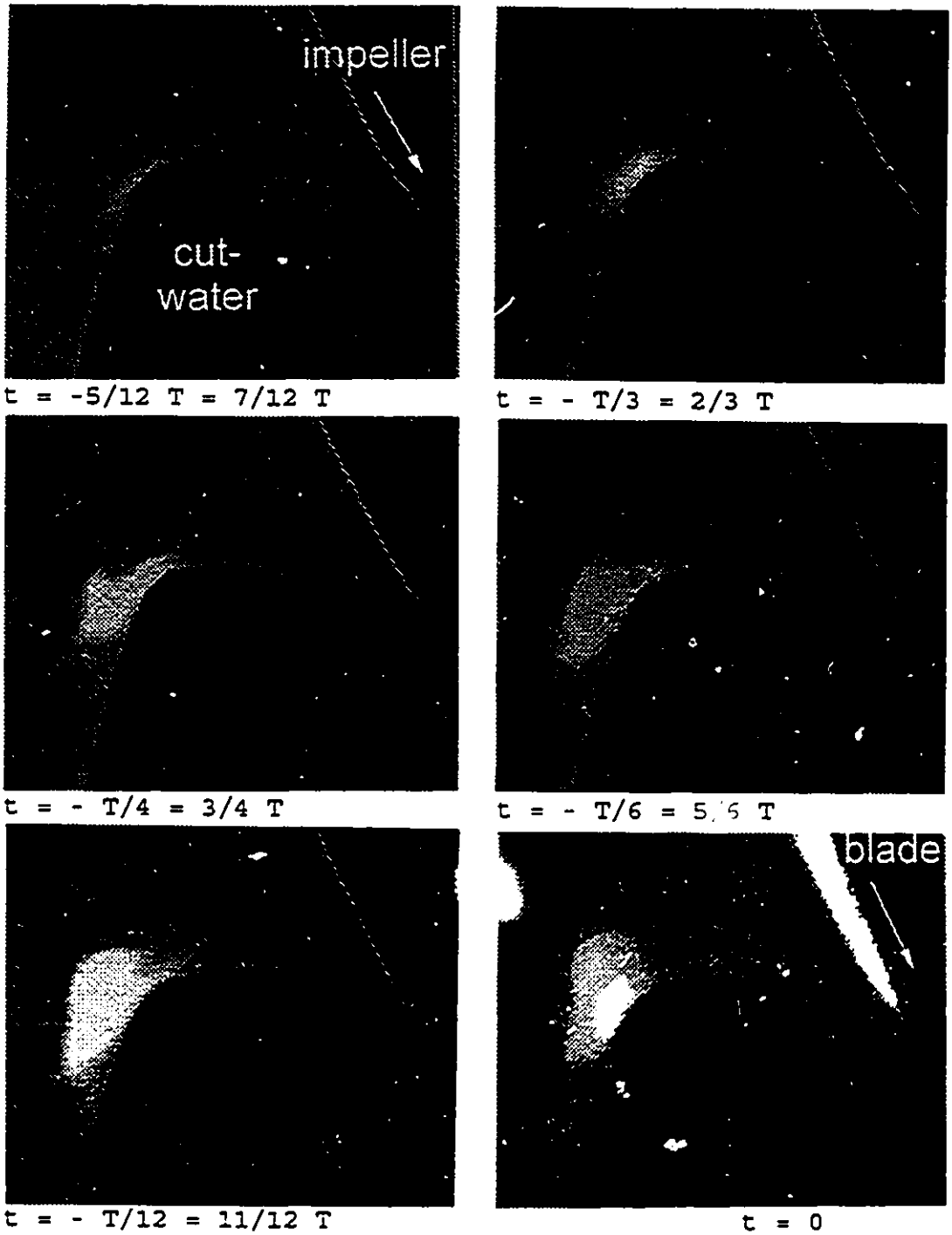

Figure 6.9: Flow Images at 40 % Flow, Tip Radius 5 mm

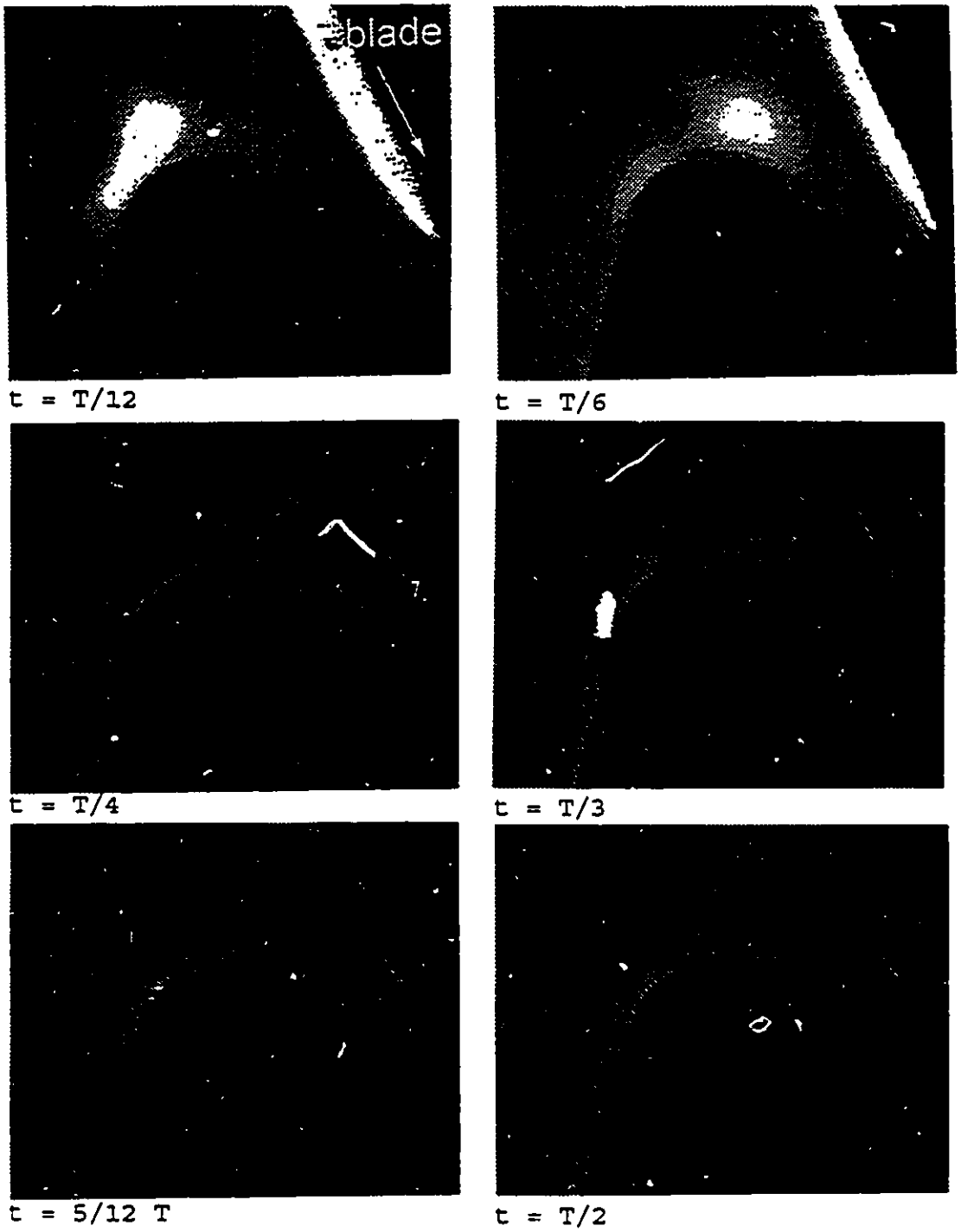

Figure 6.9: Flow Images at 40 % Flow, Tip Radius 5 mm, Continued

earlier than when the pressure side of the impeller blade passes the cut-water (Δt_v = 10 ms). It reaches its maximum size at about the time when the blade reaches alignment with the cut-water. With basically unchanged size the impeller wake carries the separation vortex around the tip of the cut-water and convects it down the recirculation channel of the pump.

Comparing this process with the corresponding cycle for a sharp tipped cut-water the timing of the vortex evolution is very similar. Only a time shift of about 1/12 of a period (2 ms) earlier is observed for the blunt geometry and this is most likely just a time resolution effect of the recording system (2 ms at 500 fps).

To appreciate the different behaviour, which is observed mainly with respect to the size and shedding process of the vortex, it should be mentioned that the bleeding location for the tracer fluid is more difficult to determine for a blunt cut-water. The intention was to locate the bleed hole at the corresponding place as for the sharp tipped geometry. In that case, however, the separation location is fixed in space by the geometry while for a blunt geometry the stagnation point is oscillating with blade position in time around a mean location given by the pump mean flow. Therefore, dye will be released during one cycle to the outside or inside of the instantaneous stagnation point. This may result in less tracer fluid being released during the time that the bleed hole is located in a favourable position with respect to the

separation region. However, the separation streamline should become visible regardless of bleeding inside the separation region or just upstream of it.

The size of the separation bubble is observed to be smaller for a blunter geometry. Since the separation point is not well defined, it can move around, depending on instantaneous flow condition (with the blade position). Thus, the size of the separation region will be reduced, leading to a smaller growth rate. It appears to the observer as if the vortex is "hugging" the contour or being squeezed against it while traversing the cut-water tip without any sharp discontinuities. The process of the formation and shedding of the separation vortex is much quieter with less potential for sound generation and probably a higher hydraulic efficiency as well.

Figure 6.10 shows a sequence of flow pictures of a flow above nominal (120 % relative flow) for a blunt cut-water tip. The general observations mentioned for the flow below nominal hold true for this flow condition also: The general behaviour of vortex evolution are in close correspondence with those for a sharp cut-water tip. The process in its overall pattern is only smoother and more harmonic in nature with separation eddies moving stretched out along the round cut-water contour.

In summary, the effect of cut-water tip rounding is that of a smoother flow with less tendency to separate. General timing of separation vortex formation and shedding are

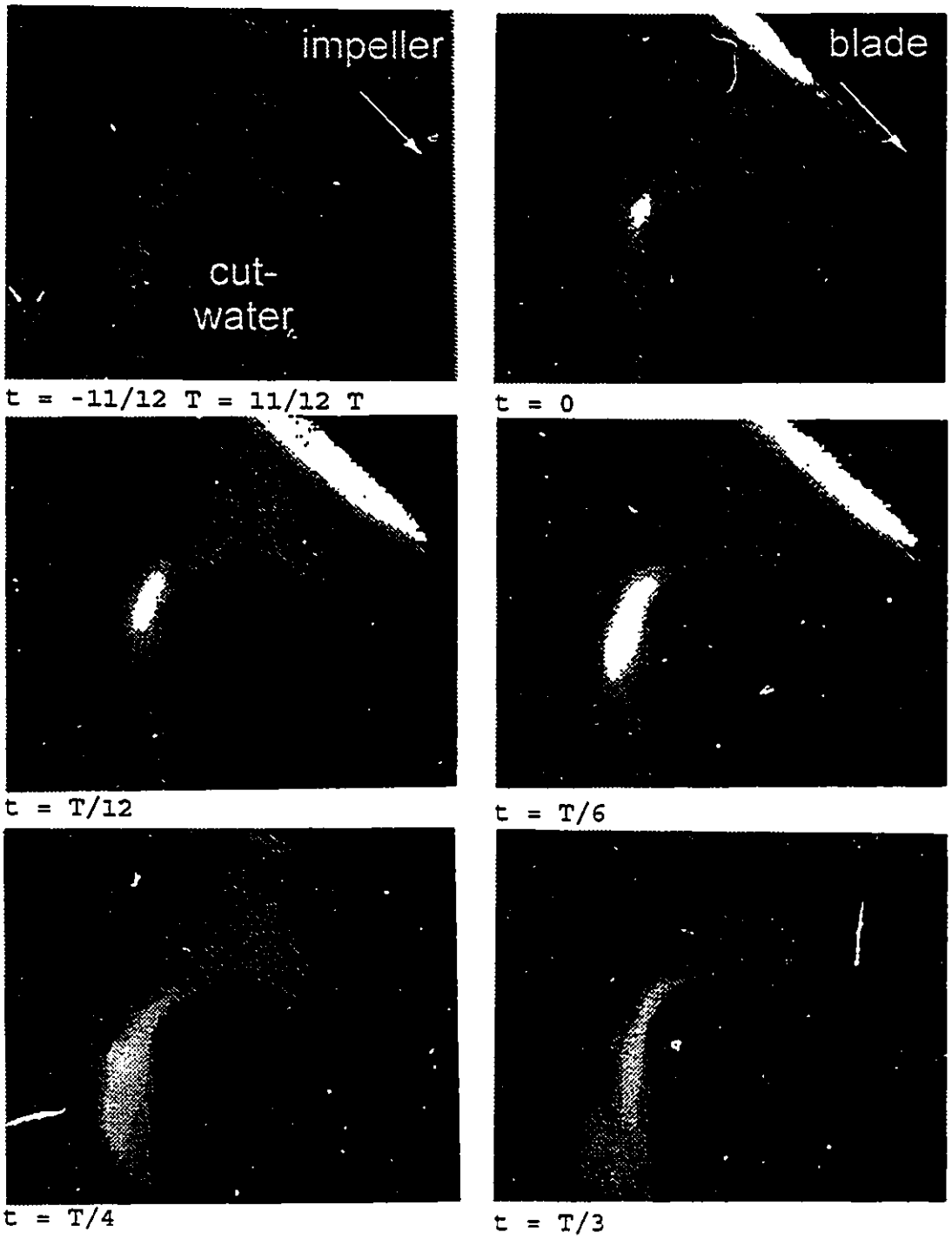

Figure 6.10: Flow Images at 120 % Flow, Tip Radius 5 mm

very similar to the behaviour with a sharp cut-water tip in the case of flow below as well that above nominal but instantaneous accelerations due to geometric discontinuities exist to a much lesser degree.

The instantaneous velocities play the dominant role in sound generation and can successfully be controlled to some degree by a careful geometric design. The potential for an optimization of the sound generation behaviour probably goes far beyond as simple a geometric modification as rounding the cut-water tip in a circular shape. An iterative approach considering the interaction of geometry change and flow field change could probably be used to optimize the sound generation behaviour for a given pump operating condition. Optimum shapes could, however, look very different for different pump mean flows. A cut-water shape dependent on the flow rate is in most cases not practical because the pump operating conditions are not necessarily defined in the design stage. Therefore, the rounding of the cut-water tip constitutes a good compromise for all operating conditions.

Only for 40 % and 120 % flow could the local flow behaviour could be observed in an attempt to understand how the acoustic performance is improved. The behaviour at nominal flow was experimentally shown in chapter 5 to benefit also from a rounding of the tip. The mechanism of performance improvement can be expected to be very similar to that off-design shown in this chapter.

CHAPTER 7: CONCLUSIONS AND RECOMMENDATIONS

"A collection of facts is no more a science than a heap of stones is a house."
Jules Henri Poincare, 1908

The closing remarks in a thesis are typically reserved for summarizing the findings and providing a prospect into the future. This chapter follows that tradition. Section 7.1 summarizes the findings and their interpretation. Section 7.2 is subdivided in a section 7.2.1 that suggests work that could be carried out in immediate extension of the presented investigation while section 7.2.2 recommends further work that would be useful in the context but would also require greater modification to the test apparatus.

7.1 Conclusions

The presented research was concerned with the sound generation of a five vane, centrifugal volute pump and its interaction with a simple piping system at Blade Pass Frequency (BPF). The investigation was chiefly of an experimental nature.

The experimental apparatus that was designed and

constructed for this research consisted of a closed loop system. The acoustic tuning between BPF and acoustic natural frequency of the system was achieved by a shaft speed control of the pump. The adjustment of operating condition, the relative pump flow rate, was realised by an in-line control valve. Dynamic pressure measurements were possible by regularly spaced piezoelectric transducers. It was provided for flow visualization in the cut-water region of the pump casing. Details of the apparatus are described in chapter 3.

The main objective of this investigation was, first, to understand better the sound generation behaviour of the pump, in view of a design optimization to minimize acoustic pressure pulsations. A second objective was to investigate the possibility of an acoustic pump pipeline interaction that alters the acoustic near field around the pump cut-water.

In pursuit of the first objective, a semi-empirical numerical model was devised that allowed for a separation of acoustic and hydraulic component of the pressure pulsations. This model was based on a linear superposition of an acoustic term, related to the acoustic mode shapes of the system, and a hydraulic term, representing a exponential decay with distance from the pump. Modelling the pump as a pressure source, an acoustic monopole, could capture the spatial distribution of measured pressure fluctuations at BPF well. The model was found in good agreement with measured pressure fluctuations in a range of the Helmholtz number, the loop

length over the wave length at BPF, from about 0.3 to 0.8. The lower limit was given by an assimilation of shape functions for acoustic and hydraulic term, resulting in the two being inseparable. The upper limit was given by a second sound source in the physical system, the cavitating control valve, adding enough to the noise floor to make the model less accurate. The details of the model and the behaviour of the hydraulic term are presented in chapter 4.

The hydraulic component of the model displayed a roughly quadratic dependency on the Helmholtz number below a Helmholtz number of about 0.8. No dependency of the quadratic coefficient on the geometry of the cut-water was observed. Cut-water variations included a sharp tip as well as a tip radius of 2.5 mm and 5 mm. The effect of relative flow rate was an increasing quadratic coefficient with decreasing relative flow. Additionally, at the highest flow of 120 % the departure of the hydraulic pressure from the quadratic behaviour was observed earlier, at a Helmholtz number of about 0.7 due to earlier onset of valve cavitation.

The behaviour observed for the acoustic pressure fluctuations is in most cases a resonance of the system at a Helmholtz number of 0.57 to 0.59. This was interpreted as a partial reflection of the system at the pump location. The pump can act as a point of partial reflection because of a change in characteristic impedance in comparison to that of the pipeline. This impedance change is thought to take place

mainly due to a change in effective cross sectional area, a volume expansion at the pump that imposes a pressure release surface. Variation of the parameter flow rate rendered a minimum of the acoustic pressure fluctuations around the nominal pump operating point. The interpretation was that a better pump efficiency, with less hydrodynamic perturbation in the local flow field, resulted also in a superior performance with respect to sound generation. However, significant flow rate effects were only observed for a sharp cut-water tip geometry. The effect of changing the pump cut-water tip radius from a sharp tip to a rounded shape had, generally, the effect of decreasing the sound generation of the pump while leaving the hydraulic characteristic nearly unchanged. A reduction in acoustic pressure fluctuations by about a factor of two could be observed. However, it came obvious that geometry effects are more complicated than the general trend mentioned above. For example, a sharp tipped cut-water at low relative flow featured a resonance at a Helmholtz number of 0.25. In combination with the acoustic mode shape unexpectedly being a half sine wave instead of a quarter sine wave a change of source type from pressure source (monopole) to velocity source (dipole) seemed a possibility. Acoustic behaviour was treated in chapter 5.

The second objective of the investigating, the possibility of acoustic source system interaction, relied heavily on flow visualization of the local flow field around

the cut-water of the pump casing. Fluorescent flow tracer was released at the cut-water tip into the flow. Illumination came from conventional lighting in a direction perpendicular to the observation generating a light sheet that illuminates the pump centre plane. For flow observation a digital high speed camera allowed for enough pictures per blade pass cycle to observe the evolution of vortex growth and shedding at the cut-water. The separation region forming behind the cut-water was observed to switch from the recirculation side at low flow to the discharge side at flows above nominal. This was most pronounced for a sharp tip geometry corresponding to the strongest dependency of acoustic pressures on relative flow rate. While for a sharp tip geometry the stagnation point remained fixed over a cycle a rounded tip displayed the instantaneous stagnation point moving with blade position. The latter resulted in smaller separation regions and, probably, is the cause for the lower sound generation. Variation of the Helmholtz number to produce off-resonant and resonant conditions produced no obvious flow field modifications. A quantitative representative of the flow field, the vortex Mach number, was defined as an average vortex growth rate over the time between vortex initiation and maximum size. The attempt to correlate this vortex Mach number with the Helmholtz number could be approximated to be a proportional relationship. No correlation between this vortex Mach number and the measured acoustic pressures was found. The interpretation was offered

that local velocities, representing the vortex growth, scale with the mean velocity triangles and no acoustic source modifications took place. The observed resonance phenomena would then be of a mere acoustic system amplification type, not of a self-excitation type.

In summary, the contribution to technology are that the investigated pump can be modelled mostly as an acoustic pressure source. Then the pump acts as a system discontinuity of the volume expansion type with dominant partial reflections. Only in the geometry variation of a sharp cut-water tip in the flow rate range below nominal flow the pump acoustic behaviour seems to be modelled better as a velocity source. A transition between dipole and monopole source occurs for this geometry from flows below nominal to those above nominal. Cut-water tip rounding in the pump can yield a significant reduction of sound generation without evidence for a performance penalty. And finally, an acoustic feed back from the piping system to modify the local flow field in the pump cut-water region is not observable for the investigated pump.

7.2 Recommendations

This section is subdivided into one part dealing with immediate recommendations for improvements of the existing test apparatus or experimental methodology and a second dealing with potential further studies that require allocation of significant additional resources.

7.2.1 Recommendations for Improvements of Existing Apparatus

This part consists of a list of independent measures to improve performance or facilitate the use of the existing test apparatus. Some of the measures are minor details with little effort necessary for their implementation others require a new approach or additional resources.

i) The availability of the shaft speed exclusively as a Transistor-Transistor-Logic (TTL) digital signal from a proximity sensor posed some inconvenience. This signal can be used by a counter of the computer A/D board but not used as an analog input channel, thus prohibiting a direct correlation with other signals that are available for input.

ii) Another improvement that rather falls into the category of convenience is the amplification of the thermocouple reading. Using a Cold Junction Compensation (CJC) available on the board two channels are consumed for the relatively

unimportant temperature measurement in the flow. So if a monitoring of the temperature is desired simultaneously with dynamic measurements a separate thermocouple amplifier and display, possibly with an output signal 0 to 10 V, would be advantageous.

iii) And yet another improvement of the handling: The external trigger utilized for starting the measurement of sound speed often failed to trigger successfully owing to the fact that the switch has to instantaneously close and remain closed. With a sampling rate of 50 000 Hz the meaning of instantaneous becomes so severe that the currently used switch is not capable of reliably remaining closed in the short time interval. Improvement of the switch or perceivably a complete automation of the currently still manual operation could contribute to better handling of the measurement.

iv) Ease of operation could further be improved by fitting a transparent level gauge to the overhead tank instead of relying on the audibility of spill flow through the tank overflow discharge for a check on filling status.

v) More challenging but with the potential to improve the experimental results at higher flow rates where apparently the control valve cavitation constitutes a second sound source in the loop that contaminates the dynamic pressure measurements is an acoustic isolation of the loop from the control valve. Design options include rubber compensators or expansion chambers effectively mismatching the specific acoustic

impedance enough to yield a large reflection upstream of the control valve. However, all options have to be paid for with more friction losses and thus a diminished range of flow rate to operate the pump on.

vi) If a correlation of pressure pulsations with pump efficiency is desired equipping the loop with instrumentation for mechanical shaft torque is imperative. Reaction mounting of the pump motor was earlier discarded due alinement and problems with frictional errors for the measurement. Direct torque measurement of the rotating shaft can be done with torsional load cells mounted between the motor pump shaft coupling. Modifications to the base frame due to the required space will be necessary. Transmitting the signal via slip rings or radio transmitters are design options to be considered.

vii) To improve means of externally exciting the system might take additional improved hardware and some more analytical backing about the appropriate reference for dynamic pressure measurements. This pertains to the question what portion of a side branch mounted piston is really producing an acoustic signal. Hardware improvements found necessary are stiffness of the mounting frame, power of the shaker and lubrication of the piston or a more adequate selection of the primary device to produce the pressure pulses (e.g. diaphragm). An immediate outcome from these improvements could be the determination of acoustic damping which would pave the

road to separate acoustic source strength from acoustic loop amplification and give further evidence with respect to the magnitude of a self-excitation phenomenon.

viii) The limiting factor for the repeatability of dynamic pressure measurements was felt to be the consistency of water quality, most prominent probably aeration and dissolved gases. By pressurizing the complete loop, cavitation at the control valve could be suppressed and the aeration remain consistent. An additional redesign of the tank discharge for better mixing with the whole tank content could further optimize the constancy of fluid properties. This change to the loop could be a costly one because it might require a new overhead tank and therefore a change of the loop location. Difficulties with the current mechanism for dye injection for flow visualization and the safety of the flow visualization windows in the pump casing have to be anticipated due to higher internal pressures. Especially the latter might call for considerable reinforcing efforts.

7.2.2 Recommendations for Further Studies

The decision about further studies is a strategic one. For this reason various possibilities, each leading in a different direction, are mapped out.

However, crucial to all studies that want to further

the understanding of how the local near field relates to sound levels measured in the system is a good methodology for flow visualization. Since the limiting factor is the concentration of sufficient light intensity in one or more planes perpendicular to the impeller axis the abandoning of conventional lighting in favour of a laser light sheet will have to have highest priority. Availability of a laser and the appropriate optics for light sheet generation will permit higher quality qualitative flow visualization and also serve as a platform for employing quantitative flow visualization by Particle Image Velocimetry (PIV).

The two major possible directions of investigation are on the one hand the improvement of pump modelling in complex piping networks, denominated "transfer matrixes" approach. It pursues the route of earlier mentioned efforts for a better description of a piping system and especially the acoustic damping. On the other hand, alternately or complementary, the investigation of the effect of various pump designs on the sound generation is a major direction of investigation. Where the former direction has potential to produce a better model of complicated piping systems including centrifugal pumps, the latter direction could yield a optimized pump design with respect to sound generation.

To devise a method to measure the acoustic transfer matrix of the pump it is necessary to provide a variety of different up and downstream impedances in order to have a

statistically significant number of observations from which the pump transfer matrix can be extracted. Taking measurements upstream of the pump for this purpose as well as to confirm the model for acoustic-hydraulic pressure separation will be needed. This is with the existing apparatus not possible because of space confinement and proximity to the tank inlet. When changing the loop configuration, a possibility to place the pump in various locations with respect to the piping length should be designed into the modification. Impedance changes can for example be incorporated by a series of side branch Helmholtz resonators that can be connected and disconnected to the main line by means of valves.

The other avenue of investigating is to investigate the mere source strength of the pump under various operating conditions. This could ideally be achieved in a test apparatus incorporating acoustic anechoic termination up- and downstream of the pump. This, clearly, would also require extensive redesign of the loop. However, using the present work as bench mark, comparative source strength values could be obtained on this basis which also allow for design optimization.

The following contains a list of design changes that are viewed as potentially significant from the experience gained on this work or from the literature.

The separation regions observed on either side of the cut-water (see chapter 6) play a major role in sound

generation. The suggested measures to be investigated are based on the assumption that reducing the cyclic growth and collapsing of these separation regions will lower the discrete frequency sound source at BPF in the pump flow.

A geometrical filling of the separation region in the form of a protrusion, shaped according to the observed separation, has some potential for source strength reduction. However, the separation region shape will depend on the immediate blade position and on the relative flow rate. Thus an optimization is most promising for a single, known operating conditions for the pump, an unpractical start point for pump design.

The following suggestions go beyond the immediate experience from this work but promise positive effects.

The suction of the boundary layer and in such a way eliminating or reducing the separation is attractive for its design simplicity. A slot cut into the cut-water connected by a short piece of tubing and a regulation valve to the suction flange of the pump could provide an device for controlling sound generation that is easy to retrofit and operate. The user would remain with the option of minimizing sound generation or minimizing leakage flow (associated with lesser hydraulic performance of the pump) by switching a valve in the connecting line.

Moving surface boundary layer control by means of a roller at the tip of the cut-water would involve a much higher

design effort but also promises some potential. With typical ratios of surface speed over flow speed of 4 for best boundary layer control, however, the roller speeds would need to be about 4 times the ratio of roller diameter over impeller diameter which easily brings speeds up to tens of thousands of revolutions per minute. This can cause secondary problems of additional energy supply, sealing leaks and bearing wear problems plus the potential for new noise sources.

Borrowed from the fan and blower literature the use of a side branch resonator connected to the cut-water seems an interesting self-sufficient way of boundary layer control. However, dimensions, which are about a factor of three smaller in air, can easily can amount to 6 m to 7 m for a quarter wavelength resonator in a water pump.

A whole new area of design modifications is opened with the changes to the impeller geometry. Obviously, there must be room for improvements since the flow field inside the pump results from an interaction between impeller and casing. Especially, the impeller tip volute tongue gap was reported to be an important design parameter, but its increase generally is associated with a performance penalty. Irregular spacing of impeller blades would widen the excitation peak at BPF, but might not affect overall noise generation. Slanting, tapering or perforating in various forms the impeller tip may also have potential for improvement of the sound generation behaviour.

BIBLIOGRAPHY

"This will never be a civilized country
until we expend more money on books
than we do for chewing gum."
Elbert Hubbard, 1915

[1] Brown, E.B., (1945) "Optical Instruments", Chemical Publishing Co., Brooklyn, N.Y.

[2] Randall, R.H., (1951) "An Introduction to Acoustics", Addison - Wesley Publishing, Reading

[3] Lighthill, M.J., (1952) "On Sound Generated Aerodynamically: I. General Theory", Proceedings of the Royal Society, London, vol 211, pp 564-587

[4] The M.W. Kellog Company (editor), (1953) "Design of Piping Systems", John Wiley & Sons, Inc., 2nd edition, New Ypork, London, Sidney

[5] Lighthill, M.J., (1954) "On Sound Generated Aerodynamically: II.Turbulence as a Source of Sound", Proceedings of the Royal Society, London, vol 222, pp 1-32

[6] Curle, N., (1955) "The Influence of Solid Boundaries upon Aerodynamic Sound", Proceedings of the Royal Society, London, vol 231, pp 505-514

[7] Lighthill, M.J., (1956) ""Viscosity Effects in Sound Waves of Finite Amplitude" in Batchelor, G. K., Davies, R. M.: "Surveys in Mechanics"", Cambridge University Press

[8] Ribner, H.S., (1958) "Strength Distribution of Noise Sources along a Jet", The Journal of the Acoustic Society of America, vol 30, p. 876

[9] Doak, P.E., (1959) "Acoustic Radiation from a Turbulent Fluid Containing Foreign Bodies", Proceedings of the Royal Society, London, vol 254, pp 129-145

[10] Dean, R.C., and Senoo, Y., (1960) "Rotating Wakes in Vaneless Diffusers", ASME - Journal of Basic Engineering, vol 82, n 3, pp 563-574

[11] Iversen, H.W., Rolling, R.E., and Carlson, J.J., (1960) "Volute Pressure Distribution, Radial Force on the Impeller and Volute Mixing Losses of a Radial Flow Centrifugal Pump", ASME - Journal of Engineering for Power, vol 82, n 2, pp. 136-144

[12] Chen, Y.N., (1961) "Wasserdruckschwingungen in Spiralgehaeusen von Speicherpumpen", Technische Rundschau Sulzer, Forschungsheft, pp 21-34

[13] Embleton, T.F.W., (1963) "Experimental Study of Noise Reduction in Centrifugal Blowers", The Journal of the Acoustic Society of America, vol 35, n 5, pp 700-705

[14] Ffowcs Williams, J.E., (1963) "On the Noise Produced by Boundary-Layer Turbulence", The Journal of the Acoustic Society of America, vol 35, pp 930-931

[15] Meecham, W.C., (1963) "Further Discussion of Noise Produced by Boundary-Layer Turbulence", The Journal of the Acoustic Society of America, vol 35, pp 931-932

[16] Powell, A., (1964) "Theory of Vortex Sound", The Journal of the Acoustical Society of America, vol 36, n 1, pp 177-195

[17] Chanaud, R.C., (1965) "Aerodynamic Sound from Centrifugal-Fan Rotors", The Journal of the Acoustic Society of America, vol 37, pp 969-974

[18] Lazarkiewicz, S., and Troskolanski, A.T., (1965) "Impeller Pumps", Pergammon Press, Oxford

[19] Ribner, H.S., (1966) "Noise Generation Mechanisms", Canadian Aeronautics and Space Institute Journal, n 1, pp 1-6

[20] Baade, P.K., (1967) "Accuracy Considerations in Fan Sound Measurement", ASHRAE - 74th Annual Meeting in Minneapolis, June 26-28, No. 2055

[21] Clayton, B.R., and Massey, B.S., (1967) "Flow Visualization in Water: A Review of Techniques", Journal of Scientific Instrumentation, vol 44, pp 2-11

[22] Simpson, H.C., Clark, T.A., and Weir, G.A., (1967) "A Theoretical Investigation on Hydraulic Noise in Pumps", Journal of Sound and Vibration, vol 5, n 3, pp 456-488

[23] Stepanoff, A.J., (1967) "Centrifugal and Axial Flow Pumps", 2nd edition, 5th printing, John Wiley & Sons, New York

[24] Morse, P.M, and Ingard, K.U, (1968) "Theoretical Acoustics", McGraw - Hill Book Company, New York

[25] Schlichting, H., (1968) "Boundary-Layer Theory", McGraw - Hill Book Comp., New York

[26] Ffowcs Williams, J.E., and Hawkings, D.L., (1969) "Sound Generation by Turbulence and Surfaces in Arbitrary Motion", Philosophical Transactions of the Royal Society of London, vol A264, pp 321-342

[27] Peterka, J.A, and Richardson, P.D., (1969) "Effects of Sound on Seperated Flows", Journal of Fluid Mechanics, vol 37, part 2, pp 265-287

[28] Werle, H., (1973) "Hydrodynamic Flow Visualization", Annual Review of Fluid Mechanics, vol 5, pp 361-382

[29] F.A.A Adubi, (1974) "The Hydroelastic Vibration of a Hydraulic Swing Check Valve", Ph.D. Thesis, McMaster University, Hamilton, Canada

[30] Merzkirch, W., (1974) "Flow Visualization", Academic Press, New York

[31] Moreland, J.B., (1974) "Housing Effect on Centrifugal Blower Noise", Journal of Sound and Vibration, vol 36, n 2, pp 191-205

[32] Archibald, F.S., (1975) "Self - Excitation of an Acoustic Resonance by Vortex Shedding", Journal of Sound and Vibration, vol 38, n 1, pp 81-103

[33] Howe, M.S., (1975) "Contribution to the Theory of Aerodynamic Sound, with Application to Excess Jet Noise and the Theory of the Flute", Journal of Fluid Mechanics, vol 71, part 4, pp 625-673

[34] Neise, W., (1975) "Application of Similarity Laws on the Blade Passage Sound of Centrifugal Fans", Journal of Sound and Vibration, vol 43, n 1, pp 61-75

[35] Chang, P.K., (1976) "Control of Flow Separation", Hemisphere Publishing, Washington

[36] Eckardt, D., (1976) "Detailed Flow Investigation within a High-Speed Centrifugal Compressor Impeller", ASME - Journal of Fluids Engineering, n 3, pp 390-402

[37] Goldstein, M.E., (1976) "Aeroacoustics", McGraw - Hill International, New York

[38] Margolis, D.L, and Brown, F.T., (1976) "Measurement of the Propagation of Long-Wavelength Disturbances through Turbulent Flow in Tubes", ASME-Journal of Fluids Engineering, vol 98, March, pp 70-78

[39] Neise, W., (1976) "Noise Reduction in Centrifugal Fans: A Literature Survey", Journal of Sound And Vibration, vol 45, n 3, pp 375-403

[40] Tritton, D.J., (1977) "Physical Fluid Dynamics", Van Nostrand Reinhold, New York

[41] Mueller, E.-A., ed., (1979) "Mechanics of Sound Generation in Flow", Springer Verlag, Berlin

[42] Rockwell, D., and Naudascher, E., (1979) "Self - Sustained Oscillations of Impinging Free Shear Layers", Annual Review of Fluid Mechanics, vol 11, pp 67-94

[43] To, C.W.S., and Doige, A.G., (1979) "A Transient Testing Technique for the Determination of Matrix Parameters of Acoustic Systems, 1: Theory and Principles", Journal of Sound and Vibration, vol 62, n 2, pp 207-222

[44] To, C.W.S., and Doige, A.G., (1979) "A Transient Testing Technique for the Determination of Matrix Parameters of Acoustic Systems, 2: Experimental Procedures and Results", Journal of Sound and Vibration, vol 62, n 2, pp 223-233

[45] Yuasa, T, and Hinata, T., (1979) "Fluctuating Flow behind the Impeller of Centrifugal Pump", Bulletin of the JSME, vol 22, n 174, pp 1746-1753

[46] Chung, J.Y., and Blaser, A.D., (1980) "Transfer Function Method of Measuring In-Duct Acoustic Properties. I. Theory", Journal of the Acoustic Society of America, vol 68, n 3, pp 907-913

[47] Chung, J.Y., and Blaser, A.D., (1980) "Transfer Function Method of Measuring In-Duct Acoustic Properties. II. Experiment", Journal of the Acoustic Society of America, vol 68, n 3, pp 914-921

[48] Florjancic, D, Schoeffler, W., and Zogg, H., (1980) "Primaere Geraeuschminderung an Kreiselpumpen", Technische Rundschau Sulzer, n 1, pp 24-26

[49] Krain, H., (1981) "A Study on Centrifugal Impeller and Diffuser Flow", ASME - Journal of Engineering for Power, vol 103, pp 688-697

[50] Nelson, P.A., Halliwell, N.A., and Doak, P.E., (1981) "Fluid Dynamics of a Flow Excited Resonance, Part I: Experiment", Journal of Sound and Vibration, vol 78, n 1, pp 15-38

[51] Neise, W., (1982) "Review of Noise Reduction Methods for Centrifugal Fans", ASME - Journal of Engineering for Industry, vol 104, n 2, pp 151-161

[52] Netsch, H., and Giacometti, A., (1982) "Axial Flow - Induced Vibrations in Large High-Head Machines", Int. Water Power & Dam Construction, vol 34, n 8, pp 21-27

[53] Dowling, A.P., and Ffowcs Williams, J.E., (1983) "Sound and Sources of Sound", Ellis Harwood Ltd, Chichester

[54] Nelson, P.A., Halliwell, N.A, and Doak, P.E., (1983) "Fluid Dynamics of a Flow Excited Resonance, Part II: Flow Acoustic Interaction", Journal of Sound and Vibration, vol 91, n 3, pp 375-402

[55] Veret, C., (1983) "Flow Visualization by Light Sheet", Proceedings of the 3rd International Symposium on Flow Visualization, pp 106-112, University of Michigan, Michigan, USA, Sept 6-9

[56] Bronstein, I.N., and Semendjajew, K.A., (1984) "Taschenbuch der Mathematik", 21. Auflage, Verlag Harri Deutsch, Thun

[57] Lauterborn, W., and Vogel, A., (1984) "Modern Optical Techniques in Fluid Mechanics", Annual Review of Fluid Mechanics, vol 16, pp 223-244

[58] Panton, R.L., (1984) "Incompressible Flow", John Wiley & Sons, New York

[59] Reader-Harris, M.J., (1984) "The Decay of Swirl in a Pipe", International Journal of Heat and Fluid Flow, vol 15, n 3, June, pp 212-217

[60] Brownell, R.B., Flack, R.D., and Kostrzewsky, G.J., (1985) "Flow Visualization in the Tongue Region of a Centrifugal Pump", The Journal of Thermal Engineering, vol 4, n 2, pp 35-45

[61] Tourret, J., Badie-Cassagnet, A., Bernard, G., Foucolt, J.P., and Kermarec, J., (1985) "Experimental Studies of Noise Emission and Noise Generation from a Centrifugal Pump", Winter Annual Meeting - ASME, 85 - WA/FE-8

[62] Tourret, J., and Millouet, J., (1985) "Examen Critique des Methodes de Characterisation de l'Energie Acoustic Produit par une Pompe", La Houille Blanche, n 8, pp 647-662

[63] Blake, W.K., (1986) "Mechanics of Flow - Induced Sound and Vibration", 2 Volumes, Academic Press, London

[64] Blake, W.K., and Powell, A., (1986) "The Development of Contemporary Views of Flow-Tone Generation", in Krothapali, A, Smith, C.A.: "Recent Advances in Aeroacoustics", Springer Verlag, New York

[65] Comte - Bellot, G., and Ffowcs Williams, J.E., (1986) "Aero - and Hydroacoustics", Springer Verlag, Berlin

[66] Dubbel, ed., (1986) "Taschenbuch fuer den Maschinenbau", 15. Auflage, Springer Verlag, Berlin

[67] Gad-El-Hak, M., (1986) "Review of Flow Visualization Techniques for Unsteady Flows", Proceedings of the 4th International Symposium on Flow Visualization, pp 3-14, Ecole Nationale Superior de Techniques Avancees, Paris, France, Aug 26 - 29

[68] Hentschel, W., and Stoffregen, B., (1986) "Flow Visualization with Laser Light-Sheet Techniques in Automotive Research", Proceedings of the 4th International Symposium on Flow Visualization, pp 839-846, Ecole Nationale Superior de Techniques Avancees, Paris, France, Aug 26 - 29

[69] Karassik, I.J., et al., (1986) "Pump Handbook", 2nd edition, McGraw Hill, New York

[70] Legendre, R., (1986) "Internal Acoustics in Turbomachinery", Recherche Aerospatial, n 3, pp 75-79

[71] Lein, G., (1986) "Hydraulische Stroemungsmaschinen", Institut fuer Hydraulische Stroemungsmaschinen, Universitaet Stuttgart

[72] Lein, G., (1986) "Instationaere Vorgaenge in Hydraulischen Anlagen", Institut fuer Hydraulische Stroemungsmaschinen, Universitaet Stuttgart

[73] Lein, G., (1986) "Technische Stroemungslehre", Institut fuer Hydraulische Stroemungsmaschinen, Universitaet Stuttgart

[74] Lighthill, M.J., (1986) "An Informal Introduction to Theoretical Fluid Mechanics", Clarendon Press, Oxford

[75] Lorett, J.A., and Gopalakrishnan, S., (1986) "Interaction between Impeller and Volute of Pumps at Off-Design Conditions", ASME - Journal of Fluids Engineering, vol 108, pp 12-18

[76] Roco, M.C., Nair, P., and Addie, G.R., (1986) "Casing Headloss in Centrifugal Slurry Pumps", ASME - Journal of Fluids Engineering, vol 108, pp 453-464

[77] Round, G.F., and Garg, V.K., (1986) "Applications of Fluid Dynamics", Edward Arnold, London

[78] Saxena, S.V., Biegel, M., Hunnekuhl, G., and Mueller, H.A., (1986) "Koerperschallspektrum einer Pumpe in Abhaengigkeit von Grundparametern der Hydrodynamik und Konstruktion", Thyssen Technische Berichte, Heft 1, pp 81-93

[79] Thomas, R.N., Kostrzewsky, G.J., and Flack, R.D., (1986) "Velocity Measurements in a Pump Volute with a Non-Rotating Impeller", Int. Journal of Heat and Fluid Flow, vol 7, n 1, pp 11-20

[80] Tourret, J., and Bernard, G., (1986) "Complementary Methods for the Evaluation of the Total Acoustical Energy Emitted by the Hydraulic System", Proceedings - 1986 International Conference on Noise Control Engineering, pp 205-210

[81] Eppler, R., (1987) "Stroemungsmechanik", Institut A fuer Mechanik, Universitaet Stuttgart

[82] Hamkins, C.P., and Flack, R.D., (1987) "Laser Velocimeter Measurements in Shrouded and Unshrouded Radial Flow Pump Impellers", ASME - Journal of Turbomachinery, vol 109, pp 70-76

[83] Monin. A.S., and Yaglom, A.M., (1987) "Statistical Fluid Mechanics: Mechanics of Turbulence", MIT Press, Cambridge, Massachusetts

[84] Stirnemann, A., Eberl, J., Bolleter, U., and Pace, S., (1987) "Experimental Determination of the Dynamic Transfer Matrix for a Pump", ASME - Journal of Fluids Engineering, vol 109, n 3 pp 218-225

[85] Walker, D.A., (1987) "A Flourescent Technique for Measurement of Concentration in Mixing Liquids", Journal of Physics E: Instrumentation, vol 20, pp 217-224

[86] Zogg, H., Eberl, J., Bolleter, U., and Pace, S., (1987) "Noise Tests on Single - Stage Volute Pumps by Measurement of Sound Integrity", World Pumps, n 5, pp 138-140

[87] Adkins, D.R., and Brennen, C.E., (1988) "Analysis of Hydrodynamic Radial Forces on Centrifugal Pump Impellers", ASME - Journal of Fluids Engineering, vol 110, n 1, pp 20-28

[88] Bolleter, U., (1988) "Blade Passage Tones in Centrifugal Pumps", Vibrations, vol 4, n 3

[89] Eck, B., (1988) "Technische Stroemungslehre", 9. Auflage, Springer Verlag, Berlin

[90] Seybert, A.F., (1988) "Two-Sensor Method for the Measurement of Sound Intensity and Acoustic Properties in Ducts", Journal of the Acoustic Society of America, vol 83, n 6, pp 2233-2239

[91] Tsujimoto, Y, Acosta, A.J., and Brennen, C.E., (1988) "Theoretical Study of Fluid Forces on a Centrifugal Impeller Rotating and Whirling in a Volute", ASME - Journal of Vibration, Acoustics, Stress and Reliability in Design, vol 110, n 3, pp 263-269

[92] Welsh, M.C., Hourigan, K., Welch, L.W., Downie, R.J., Thompson, M.C., and Stokes, A.N., (1988) "Acoustics and Experimental Methods: The Influence of Sound on Flow and Heat Transfer", Experimental Heat Transfer, Fluid Mechanics and Thermodynamics, pp 141-159

[93] Arndt, N., Acosta, A.J., Brennen, C.E, and Caughey, T.K., (1989) "Rotor-Stator-Interaction in a Diffuser Pump", ASME - Journal of Turbomachinery, vol 111, n 3, pp 213-221

[94] Burchett, P.R., (1989) "Dynamic Performance of Centrifugal Pumps in a Two-Phase-(Steam/ Water) System", ASME - PVP Conference, vol 180, pp 1-6

[95] Chin, S.L., (1989) "Fundamentals of Laser Optoelectronics", World Scientific, Singapore

[96] Drazin, P.G., and Reid, W.H., (1989) "Hydrodynamic Stability", Cambridge University Press, Cambridge

[97] Kawashima, G., and Yang, W.-J., (1989) "Light Sheet Visualization of Unsteady Recirculating Flow inside Rotating Drum", Proceedings of the 5th International Symposium on Flow Visualization, Prague, Czechoslovakia, Aug 21 - 25

[98] Marek, I., and Hrabowsky, M., (1989) "Automated System for Quantitative Flow Visualization in Pumping Equipment", Proceedings of the 5th International Symposium on Flow Visualization, Prague, Czechoslovakia, Aug 21 - 25

[99] Miner, S.M., Beaudoin, R.J., and Flack, R.D., (1989) "Laser Velocimeter Measurements in a Centrifugal Flow Pump", ASME - Journal of Turbomachinery, vol 111, pp 205-212

[100] Paone, N., Riethmuller, M.L., and Van den Brambussche, R.A., (1989) "Experimental Investigation of the Flow in the Vaneless Diffuser of a Centrifugal Pump by Particle Image Displacement Velocimetry", Experiments in Fluids, vol 7, pp 371-378

[101] Ye, J., Roco, M.C., and Hamelin, P., (1989) "Experimental Investigation of Dilute Suspension Flow in a Rectangular Venturi Section", Cavitation and Multiphase Flow Forum, ISBN 0791803422, pp 93-99

[102] Arndt, N., Acosta, A.J., Brennen, C.E, and Caughey, T.K., (1990) "Experimental Investigation of Rotor-Stator-Interaction in a Centrifugal Pump with several Vaned Diffusors", ASME - Journal of Turbomachinery, vol 112, n 1, pp 98-108

[103] Bolleter, U., Stirnemann, A., Eberl, J., and McCloskey, T., (1990) "The Dynamic Transfer Matrix of a Pump and its Use in Pumping System Design", 3rd International Symposium on Transport Phenomena and Rotating Machinery, pp 493-504

[104] Chiang, H.-D., and Fleeter, S., (1990) "Cascade Aeronautics Including Steady Loading Effects", Noise Control Engineering Journal, vol 34, n 2, pp 61-72

[105] Denger, G.R., and McBride, M.W., (1990) "Three-Dimensional Flow Field Characteristics Measured in a Forward-Curved Centrifugal Blower using Particle Tracing Velocimetry", Fluid Measurement and Instrumentation Forum, pp 49-56

[106] Edge, K.A., and Johnston, D.N., (1990) "The 'Secondary Source' Method for the Measurement of Pump Pressure Ripple Characteristics", Proceedings of the Institute of Mechanical Engineers, Part A, vol 204, n 1, pp 33-46

[107] Franz, R., Acosta, A.J., Brennen, C.E, and Caughey, T.K., (1990) "The Rotordynamic Forces on a Centrifugal Pump Impeller in the Presence of Cavitation", ASME - Journal of Turbomachinery, vol 112, Sept, pp 264-271

[108] Godefroi, B., Tourret, J., Bertinier, M., and Pluviose, M., (1990) "Mesures Instationnaires dans les Pompes en Vue de Characteriser leur Acoustic Interne", Revue Francais de Mechanique, n 1990-3, pp 185-190

[109] Kodama, H., and Namba, M., (1990) "Unsteady Lifting Surface Theory for a Rotating Cascade of Swept Blades", ASME - Journal of Turbomachinery, vol 112, n 3, pp 411-417

[110] Shoureshi, R., Kubota, N., and Batta, G., (1990) "A Modern Approach to Active Noise Control", Winter Annual Meeting of the ASME, Dallas, Texas, Active Noise and Vibration Control, NCA, vol 8

[111] Stirnemann, A., (1990) "Instabilities in Pumping Systems", Sulzer Technical Review, 1

[112] Tennekes, H., and Lumley, J.L., (1990) "A First Course in Turbulence", 13th Printing, MIT Press, Cambridge

[113] Yu, F.T.S., and Khoo, I.C., (1990) "Principles of Optical Engineering", John Wiley & Sons, New York

[114] Dong, R., Chu, S., and Katz, J., (1991) "Quantitative Visualization of the Flow Within the Volute of a Centrifugal Pump", 1st ASME/JSME Joint Fluids Engineering Conf., Portland, Oregon

[115] Dong, R., Chu, S., and Katz, J., (1991) "The Three Dimensional Flow Structure Near the Cut-Off Region of a Centrifugal Pump", 4th Int. Conf. on Laser-Anemometry - Advances and Application, Cleveland, Ohio

[116] Morfiadakis, E.E., Voutsinas, S.G., and Papantonis, D.E, (1991) "Unsteady Flow Calculation in a Radial Flow Centrifugal Pump with Spiral Casing", Int. Journal for Numerical Methods in Fluids, vol 12, pp 895-908

[117] Pierce, A.D., (1991) "Acoustics - an Introduction to its Physical Principles and Application", 2nd Printing, Acoustic Society of America, Woodbury

[118] Dong, R., Chu, S., and Katz, J., (1992) "Quantitative Visualization of the Flow Within the Volute of a Centrifugal Pump. Part B: Results and Analysis", ASME - Journal of Fluids Engineering, vol 114, pp. 396-403

[119] Dong, R., Chu, S., and Katz, J., (1992) "Quantitative Visualization of the Flow Within the Volute of a Centrifugal Pump. Part A: Technique", ASME - Journal of Fluids Engineering, vol 114, pp. 390-395

[120] Durgin, W.W., and Graf, H.R., (1992) "Flow Excited Acoustic Resonance in a Deep Cavity: An Analytical Model", ASME - AMD, vol 151, and PVP Conference, vol 247, Symposium on Flow Induced Vibration and Noise, vol 7, ASME

[121] Fukano, T., Hayashi, H., Isobe, H., Hironaka, Y., and Fukahara, M., (1992) "Periodic Velocity Fluctuation in the Near Wake of a Rotating Flat-Plate Blade and their Role in the Generation of Turbulent Noise", ASME - PVP Conference, vol 243, Symposium on Flow Induced Vibration and Noise, vol 4, ASME

[122] Guehlich, J.F., and Bolleter, U., (1992) "Pressure Pulsations in Centrifugal Pumps", ASME - Journal of Vibration and Acoustics, vol 114, pp 273-279

[123] Hartlen, R.T., (1992) "Testing of Five and Seven-Vane Darlington Pump Impellers", Ontario Hydro Report No. 92-261-K, not published

[124] Morgenroth, M., (1992) "Numerical Model of the Vane Passage of a Rotating Impeller", McMaster University, Hamilton, Ontario, not published report

[125] Park, D.S., Ladd, D.M., and Hendricks, E., (1992) "Feedback Control of Karman Vortex Shedding", Active Control of Noise and Vibration, Winter Annual Meeting of the ASME, Anaheim, California

[126] Afonin, E., and Novozhilov, K., (1993) "Prediction of Hydrodynamic Noise Levels Generated by Blade Pumps using Principal Energetic Parameters", CETIM - 1st Int. Symposium on Pump Noise and Vibrations, Clamard, France, July 7-9, pp 161-164

[127] Barrand, J.P., Jaremczak, M., and Talha, M., (1993) "Pressure Fluctuations and Waves within a Pump Impeller", CETIM - 1st Int. Symposium on Pump Noise and Vibrations, Clamard, France, July 7-9, pp 35-42

[128] Bolleter, U., (1993) "Generation and Propagation of Pressure Pulsation in Centrifugal Pump Systems", Seminar on Acoustic Vibrations and Pressure Pulsations in Rotating Machinery, AECL CANDU, Oakville, Canada

[129] Bolleter, U., (1993) "Interaction of Pump and Piping Systems with regard to Pressure Pulsations", CETIM - 1st Int. Symposium on Pump Noise and Vibrations, Clamard, France, July 7-9, pp 3-12

[130] Brekke, H., Jernsletten, J., and Svingen, B., (1993) "Experimental Analysis of Pressure Pulsations in a Reversible Pump Turbine and Self Excited Pulsations from a Leaking Check Valve", CETIM - 1st Int. Symposium on Pump Noise and Vibrations, Clamard, France, July 7-9, pp 301-312

[131] Chatel, G., Lauro, J.F., and Trollat, C., (1993) "Experimental Analysis of Noise Generation Mechanism in a Centrifugal Pump", CETIM - 1st Int. Symposium on Pump Noise and Vibrations, Clamard, France, July 7-9, pp 137-144

[132] Chu, S., Dong, R., and Katz, J., (1993) "The Effect of Blade-Tongue Interaction on the Flow Structure, Pressure Fluctuations and Noise within a Centrifugal Pump", CETIM - 1st Int. Symposium on Pump Noise and Vibrations, Clamard, France, July 7-9, pp 13-34

[133] Cooper, P., (1993) "System Pulsations Associated with a 60,000 hp Vertical Water Pump", Seminar on Acoustic Vibrations and Pressure Pulsations in Rotating Machinery, AECL CANDU, Oakville, Canada

[134] Croba, D., Kueny, J.L., Hureau, F., and Kermarec, J., (1993) "Numerical and Experimental Unsteady Flow Analysis in Centrifugal Pumps, Impellers and Volute Interaction", CETIM - 1st Int. Symposium on Pump Noise and Vibrations, Clamard, France, July 7-9, pp 111-120

[135] De Jong, C.A.F., Kriesels, P.C., Bruggeman, J.C., and van Bokhorst, E., (1993) "Measurement of the Characteristics of a Centrifugal Pump as a Source of Pressure Pulsations", CETIM - 1st Int. Symposium on Pump Noise and Vibrations, Clamard, France, July 7-9, pp 165-174

[136] Denton, J.D., (1993) "Loss Mechanisms in Turbomachinery", ASME - Journal of Turbomachinery, vol 115, n 4, pp 621-656

[137] France, D., and Bilyk, D.W., (1993) "The Measurement of Pump Dynamic Impedance for use in Piping System Dynamic Analysis", CETIM - 1st Int. Symposium on Pump Noise and Vibrations, Clamard, France, July 7-9, pp 251-262

[138] Hartlen, R.T., Urbanowicz, J.T., and Barecca, S.L., (1993) "Dynamic Interaction between Pump and Piping System", CETIM - 1st Int. Symposium on Pump Noise and Vibrations, Clamard, France, July 7-9, pp 485-492

[139] Jaremczak, M., and Caignaert, G., (1993) "Theoretical and Experimental Analysis of Hydraulic Noise of Three Centrifugal Pumps", CETIM - 1st Int. Symposium on Pump Noise and Vibrations, Clamard, France, July 7-9, pp 103-110

[140] Klaeui, E., (1993) "A Simulation Study on the Attenuation of Fluid Borne Noise of Centrifugal Pumps by Influencing the Acoustic Impedance of the Pump", CETIM - 1st Int. Symposium on Pump Noise and Vibrations, Clamard, France, July 7-9, pp 509-514

[141] Pauls, R.E., Misra, A., Vijay, D.K., Teper, W., Lin, T.C., Strezelczyk, A., and Hemraj, R., (1993) "Acoustic Modelling in Support of Darlington n 12 Investigations", Seminar on Acoustic Vibrations and Pressure Pulsations in Rotating Machinery, AECL CANDU, Oakville, Canada

[142] Rzentkowski, G., and Forest, J.W, (1993) "Acoustical Characterization of the Heat Transport System of Darlington Nuclear Generation Station: Analysis Technique and Result", CETIM - 1st Int. Symposium on Pump Noise and Vibrations, Clamard, France, July 7-9, pp 289-300

[143] Schwirian, R.E., (1993) "Pump-Induced Acoustical Analysis of the Primary Coolant System in a Pressurized Water Reactor", CETIM - 1st Int. Symposium on Pump Noise and Vibrations, Clamard, France, July 7-9, pp 427-434

[144] Steward, B., (1993) "Darlington Fuel Damage Investigations", Seminar on Acoustic Vibrations and Pressure Pulsations in Rotating Machinery, AECL CANDU, Oakville, Canada

[145] Telfer, A.D., (1993) "Darlington Fuel Damage Investigation", CETIM - 1st Int. Symposium on Pump Noise and Vibrations, Clamard, France, July 7-9, pp 443-456

[146] Timushev, S.F., and Nedashkovsky, A.K., (1993) "Computational and Experimental Study of Acoustical Resonances in Centrifugal Pump Working Cavity", CETIM - 1st Int. Symposium on Pump Noise and Vibrations, Clamard, France, July 7-9, pp 271-278

[147] To, S., (1993) "Characterization of Flow Induced Vibrations and Pulsations of Complicated Piping Systems", Seminar on Acoustic Vibrations and Pressure Pulsations in Rotating Machinery, AECL CANDU, Oakville, Canada

[148] Verhoeven, J., and Gutierez, J.R., (1993) "Hydraulic Interaction between Pump and Piping Systems a Prime Source of Pressure Pulsations in Boiler Feed Pump Systems", Seminar on Acoustic Vibrations and Pressure Pulsations in Rotating Machinery, AECL CANDU, Oakville, Canada

[149] Weaver, D.S., (1993) "Interactions of Fluid Flow Oscillations and Acoustic Fields", Seminar on Acoustic Vibrations and Pressure Pulsations in Rotating Machinery, AECL CANDU, Oakville, Canada

[150] Whitson, R.J., and Benson, I.M., (1993) "Investigation of the Fluid Borne Noise Source Flow and Source Impedance Characteristics of a Single Stage Centrifugal Pump using Secondary Noise Source", CETIM - 1st Int. Symposium on Pump Noise and Vibrations, Clamard, France, July 7-9, pp 175-184

[151] Wu, J.-S., and Faeth, G.M., (1993) "Sphere Wakes in Still Surrounding at Intermediate Reynolds Numbers", AIAA Journal, vol 31, n 8, pp 1448-1455

[152] Yu, S.K.W., (1993) "Design for Control of Acoustic Pulsations and Vibrations", Seminar on Acoustic Vibrations and Pressure Pulsations in Rotating Machinery, AECL CANDU, Oakville, Canada

[153] Ziada, S., (1993) "Flow Excited Resonances of Piping Systems Containing Side Branches", Seminar on Acoustic Vibrations and Pressure Pulsations in Rotating Machinery, AECL CANDU, Oakville, Canada

[154] Zogg, H., and Bolleter, U., (1993) "Generation and Propagation of Hydraulic Noise in Centrifugal Pumps", CETIM - 1st Int. Symposium on Pump Noise and Vibrations, Clamard, France, July 7-9, pp 263-270

[155] Akin, O., and Rockwell, D., (1994) "Actively Controlled Radial Flow Pumping System: Manipulation of Spectral Content of Wakes and Wake-Blade Interactions", ASME - Journal of Fluids Engineering, vol 116, n 3, pp 528-537

[156] Akin, O., and Rockwell, D., (1994) "Flow Structure in a Radial Flow Pumping System Using High-Image-Density Particle Image Velocimetry", ASME - Journal of Fluids Engineering, vol 116, n 3, pp 538-544

[157] Badie, R., Jonker, J.B., and van den Braembussche, R.A., (1994) "Finite Element Calculations and Experimental Verification of the Unsteady Potential Flow in a Centrifugal Volute Pump", Internatiol Journal for Numerical Methods in Fluids, vol 19, pp 1083-1102

[158] Benedek, S., (1994) "Fluid Vibration Induced by a Pump", Journal of Sound and Vibration, vol 177, n 3, pp 337-348

[159] Lee, K.B., and Im, I.Y., (1994) "An Analytical Study on the Pump-Induced Acoustic Pressure in a Pressurized Water Reactor", Nuclear Engineering and Design, vol 147, pp 275

[160] Misra, A., Pauls, R.E, Vijay, D.K., Teper, W., Lin, T.C., Strzelcyk, A., Liu, J., and Hemraj, R., (1994) "Acoustic Modeling in Support of Fuel Failure Investigation in a CANDU Nuclear Generating Station", ASME - PVP Conference, vol 279, Minneapolis

[161] Ohashi, H, (1994) "Case Study of Pump Failure due to Rotor-Stator Interaction", International Journal of Rotating Machinery, vol 1, n 1, pp 53-60

[162] Chu, S., Dong, R., and Katz, J., (1995) "Relationship between Unsteady Flow, Pressure Fluctuations, and Noise in a Centrifugal Pump - Part B: Effects of Blade-Tongue Interactions", ASME - Journal of Fluids Engineering, vol 117, n 1, pp 30-41

[163] Chu, S., Dong, R., and Katz, J., (1995) "Relationship Between Unsteady Flow, Pressure Fluctuations, and Noise in a Centrifugal Pump - Part A: Use of PDV Data to Compute the Pressure Field", ASME - Journal of Fluids Engineering, vol 117, n 1, pp 24-29

[164] Crandall, S.H., (1995) "Canonical Physical Models of Dynamic Instability", 15th Canadian Congress of Applied Mechanics, University of Victoria, BC, Canada, May 28 - June 1

[165] Miyamoto, H., and Ohba, H., (1995) "The Effect of Flow Rate on Passage Flows in Centrifugal Impellers", JSME International Journal Part B: Fluids and Thermal Engineering, vol 38, n 1, pp 17-24

[166] Miyamoto, H., and Ohba, H., (1995) "The Effect of Flow Rate on Characteristics in Centrifugal Impellers", JSME International Journal Part B: Fluids and Thermal Engineering, vol 38, n 1, pp 25-30

[167] Miyano, H., Saito, N., and Hagiwara, T., (1995) "Study of Elbow Effect on Pulsation in Piping System", ASME - PVP Conference, Honolulu, vol 298, Flow Induced Vibration, pp 55-58

[168] Modi, V.J., (1995) "Moving Surface Boundary-Layer Control: Experiments, Analyses and Application", 15th Canadian Congress of Applied Mechanics, University of Victoria, BC, Canada, May 28 - June 1

[169] Morgenroth, M., and Weaver, D.S., (1995) "Pump Acoustics: An Experimental Investigation", 15th Canadian Congress of Applied Mechanics, University of Victoria, BC, Canada, May 28 - June 1

[170] Rzentkowski, G., (1995) "Analysis of Two-Phase Flow Instability in a Closed-Loop Pump-Piping System", ASME - PVP Conference, Honolulu, vol 298, Flow Induced Vibration, pp 71-82

[171] Sharma, S.D., and Sahoo, R.K., (1995) "Near Wake of a Blunt-Based Aerofoil with Boundary Layer Suction on One Side", 15th Canadian Congress of Applied Mechanics, University of Victoria, BC, Canada, May 28 - June 1

[172] Morgenroth, M., and Weaver, D.S., (1996) "Pump Acoustics: Effects of Cut-Water Geometry on Sound Generation at Blade Pass Frequency", accepted for CSME Forum '96, May 7-9, McMaster University, Hamilton, Ontario, Canada

APPENDIX A: LIST OF EQUIPMENT

Hydraulic Hardware

[a] Ball Valve, Newco 51FC8M4, 4" diameter, ANSI 150 flanged, stainless steel SS 316, lever operated

[b] Centrifugal Volute Pump, Smart Turner Model 3LIUE, Serial No. 939135, 4" x 3" x 13.5", all bronze construction, flow rate 17.4 l/s, head 19.2 m water, efficiency > 70 % nominal at 1150 rpm

[c] Globe Valve, Newco 21FC8M4, 3" diameter, ANSI 150 flanged, stainless steel SS 316, handwheel operated

[d] Electric AC Motor, Brook Crompton, Model 2425311-99 M, 575 V, 60 Hz, 3 phase, nominal power: 7.46 kW, nominal shaft speed: 1165 rpm

[e] Flanges, ANSI 150, stainless steel SS 304 L

[f] Gaskets, ANSI 150, full face, red rubber

[g] Instrumentation Fittings, Swagelock, bronze

[h] Piping, 3" and 4", stainless steel SS 304 welded, schedule 40s

Instrumentation

[i] Accelerometer, Entran EGAL-125F-10D

[j] Differential Pressure Transducer, Lucas-Schaewitz P-3061, inductive type, range: 0-3500 mbar, combined static error: < 0.5 % of full scale

[k] Dynamic Pressure Transducer, PCB Piezotronics, Model No. 112M284, charge mode, resolution 0.28 mbar, sensitivivity (nominal 1.45 pC/mbar):
Transducer:1 2 3 4 5 6 7 8
Serial#:10656,10280,10282,10418,10419,10444,10499,10662
Sens. : 1.60, 1.74, 1.81, 1.70, 1.83, 1.61, 1.71, 1.51
complete system including individual preamplifier, amplifier channel (10x), board gain, software gain factor and all cables physically calibrated wrt transducer no. 4

[l] Flow Meter, Sparling FM 621 Waterhawk, pulsed dc magnetic flow meter, accuracy +/- 2 % of rate for flow velocity greater then 0.3 m/s, +/- 6 mm/s constant for flow velocity less then 0.3 m/s, calibration constant 424.625 pulses /gallon

[m] Proximity Sensor, Micro Switch PK 8056 1, Series 922, 12 mm

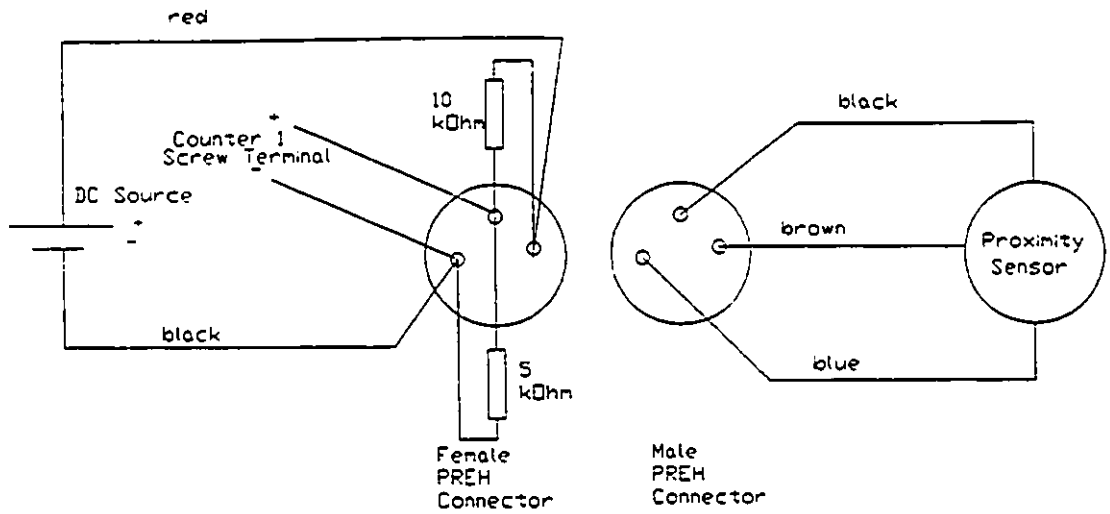

Figure A.1: Wiring Diagram for Proximity Sensor

[n] Pressure Transducer, Data Instruments, Model EA, strain gauge type, range: 0-414 and 0-3450 mbar, combined static error: < 1% of full scale

[o] Thermocouple, Omega Engineering, EMQSS-062U-3, type E, 1/16" diameter, 3" long, ungrounded

Signal Generating Equipment

[p] Electromagnetic Shaker, MB Electronics, Model No. EA-1500, Serial No. 673

[q] External Trigger for A/D Computer Board

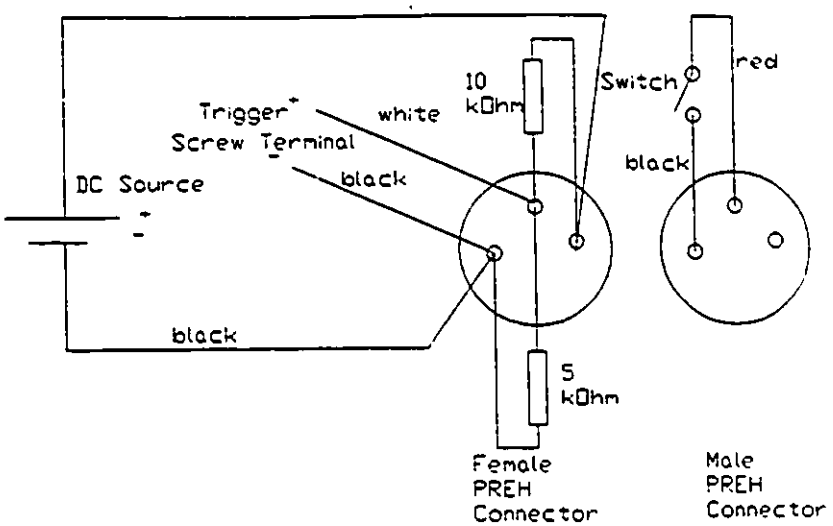

Figure A.2: Wiring Diagram for External Trigger

[r] Function Generator, Philips PM5133

[s] Power Amplifier, MB Electronics, Model No. 2250MB

[t] Sine Random Generator, Brüel & Kjaer Type 1024

[u] Variable Frequency Motor Controler, TB Wood's E-TRac AC Inverter, WCC50100 C Series, 7.46 kW, output voltage 575 V AC, frequency: 0.1-120 Hz, resolution 0.05 of max. frequency, stability: +/- 0.00006 %/°C

Signal Processing Equipment

[v] Amplifier, Vishay Instruments, Signal Conditioning Amplifier 2310

[w] Charge Amplifier, PCB, In-Line Charge Amplifier, Model No. 422 D02

[x] Charge Amplifier, PCB Model No. 483 B07, Serial No. 393, 16 channels, 1 to 8 used

[y] Data Acquisition Board, Data Translation DT2835, 12 Bit resolution, 50 kHz throughput, 8 double entry channels, gains of 1, 10, 100 and 500

[z] Dynamic Analyser, HP 35670A, 4 channel

[aa] Filter, Wavetek 852, Serial No. 6871210

[ab] High Speed Video Camera, Kodak Ektapro 1000, 1000 frames/s, 408 full frames memory

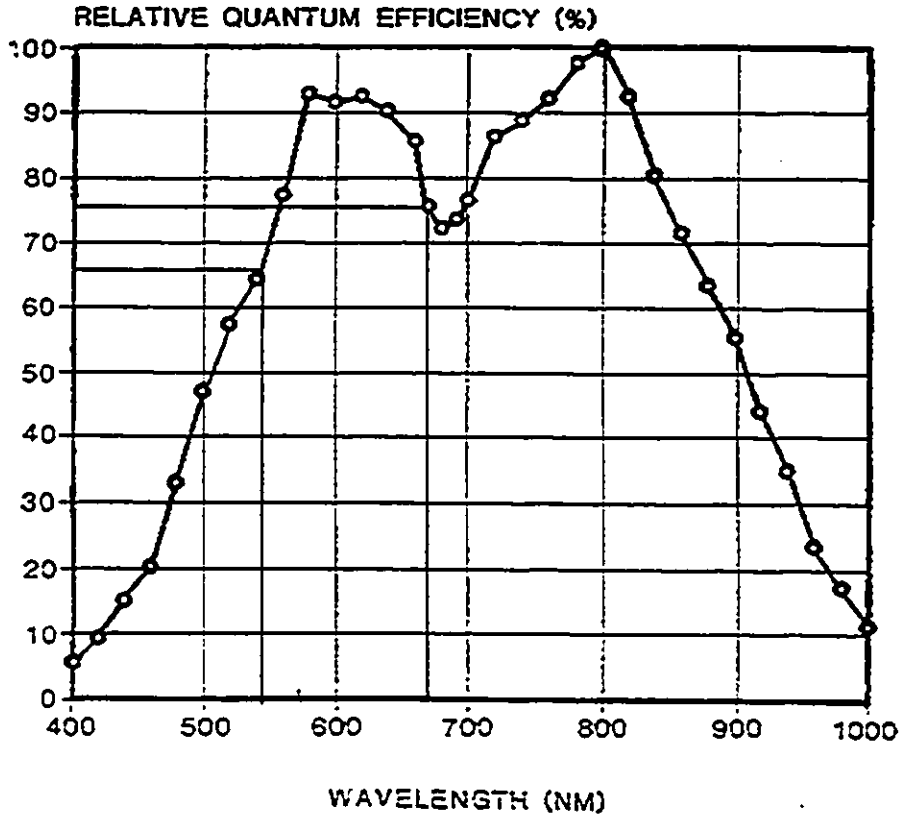

Figure A.3: Relative Spectral Response for Kodak Ektrapro 1000

[ac] Loop Current Meter, Digitec Model 2020, 4-20 mA, calibrated 0 to 69.4 l/s

Miscellaneous

[ad] Flourescein, BDH Laboratory Chemicals Group, Poole, England

[ae] Ink, Schaefer "Skript", black

[af] Metal Rebuilding Compound, Devcon Bronze Putty BR

[ag] Transparent Plastic Sheet, Chemacryl Acrylite GP

[ah] Vibration Plate, Trellcan, MDVP, 9 mm, capacity 0.4 MPa

APPENDIX B: OPERATING INSTRUCTIONS

B.1 Hardware Operating Instructions

Fill Overhead Tank

Why? Exchange (contamination with rust, algae, excess of tracer fluid, etc.) or replenish working fluid (depletion by undergraduate "Reynolds number experiment").

How? Valves are located to the left of the tank (facing it from the lab)

1) Drain pipe water to waste water system until plug of rusty water can be observed passing the acrylic pipe.
2) Fill overhead tank until flow through overflow duct can be heard (no level gauge is fitted so far)
3) Close valves slowly to avoid water hammer.

Replace Cut-Water Wedge in Pump

Why? Change geometry of pump cut-water.

How? 1) Close ball and globe valve to isolate loop from tank.

2) Drain loop water through drain hose (open one or more of the vent valve) at least below the window level.

3) When removing screws from windows be careful not to mix them up (different sizes and lengths for different taps, wood pattern is provided).

4) Ease wedge from locating dowel pin in casing by gently rocking the piece.

5) Assembly is generally the reverse process, but extreme care is required not to strip the taps!!! Sealing of the windows might require a couple of days soaking the gasket and O-Ring in water. Do not over tighten!

Disassembly of Loop Upstream of Pump

Why? Remove pump suction cover or impeller

How? 1) Overhead tank should be emptied to avoid spill (if absolutely necessary water can remain in tank but loop needs to be drained). This can be done in three ways: through loop drainage (preferably, allow about 2 hours), through pipes along the windows (undergraduate experiment), through pump next to loop (only possible while foot valve is still leaking).

2) Remove all but the two threaded rods fitted with nuts on the flow meter side from the wafer type magnetic flow meter.

3) Use the inside nuts to lift alternating the pipe assembly upstream of the flow meter (seal at the tank flange is designed to slide) by about 10 mm.

4) Remove rubber gaskets between flow meter and pipe on both sides (if they are stuck wait until they have dried)

5) Flow meter can be removed to allow access to remaining pipe assembly. Beware: Upstream part of assembly is now only held in place by friction.

6) Remove wiring and tubing where necessary.

7) To remove suction cover let sealing dry, leave bolts after loosening 2 to 3 turns in tap and hit with soft faced hammer. Lift suction cover without tilting.

8) To remove impeller remove hub nut, wedge impeller against casing and hit shaft with soft faced hammer.

9) Wooden frame is provided to be placed on open pump casing for preventing upstream pipe assembly from sliding down.

Dissembly of Loop Downstream of Pump

Why? Change system, general maintenance

How? Parts are heavy. U-Bend is cantilevered, support well with wooden blocks before removing all flange bolts. Downstream tank seal is also of the sliding type. Steel bracket needs to be removed to dissemble.

Application of Instrumentation Taps in Pipe

Why? Change location of pressure taps

How? Drilling and tapping in stainless steel is very tedious (be prepared to spend a day on a tap in an awkward location).

1) A steel stencil (for 1/8" NPT taps) attached with a hose clamp is provided to keep the hand drill perpendicular. (Predrilling with smaller diameters did not prove advantageous.)

2) The drill bit needs to be specifically ground for stainless steel.

3) Generating the axial force can be facilitated by use of a webbing ribbon with a ratchet.

B.2 Software Operating Instructions

Various pieces of software are thought to be worthy of being preserved. They fall into two categories: macro programs to complement the use of the Global Lab (GL) data acquisition software, and independent FORTRAN or Quick Basic programs for data post processing. A listing of the programs is avoided but a copy on floppy disk remains with the thesis supervisor Professor Weaver.

<u>GL Macro: SP</u>

purpose:	measure sound speed by acquiring pressure time history from two transducers
file needed:	sp.mac, (sp.asc), sp.asu
file produced:	sp.dat
input format:	n/a
output format:	GL intern
comments:	signals from transducer 2 and 4 is sampled at total sampling rate of 50 000 Hz for a duration of 0.5 s, relevant part of signal needs to be extracted and translated to ASCII format semi-manually, auxiliary macros are a.mac, b.mac, spimp.mac

<u>GL Macro: HQ</u>

purpose:	measure static head and flow rate of pump
file needed:	hq.mac, (hq.asc), stat.asu, pumpnois.ulb
file produced:	flow.asc, head.asc (append mode)
input format:	n/a
output format:	ASCII, single value per line in l/s and mbar respectively
comments:	acquisition at 10 Hz/channel for 10 s, mean flow rate and head are appended to corresponding file

GL Macro: AQ

purpose: acquire dynamic pressure signals for all channels
file needed: aq.mac, (aq.asc), pd.asu, pumpnois.ulb
file produced: pd.dat
input format: n/a
output format: GL intern, sequence of channels: 0-7, values in units of mbar
comments: sampling frequency 511.87551 Hz for 61 s

GL Macro: FF

purpose: compute FFT transform of dynamic pressures
file needed: ff.mac, (ff.asc), pd.dat
file produced: fft.asc, fft.dat
input format: GL intern, sequence of channels: 0-7, values in units of mbar
output format: GL intern and ASCII, sequence of transforms: 1-8, values in units of mbar rms
comments: FFT size is 1024 resulting in 30 averages and about 0.5 Hz resolution in frequency domain, frequency limits: 0-200 Hz

Quick Basic Program: CROSS

purpose: compute cross correlation function of two signals
file needed: cross.exe, (cross.bas), cross.in
file produced: taumax.prn
input format: ASCII, 2 values per line
output format: ASCII, single value per line: cross correlation factor normalized by auto correlation of first signal at θ=0
comments: direct integration of cross correlation factor, ∂t = 0.04 ms, time θ at maximum of parabolic fit to 3 highest values of cross correlation function is appended to taumax.prn

Quick Basic Program: EXTRACT

purpose: extract peaks at BPF from pressure spectrum
file needed: extract.exe, (extract.bas), input file
file produced: output file
input format: ASCII
output format: ASCII
comments: name(s) of input file(s), output file(s), frequency resolution, number of channels observed, pump shaft speed(s) and number of BPF harmonics are adjusted in the code. Versatility also includes calculation of frequency band integration and equivalent viscous damping parameter for peaks.

FORTRAN Program: GREEN

purpose:	curve fit combined model (see chapter 4) to measured peaks at BPF
file needed:	green.exe, (green.for), fit.in
file produced:	green.out, green.dat, green.par
input format:	ASCII, 3 lines skipped (comments), 2. column independent, 3. column dependent variable
output format:	ASCII, green.out: initial guesses, iteration parameters, statistical results, etc. green.par: only parameters of model and residual green.dat: separately acoustic and hydraulic part of model in specified range of independent variable
comments:	code bases on public domain software VARPRO, subroutines for green's function and decay function are verified using MAPLE V, input format is matched to use output from EXTRACT